NASA-CR-194838

N-
202113
123 p

Determination of the Stability and Control Derivatives of the NASA F/A-18 HARV Using Flight Data

Contractor Report
for
NASA Grant # NCC 2-759

NASA Technical Contact
Albion H. Bowers
NASA Dryden Flight Research Facility

Authors
Principal Investigator: Marcello R. Napolitano
Graduate Student: Joelle M. Spagnuolo

May 15, 1993 - December 15, 1993

(NASA-CR-194838) DETERMINATION OF THE STABILITY AND CONTROL DERIVATIVES OF THE NASA F/A-18 HARV USING FLIGHT DATA Contractor Report, 15 May - 15 Dec. 1993 (West Virginia Univ.) 123 p

N94-24804

Unclas

G3/08 0202113

Determination of the Stability and Control Derivatives of the NASA F/A-18 HARV Using Flight Data

Contractor Report
for
NASA Grant # NCC 2-759

NASA Technical Contact
Albion H. Bowers
NASA Dryden Flight Research Facility

Authors
Principal Investigator: Marcello R. Napolitano
Graduate Student: Joelle M. Spagnuolo

December 1993

ABSTRACT

This report documents the research conducted for the NASA-Ames Cooperative Agreement No. NCC 2-759 with West Virginia University. The NASA technical officer for this grant is Albion H. Bowers, an aerospace engineer at NASA

A complete set of the stability and control derivatives for varying angles of attack from 10° to 60° were estimated from flight data of the NASA F/A-18 HARV. The data were analyzed with the use of the pEst software which implements the output-error method of parameter estimation. Discussions of the aircraft equations of motion, parameter estimation process, design of flight test maneuvers, and formulation of the mathematical model are presented. The added effects of the thrust vectoring and single surface excitation systems are also addressed. The results of the longitudinal and lateral directional derivative estimates at varying angles of attack are presented and compared to results from previous analyses. The results indicate a significant improvement due to the independent control surface deflections induced by the single surface excitation system, and at the same time, a need for additional flight data especially at higher angles of attack.

ACKNOWLEDGMENTS

The authors would like to express their sincere gratitude to Mr. Albion Bowers, the NASA technical monitor, Mr. Brent Cobleigh, Dr. Kenneth Iliff and the other researchers at NASA Dryden Flight Research Facility for their much appreciated advice and assistance.

TABLE OF CONTENTS

	Page
TITLE PAGE	i
ABSTRACT	ii
ACKNOWLEDGEMENTS	iii
TABLE OF CONTENTS	iv
LIST OF TABLES AND FIGURES	vi
NOMENCLATURE	x
CHAPTER 1: INTRODUCTION	1
1.1 Literature Review	3
CHAPTER 2: AIRCRAFT STABILITY AND CONTROL	8
2.1: Aircraft Stability and Control Definition	8
2.2: Aerodynamic Force and Moment Representation	9
CHAPTER 3: PARAMETER ESTIMATION	11
3.1: Purpose	11
3.2: Techniques	11
3.3: The Maximum Likelihood Method	13
CHAPTER 4: AIRCRAFT EQUATIONS OF MOTION	21
4.1: Newtonian Mechanics	21
4.2: Applied Forces	23
4.3: Applied Moments	24

4.4: Euler Angles 26

4.5: Velocity Components (Polar Form) 29

4.6: Six-Degree-of-Freedom Equations of Motion 31

4.7: Observation Equations 32

CHAPTER 5: HIGH ALPHA RESEARCH 37

5.1: Purpose of High Alpha Technology Program 37

5.2: High Alpha Research Vehicle (HARV) Description 39

5.3: Instrumentation and Airdata Systems 41

CHAPTER 6: FLIGHT TEST MANEUVERS 46

6.1: Design Considerations 46

6.2: Maneuvers Developed for the HARV 48

CHAPTER 7: HARV AERODYNAMIC MODEL 56

7.1: Equation Modification 56

7.2: Sign Convention 59

CHAPTER 8: RESULTS AND CONCLUSIONS 62

8.1: Lateral Directional Derivatives 63

8.2: Longitudinal Directional Derivatives 68

8.3: Conclusions 71

REFERENCES 104

LIST OF TABLES AND FIGURES

PAGE

TABLES

Table 5.1: Physical Characteristics of the F/A-18 HARV 43

FIGURES

Figure 3.1: Block Diagram of the Parameter Estimation Process 18

Figure 3.2: Geometric Meaning of the Modified Newton-Raphson Method 19

Figure 3.3: A Qualitative Trend of J with the Number of Iterations, K 20

Figure 4.1: Body Axis System 35

Figure 4.2: Representation of Euler Angles 36

Figure 5.1: Three-view Drawing of the F-18 HARV 44

Figure 5.2: F-18 HARV Engine Thrust Vectoring Vane Configuration 45

Figure 6.1: Flight Test Maneuver Input Shapes 51
(a) Frequency Sweep (b) 3211 (c) Pulse-Type (Doublet)

Figure 6.2: Control Surface Deflection Time Histories without OBES 52

Figure 6.3: Correlation between the Rudder & Aileron Deflections without OBES 53

Figure 6.4: Control Surface Deflection Time Histories with OBES 54

Figure 6.5: Correlation between the Rudder & Aileron Deflections with OBES 55

Figure 7.1: Thrust Vectoring Vane Positions 61

Figure 8.1: Computed and Measured Response Time Histories for α = 10° in the 73
Lateral Direction (a) Sideslip Angle (b) Rolling Moment
(c) Yawing Moment (d) Roll Angle (e) Lateral Acceleration

Figure 8.2: Computed and Measured Response Time Histories for α = 25° in the 74
Lateral Direction (a) Sideslip Angle (b) Rolling Moment
(c) Yawing Moment (d) Roll Angle (e) Lateral Acceleration

Figure 8.3: Computed and Measured Response Time Histories for α = 30° in the Lateral Direction (a) Sideslip Angle (b) Rolling Moment (c) Yawing Moment (d) Roll Angle (e) Lateral Acceleration 75

Figure 8.4: Computed and Measured Response Time Histories for α = 40° in the Lateral Direction (a) Sideslip Angle (b) Rolling Moment (c) Yawing Moment (d) Roll Angle (e) Lateral Acceleration 76

Figure 8.5: Computed and Measured Response Time Histories for α = 50° in the Lateral Direction (a) Sideslip Angle (b) Rolling Moment (c) Yawing Moment (d) Roll Angle (e) Lateral Acceleration 77

Figure 8.6: Computed and Measured Response Time Histories for α = 60° in the Lateral Direction (a) Sideslip Angle (b) Rolling Moment (c) Yawing Moment (d) Roll Angle (e) Lateral Acceleration 78

Figure 8.7: Aerodynamic Bias Derivatives (Lateral-Directional) (a) Lateral Force (b) Rolling Moment (c) Yawing Moment 79

Figure 8.8: Sideslip Derivatives (Lateral-Directional) (a) Lateral Force (b) Rolling Moment (c) Yawing Moment 80

Figure 8.9: Roll Rate Derivatives (Lateral-Directional) (a) Lateral Force (b) Rolling Moment (c) Yawing Moment 81

Figure 8.10: Yaw Rate Derivatives (Lateral-Directional) (a) Lateral Force (b) Rolling Moment (c) Yawing Moment 82

Figure 8.11: Aileron Derivatives (Lateral-Directional) (a) Lateral Force (b) Rolling Moment (c) Yawing Moment 83

Figure 8.12: Rudder Derivatives (Lateral-Directional) (a) Lateral Force (b) Rolling Moment (c) Yawing Moment 84

Figure 8.13: Differential Horizontal Tail Derivatives (Lateral-Directional) (a) Lateral Force (b) Rolling Moment (c) Yawing Moment 85

Figure 8.14: Pitch Vane Derivatives (Lateral-Directional) (a) Lateral Force (b) Rolling Moment (c) Yawing Moment 86

Figure 8.15: Yaw Vane Derivatives (Lateral-Directional) (a) Lateral Force (b) Rolling Moment (c) Yawing Moment 87

Figure 8.16: Calculated Thrust Moment Arm at Varying Angles of Attack 88

Figure 8.17: Computed and Measured Response Time Histories for α = 10° in the Longitudinal Direction (a) Angle of Attack (b) Pitching Moment (c) Pitch Angle (d) Normal Acceleration (e) Axial Acceleration 89

Figure 8.18: Computed and Measured Response Time Histories for α = 25° in the Longitudinal Direction (a) Angle of Attack (b) Pitching Moment (c) Pitch Angle (d) Normal Acceleration (e) Axial Acceleration 90

Figure 8.19: Computed and Measured Response Time Histories for α = 30° in the Longitudinal Direction (a) Angle of Attack (b) Pitching Moment (c) Pitch Angle (d) Normal Acceleration (e) Axial Acceleration 91

Figure 8.20: Computed and Measured Response Time Histories for α = 40° in the Longitudinal Direction (a) Angle of Attack (b) Pitching Moment (c) Pitch Angle (d) Normal Acceleration (e) Axial Acceleration 92

Figure 8.21: Computed and Measured Response Time Histories for α = 50° in the Longitudinal Direction (a) Angle of Attack (b) Pitching Moment (c) Pitch Angle (d) Normal Acceleration (e) Axial Acceleration 93

Figure 8.22: Computed and Measured Response Time Histories for α = 60° in the Longitudinal Direction (a) Angle of Attack (b) Pitching Moment (c) Pitch Angle (d) Normal Acceleration (e) Axial Acceleration 94

Figure 8.23: Aerodynamic Bias Derivatives (Longitudinal-Directional) (a) Normal Force (b) Pitching Moment (c) Axial Force 95

Figure 8.24: Angle of attack Derivatives (Longitudinal-Directional) (a) Normal Force (b) Pitching Moment (c) Axial Force 96

Figure 8.25: Pitch Rate Derivatives (Longitudinal-Directional) (a) Normal Force (b) Pitching Moment (c) Axial Force 97

Figure 8.26: Trailing Edge Flap Derivatives (Longitudinal-Directional) (a) Normal Force (b) Pitching Moment (c) Axial Force 98

Figure 8.27: Leading Edge Flap Derivatives (Longitudinal-Directional) (a) Normal Force (b) Pitching Moment (c) Axial Force 99

Figure 8.28: Symmetric Aileron Derivatives (Longitudinal-Directional) (a) Normal Force (b) Pitching Moment (c) Axial Force 100

Figure 8.29: Elevator Derivatives (Longitudinal-Directional) (a) Normal Force (b) Pitching Moment (c) Axial Force 101

Figure 8.30: Pitch Vane Derivatives (Longitudinal-Directional) 102
(a) Normal Force (b) Pitching Moment (c) Axial Force

Figure 8.31: Yaw Vane Derivatives (Longitudinal-Directional) 103
(a) Normal Force (b) Pitching Moment (c) Axial Force

NOMENCLATURE

Symbol	Description	Units
a_n	Normal Acceleration	g
a_x	Longitudinal Acceleration	g
a_y	Lateral Acceleration	g
a_z	Vertical Acceleration	g
b	Reference Span	m or ft
c	Reference Chord	m or ft
C_A	Axial Force Coefficient	
C_{A_o}	Axial Force Aerodynamic Bias	
C_{A_α}	Axial Force due to α	per deg
$C_{A_{\delta E}}$	Axial Force due to δ_E	per deg
$C_{A_{\delta LEF}}$	Axial Force due to δ_{LEF}	per deg
$C_{A_{\delta TEF}}$	Axial Force due to δ_{TEF}	per deg
$C_{A_{\delta SA}}$	Axial Force due to δ_{SA}	per deg
C_{A_q}	Axial Force due to q	per rad
$C_{A_{\delta PV}}$	Axial Force due to δ_{PV}	per deg
$C_{A_{\delta YV}}$	Axial Force due to δ_{YV}	per deg
C_D	Drag Coefficient	
C_l	Rolling Moment Coefficient	

C_{lo}	Rolling Moment Aerodynamic Bias	
$C_{l\beta}$	Rolling Moment due to β	per deg
C_{lp}	Rolling Moment due to p	per rad
C_{lr}	Rolling Moment due to r	per rad
$C_{l\delta A}$	Rolling Moment due to δ_A	per deg
$C_{l\delta DHT}$	Rolling Moment due to δ_{DHT}	per deg
$C_{l\delta R}$	Rolling Moment due to δ_R	per deg
$C_{l\delta PV}$	Rolling Moment due to δ_{PV}	per deg
$C_{l\delta YV}$	Rolling Moment due to δ_{YV}	per deg
C_L	Lift Coefficient	
C_m	Pitching Moment Coefficient	
C_{mo}	Pitching Moment Aerodynamic Bias	
$C_{m\alpha}$	Pitching Moment due to α	per deg
$C_{m\delta E}$	Pitching Moment due to δ_E	per deg
$C_{m\delta LEF}$	Pitching Moment due to δ_{LEF}	per deg
$C_{m\delta TEF}$	Pitching Moment due to δ_{TEF}	per deg
$C_{m\delta SA}$	Pitching Moment due to δ_{SA}	per deg
C_{mq}	Pitching Moment due to q	per rad
$C_{m\delta PV}$	Pitching Moment due to δ_{PV}	per deg
$C_{m\delta YV}$	Pitching Moment due to δ_{YV}	per deg
C_n	Yawing Moment Coefficient	
C_{no}	Yawing Moment Aerodynamic Bias	

$C_{n\beta}$	Yawing Moment due to β	per deg
C_{np}	Yawing Moment due to p	per rad
C_{nr}	Yawing Moment due to r	per rad
$C_{n\delta A}$	Yawing Moment due to δ_A	per deg
$C_{n\delta DHT}$	Yawing Moment due to δ_{DHT}	per deg
$C_{n\delta R}$	Yawing Moment due to δ_R	per deg
$C_{n\delta PV}$	Yawing Moment due to δ_{PV}	per deg
$C_{n\delta YV}$	Yawing Moment due to δ_{YV}	per deg
C_N	Normal Force Coefficient	
C_{No}	Normal Force Aerodynamic Bias	
$C_{N\alpha}$	Normal Force due to α	per deg
$C_{N\delta E}$	Normal Force due to δ_E	per deg
$C_{N\delta LEF}$	Normal Force due to δ_{LEF}	per deg
$C_{N\delta TEF}$	Normal Force due to δ_{TEF}	per deg
$C_{N\delta SA}$	Normal Force due to δ_{SA}	per deg
C_{Nq}	Normal Force due to q	per rad
$C_{N\delta PV}$	Normal Force due to δ_{PV}	per deg
$C_{N\delta YV}$	Normal Force due to δ_{YV}	per deg
C_X	Longitudinal Force Coefficient	
C_Y	Lateral Force Coefficient	
C_{Yo}	Lateral Force Aerodynamic Bias	
$C_{Y\beta}$	Lateral Force due to β	per deg

C_{Yp}	Lateral Force due to p	per rad
C_{Yr}	Lateral Force due to r	per rad
$C_{Y\delta A}$	Lateral Force due to δ_A	per deg
$C_{Y\delta DHT}$	Lateral Force due to δ_{DHT}	per deg
$C_{Y\delta R}$	Lateral Force due to δ_R	per deg
$C_{Y\delta PV}$	Lateral Force due to δ_{PV}	per deg
$C_{Y\delta YV}$	Lateral Force due to δ_{YV}	per deg
C_Z	Vertical Force Coefficient	
DHT	Differential Horizontal Tail	
F	External Applied Force	N or lb
F_X,F_Y,F_Z	Components of External Force	N or lb
g	Gravitational Acceleration	m/sec^2 or ft/sec^2
GG	Measurement Noise Covariance	
H	Altitude	
h	Angular Momentum Vector	
I_x,I_y,I_z	Moments of Inertia	$kg\text{-}m^2$ or $slug\text{-}ft^2$
I_{xe}	Engine Moment of Inertia	$kg\text{-}m^2$ or $slug\text{-}ft^2$
I_{xy},I_{xz},I_{yz}	Cross Products of Inertia	$kg\text{-}m^2$ or $slug\text{-}ft^2$
J	Cost Function	
K_α,K_β	Upwash and Sidewash Factors	
LEF	Leading Edge Flap	
m	Mass	kg or slug

M	External Applied Moment	N-m or ft-lb
M_X, M_Y, M_Z	Components of External Moment	N-m or ft-lb
n	Measurement Noise	
n_t	Number of Time History Points	
n_z	Number of Response Variables	
N	Engine Speed	rad/sec
p	Roll Rate	rad/sec or deg/sec
P	Probability	
q	Pitch Rate	rad/sec or deg/sec
$\bar{q}$	Dynamic Pressure	N/m^2 or lb/ft^2
r	Yaw Rate	rad/sec or deg/sec
S	Reference area	m^2 or ft^2
SA	Symmetric Aileron	
t	Time Variable	
T	Thrust	N or lb
TEF	Trailing Edge Flap	
u,v,w	Velocity Components	m/sec or ft/sec
u	Input	
V	Velocity	m/sec or ft/sec
W	Response Weighting Matrix	
x	System State	
$x_\alpha, x_\beta, x_{ax}, x_{ay}, x_{an}$	Sensor Position x-axis	m or ft

$y_\alpha, y_\beta, y_{ax}, y_{ay}, y_{an}$	Sensor Position y-axis	m or ft
y	Modeled Response	
z	Measured Response	
$\tilde{z}$	Computed Response	
$z_\alpha, z_\beta, z_{ax}, z_{ay}, z_{an}$	Sensor Position z-axis	m or ft

GREEK

α	Angle of Attack	rad or deg
β	Angle of Sideslip	rad or deg
Δ	Sample Interval	sec
δ_A	Aileron Deflection	rad or deg
δ_{DHT}	Differential Horiz. Tail Def.	rad or deg
δ_E	Elevator Deflection	rad or deg
δ_{LEF}	Leading Edge Flaps Def.	rad or deg
δ_{SA}	Symmetric Ailerons Deflection	rad or deg
δ_{TEF}	Trailing Edge Flaps Def.	rad or deg
δ_{PV}	Pitch Vane Deflection	rad or deg
δ_R	Rudder Deflection	rad or deg
δ_{YV}	Yaw Vane Deflection	rad or deg
η	Measurement Noise	
θ	Pitch Attitude	rad or deg
ξ	Unknown Parameter Vector	

ϕ	Roll Attitude	rad or deg
ψ	Heading Angle	rad or deg
∇	Gradient	
ω	Angular Velocity	rad/sec or deg/sec

SUBSCRIPTS

a	Actual System
b	Bias
B	Body Axis
E	Earth Axis
K	Iteration Number
m	Modeled System
wind	Wind Axis
z	Observation

SUPERSCRIPTS

T	Transpose

ABBREVIATIONS

aoa	Angle of Attack
c.g.	Center of Gravity
HARV	High Alpha Research Vehicle
MMLE	Modified Maximum Likelihood Estimation
pEst	Parameter Estimation

PID	Parameter Identification

CHAPTER 1

INTRODUCTION

The National Aeronautics and Space Administration is currently involved in a High Alpha Technology Program which has the following objectives:

1. To provide flight validated prediction methods including experimental and computational methods that accurately simulate high angle of attack aerodynamics, flight dynamics, and flying qualities.
2. To improve aircraft agility at high angles of attack.

In undertaking this type of research, the airplane dynamics in the high alpha regimes must be understood. For this reason, part of the overall program for each test aircraft includes a parameter estimation analysis in which a complete set of stability and control parameters is extracted from flight data. Although a thorough basis of the vehicle aerodynamics is generated by analytic computations and wind tunnel tests performed during the design process, the true aerodynamic characteristics of the aircraft cannot be verified until flight test data has been analyzed. Primarily, the verification of the aircraft aerodynamics is accomplished by comparing the stability and control derivatives extracted from both wind tunnel tests and flight data. This comparison allows for validation of the prediction methods applied to the wind tunnel data and complete understanding of the vehicle aerodynamics. In addition, the results of the parameter estimation analysis are significant, for they not only compose an extensive data base of the vehicle aerodynamic qualities but are also used to update the stability and control data in flight simulators. This

is performed in order to ensure that the responses in the simulators are comparable to those experienced in flight.

The use of flight data to estimate the stability and control derivatives of aircraft has been implemented for many years. In the past, most flight testing was limited to conditions in which linear equations of motion would appropriately describe the dynamic model. Several computer programs were developed and used for this type of analysis. For these cases, the parameter estimation program *MMLE3* developed at Ames-Dryden in the early 1970's was widely used. MMLE was used for several parameter estimation analyses of many aircraft including the space shuttle throughout the 1970's and early 1980's. However, more recent research such as the high alpha research, is exploring flight regimes in which nonlinearities occur and need to be included in the dynamic model. Hence, the data analysis for these types of investigations is often performed with the more recently developed *pEst* estimation program. This software was also developed at NASA Dryden, and it is capable of supporting nonlinearities in the dynamic equations of motion.

The purpose of this report is to document the estimates of the stability and control parameters of one of the test airplanes involved in the high alpha program. The airplane under investigation is the NASA F/A-18 High Alpha Research Vehicle which has been equipped with a thrust vectoring system and an On Board Excitation System which induces independent control surface motions. The thrust vectoring system consists of axisymmetric nozzles and six post exit vanes that allow vectoring capability in both pitch and yaw. It is explained how the six vane deflections are combined to produce a single deflection value for either a pitch or yaw maneuver.

This document includes discussions of the aircraft equations of motion, parameter estimation process, design of the flight test maneuvers, and the formulation of the mathematical model. In addition, the results of the longitudinal and lateral derivative estimates at varying angles of attack are presented and compared to results from previous analyses.

1.1 LITERATURE REVIEW

This section presents a summary of some previous parameter estimation analyses. The various methods used and conclusions for each analysis are discussed.

In 1986 Richard Maine and Kenneth Iliff[1] examined the practical application of parameter estimation methodology to the problem of estimating aircraft stability and control derivatives from flight test data. In-depth discussions of all aspects of the parameter estimation process beginning with reasons why this type of analysis is performed were provided. Derivations of the aircraft equations of motion and methods in which the equations are modified to be used in the estimation process were also presented. The output error estimation technique was chosen as the focus for detailed examination. Topics such as the design of flight test maneuvers, flight safety considerations, pilot involvement, data acquisition and instrumentation systems were all extensively reviewed. The evaluation of the parameter estimation results were considered, and several suggestions to improve results were given.

A study of estimating the parameters of highly unstable aircraft was conducted by

Maine and Murray[2] in 1986. This investigation involved data from the highly unstable X-29 aircraft. It was concluded that problems exist in applying the output error method to such highly unstable aircraft. From the analysis, it was found that the more appropriate maximum likelihood estimator was the filter error method.

A parameter estimation analysis for the AD-1 Oblique Wing Research Airplane was conducted by Alex Sim and Robert Curry[3] in 1984. In this investigation, the *MMLE3* program was used to produce a complete set of both longitudinal and lateral-directional derivatives. The flight determined derivatives were compared to the predictions obtained from wind tunnel data. The results for the primary longitudinal derivatives were somewhat consistent. However, it was concluded that the discrepancies in the remaining derivatives were due to the poor quality of the time response data. This was due to the fact that the airplane was designed to be a low cost aircraft which implied that the instrumentation system was not of the best quality. Also, it was determined that the longitudinal response was heavily damped and significant aerolastic and nonlinear effects were present but not considered in the model used in *MMLE3*.

Pellicano, Krumenacker and Vanhoy[4] provided a technical overview of the procedures and analyses tools used to conduct a successful expansion of the flight envelope for the X-29 aircraft. The design of the flight test maneuvers used for the aerodynamic analysis and flight envelope clearance were discussed, and three different methods were used to update the aerodynamic database and extrapolate the results. These methods were:

1. A parameter identification program
2. An off-line closed loop simulation

3. A total aerodynamic coefficient matching method.

Specifically. the parameter estimation program *pEst* was utilized during the first expansion flights. The program was used primarily for analysis of yaw-roll doublets, lateral stick raps, and rudder pedal raps in order to obtain lateral-directional derivatives. However, it was concluded that the use of *pEst* in the longitudinal axis was impaired by the high static instability and the three-surface pitch control.

In 1989, Vladislav Klein, Kevin Breneman and Thomas Ratvasky[5] presented preliminary results of the aerodynamic parameters estimated from flight data of an advanced fighter aircraft. In this analysis, a summary of the aerodynamic parameters of the NASA F-18A High Alpha Research Vehicle and an assessment of the accuracy of the instrumentation system and parameter estimates were discussed. The parameters were estimated from transient maneuvers at different angles of attack varying from 8 to 54 degrees. A stepwise regression with the ordinary least squares technique was applied for the data analysis. Some of the conclusions suggested that insufficient excitation of the transient maneuvers resulted in large scatter of the estimated parameters. The resulting low accuracy of the parameters indicated that it was not possible to comment on their agreement with wind tunnel measurement and previous flight data.

A parameter identification study of the X-31 was performed in 1991 by Rohlf, Plaetschke, and Weib.[6] Selected results from both simulated and flight test data obtained by using a maximum likelihood method for parameter estimation in nonlinear systems were presented. In this investigation, the researchers had to implement a stabilization procedure to the Maximum Likelihood output error parameter estimation algorithm since the X-31A

aircraft is partially aerodynamically unstable. This was done in order to avoid divergence in the numerical integration. Essentially, the estimates from the flight test data compared well with the predicted values. However, the uncertainty of the values was due to the fact that flight test data was not particularly suited for aerodynamic parameter estimation.

Parameter estimation results of the F-18 stability and control derivatives were discussed in a NASA internal memo written by K. Iliff[7] in December of 1990. The parameter estimation program *pEst* was used to obtain the derivative estimates for the lateral-direction. It was explained how the estimation of stability and control derivatives at high angles of attack is always difficult due to the uncertainty of the aerodynamic mathematical model and the occurrences of uncommanded responses during the dynamic maneuvers. In general, the agreement between the flight determined derivatives and the predictions from the wind tunnel data was good considering all of the difficulties in obtaining derivative estimates from both the flight and wind tunnel data. It was concluded that many of the differences encountered in the estimates were due to the lack of independent control surface deflections.

In addition, Klein[8] estimated a complete set of stability and control derivatives for a low-wing, single engine, general aviation airplane using the equation error method and the maximum likelihood method. The mathematical model of the airplane was based on the equations of motion with linear aerodynamics. Klein utilized two standard-deviation confidence intervals obtained from repeated measurements as bounds for the comparison of the parameters determined by both methods. From the analysis, it was determined that the estimated parameters of both methods agreed within the two standard-deviation

confidence intervals for the parameter. Both estimation methods provided identical values for most of the longitudinal parameters; however, a significant difference in the derivative of the vertical force coefficient with respect to the angle of attack was found. The results showed that the maximum likelihood estimates agreed better with the computed parameters from steady flight data than with those from the equation error method. For the lateral directional derivatives, the mean values from both estimation methods agreed in general.

CHAPTER 2

AIRCRAFT STABILITY AND CONTROL

2.1: AIRCRAFT STABILITY AND CONTROL DEFINITION

The subject of aircraft stability and control involves controlling the attitude and flight path of an aircraft. The desired position of the aircraft is affected by either internally or externally generated disturbances. For instance, an internal disturbance could be the result of pilot interaction or an automatic flight control system. Some examples of these types of disturbances are changes in the airplane configuration, changes in center of gravity locations, or changes in the control surface deflections. All of these changes have an effect on the aerodynamic forces and moments on the vehicle.

External disturbances are caused by things such as turbulence, wind gusts, etc. Several factors are involved in maintaining total control of an aircraft, and many complex control systems are integrated to produce the desired result. However, in a parameter estimation process, the main concern lies with the response of the aircraft to certain control surface deflections. It is irrelevant how the surfaces are moved or what caused them to do so. The goal is to use the simplest model possible and estimate only the aerodynamic forces and moments.

2.2: AERODYNAMIC FORCE AND MOMENT REPRESENTATION

The force and moment contributions to an airplane are represented by stability and control coefficients. This method of representing the forces and moments by stability coefficients was first introduced by Bryan[9] over a half century ago. The technique proposed by Bryan assumes that the aerodynamic forces and moments can be expressed as a function of the instantaneous values of the perturbation variables. The perturbation variables are the instantaneous changes from the reference conditions of the translational velocities, angular velocities, control deflections, and their derivatives. With this assumption, the aerodynamic forces and moments can be expressed by means of a Taylor series expansion of the perturbation variables about the reference equilibrium condition. For example, the change in the force in the x direction can be expressed as follows:

$$\Delta X(u, w, \ldots, \delta_e) = \frac{\partial X}{\partial u}\Delta u + \frac{\partial X}{\partial w}\Delta w + \ldots \frac{\partial X}{\partial \delta_e}\Delta \delta_e + H.O.T. \qquad 2.1$$

The term $\partial X/\partial u$ is called the stability derivative and is evaluated at the reference flight condition. The contribution of the change in velocity u to the change ΔX in the X force is just $(\partial X/\partial u)\Delta u$. $\partial X/\partial u$ can also be expressed in terms of the stability coefficient as follows:

$$\frac{\partial X}{\partial u} = C_{x_u} \frac{1}{u_o}\bar{q}S \qquad 2.2$$

where

$$C_{x_u} = \frac{\partial C_x}{\partial(\frac{u}{u_o})} \qquad 2.3$$

and $\bar{q}$ is the dynamic pressure and S is the reference area. Note that the stability derivative has dimensions, whereas the stability coefficient is defined so that it is nondimensional.[10]

There are several theoretical methods which predict the values for the stability and control coefficients. A comprehensive collection of the aerodynamic stability and control prediction techniques is the *US Air Force Stability and Control DATCOM*,[11] which is widely used throughout the aviation industry. However, in this study, the stability and control derivatives for the NASA F/A-18 HARV are estimated from flight data.

CHAPTER 3

PARAMETER ESTIMATION

3.1: PURPOSE

Estimation of aircraft stability and control derivatives has several practical uses such as validating wind-tunnel or analytical predictions. A thorough basis of the vehicle aerodynamics is generated by these means such as the wind tunnel tests and analytical predictions, but some error may be involved. For instance, the results from the wind-tunnel tests are not expected to be truly accurate because it is practically impossible to simulate the exact flight conditions and Reynolds number. Also, differences in the vehicle configuration may be present. Therefore, it is beneficial to compare the results from both the wind tunnel tests and flight data in order to validate the prediction methods of the aircraft aerodynamics.

Another use of the derivative estimates is to update the current flight simulators. The simulators require a complete database of the vehicle's stability and control characteristics to appropriately represent the aircraft in flight.

3.2: TECHNIQUES

The number of parameter estimation computer programs has greatly increased since the first application performed with high-speed digital computers in 1968. However, the

MMLE3 (Modified Maximum Likelihood Estimation, Version 3)[12] developed at NASA Ames Dryden has been accepted as an industry standard for aircraft parameter estimation. *MMLE3* has two characteristics that somewhat limit its use in recent research:

1. It is designed for use solely in a batch processing environment.
2. The equations of motion defining the dynamic model used in the program are linear.

These characteristics do not pose serious limitations for many parameter estimation problems; however, recent flight test experience at NASA Dryden Flight Research Facility has indicated that the *MMLE3* program does not have the capabilities of handling the more modern parameter estimation problems. For instance, the newly developed test aircraft are being subjected to more extreme flight conditions where nonlinearities arise in the dynamic behavior of the aircraft. Such behavior cannot be appropriately modeled using the simple linear dynamic equations of motion. In addition, the new aircraft configurations are becoming more unique. This increases the complexity of the problem, in that it requires the analyst to interact more with the code. In response to these problems, another parameter estimation program, *pEst*, was designed by the researchers at NASA Dryden.

The *pEst* program is designed to be fully interactive; however, it can be run in a batch mode, and it supports full nonlinear capability in the dynamic equations of motion.[13] The form of the dynamic equations of motion for the aircraft system is assumed to be known. The unknowns are the values of the coefficients in these equations. The output of a parameter estimation process will therefore be an estimate of these unknown coefficients. Particularly, the aircraft system is flown and the dynamic responses following a given

maneuver are recorded, along with the input maneuver. The same input maneuver is given to an "a priori" model of the system. In the case of the Modified Maximum Likelihood Method, the likelihood cost function is maximized through the application of a particular method. This method is known as the Modified Newton-Raphson Method which provides new estimates of the unknown coefficients on the basis of the response error which is the difference between the actual and computed responses. The updated mathematical model (with the updated values of the unknown coefficients) is used to provide a new computed response, and therefore a new response error. The updating of the mathematical model continues iteratively until the response error satisfies some user-defined convergence criterion. Figure 3.1 illustrates the Maximum Likelihood Estimation Concept. More analytical details are given in the next section.

3.3: THE MAXIMUM LIKELIHOOD METHOD

The actual aircraft dynamic system can be described in the general state variable form:

$$\dot{x}_a(t) = f_a\,[x_a(t),\ u(t),\ \xi] \qquad 3.1$$

$$z(t_i) = g_a\,[x_a(t_i),\ u(t_i),\ \xi] + \eta_i \quad i=1,\ldots n_t \qquad 3.2$$

for given known initial conditions. The input vector, u, is assumed to be known as a function of time. The response vector, z from the on-board sensors, is measured at discrete time points, t_i. The variable η is the measurement noise and is assumed to be a sequence

of independent Gaussian vectors with zero mean and known covariance matrix. The objective is to estimate the unknown parameters in the vector ξ.

Similarly, a mathematical model for the aircraft system is given by

$$\dot{x}_m(t) = f_m\,[x_m(t),\ u(t),\ \xi(t)] \qquad 3.3$$

$$y(t_i) = g_m\,[x_m(t_i),\ u(t_i),\ \xi(t_i)] \quad i=1,\ldots n_t \qquad 3.4$$

for given initial conditions and initial estimates of the unknown parameters ξ, that is $\hat{\xi}(0)$.

As previously stated, independent initial estimates $\hat{\xi}(0)$ of the unknown coefficients are available from wind-tunnel analysis or theoretical methods. It is definitely desirable to use this "a priori" information so that all available information is used to help the convergence in the estimation process. When this feature is used, the Maximum Likelihood Method is known as the Modified Maximum Likelihood Method.

At this point, consider the following definitions:

$P(z/\xi)$ is the probability of having the response, z, for given values of the unknown vector ξ. $P(\xi)$ is the probability that the unknown vector ξ is a vector of "a priori" values of the unknown coefficients $\hat{\xi}(0)$ (values of the aerodynamic and control stability derivatives from wind tunnel and/or theoretical methods). Note that these two events are assumed to be independent.

Now assume that the errors (measurement noise vector and "a priori" values error vector) have a normal distribution. Therefore;

$$P(z/\xi) = \frac{1}{2\pi^{n_t \frac{n_z}{2}} \left(\frac{1}{W_1}\right)^{\frac{n_t}{2}}} e^{-\frac{1}{2}\left[\sum_{i=1}^{n_t} (z(t_i)-y(t_i))^T W_1 (z(t_i)-y(t_i))\right]} \quad 3.5$$

$$P(\xi) = \frac{1}{2\pi^{\frac{n_\xi}{2}} \left(\frac{1}{W_2}\right)^{\frac{1}{2}}} e^{-\frac{1}{2}\left[(\xi-\xi(0))^T W_2 (\xi-\xi(0))\right]} \quad 3.6$$

where n_z is the number of actual and computed responses, n_ξ is the number of coefficients to be estimated in ξ, n_t is the number of time history points, W_1 is a response weighting matrix (measurement noise covariance matrix) and W_2 is an "a priori" values weighting matrix.

Next, the assumption of independence implies that

$$P(z) = P(z/\xi) \cdot P(\xi) \quad 3.7$$

thus,

$$P(z) = \frac{1}{2\pi^{\left[n_t \frac{n_z}{2} + \frac{n_\xi}{2}\right]} \left(\frac{1}{W_1}\right)^{\frac{n_t}{2}} \left(\frac{1}{W_2}\right)^{\frac{1}{2}}} \cdot \quad 3.8$$
$$\cdot e^{-\frac{1}{2}\left[\sum_{i=1}^{n_t} (z(t_i)-y(t_i))^T W_1 (z(t_i)-y(t_i)) + (\xi-\xi(0))^T W_2 (\xi-\xi(0))\right]}$$

Hence, the parameter that must be minimized with respect to the vector of unknown coefficients ξ, is the likelihood cost functional which is given by

$$J(\xi) = \sum_{i=1}^{n_t} (z(t_i)-y(t_i))^T W_1 (z(t_i)-y(t_i)) + (\xi-\xi(0))^T W_2 (\xi-\xi(0)) \quad 3.9$$

The next computational step is to calculate the vector $\hat{\xi}$ such that $J(\xi)$ is minimized.

Therefore:

$$\xi^T = ARG \min \sum_{i=1}^{n_t} [(z(t_i) - y(t_i))^T W_1 (z(t_i) - y(t_i)) + (\xi - \xi(0))^T W_2 (\xi - \xi(0))] \qquad 3.10$$

This task is accomplished by using the Modified Newton-Raphson Algorithm to solve the associated system of non-linear equations.

Such algorithm is an iterative method for finding the zero of a non-linear function of several parameters. In this problem, the algorithm calculates the zero of the cost functional gradient with respect to the unknown parameters forming the vector ξ.

Now consider the terms of a discrete Taylor series development. At the k-th iteration:

$$(\nabla_\xi J)_{K+1} = (\nabla_\xi J)_K + (\nabla_\xi^2 J)\, \Delta\hat{\xi}_K \qquad 3.11$$

where

$$\Delta\hat{\xi}_k = \hat{\xi}_{k+1} - \hat{\xi}_k \qquad 3.12$$

and $\nabla_\xi J$ and $\nabla^2_\xi J$ are the first and second gradients of J with respect to ξ at the k-th iteration and are calculated as follows:

$$(\nabla_\xi J)_K = 2\left[\sum_{i=1}^{n_t} (z(t_i) - y(t_i))^T W_1 [\nabla_\xi (z(t_i) - y(t_i))]\right]^T + 2W_2 (\xi - \xi(0)) \qquad 3.13$$

$$(\nabla_\xi^2 J)_K = 2\left[\sum_{i=1}^{n_t} [\nabla_\xi (z(t_i) - y(t_i))]^T W_1 [\nabla_\xi (z(t_i) - y(t_i))]\right] + 2W_2 \qquad 3.14$$

The geometric meaning of the Modified Newton-Raphson Method is shown in Figure 3.2.

Note that the iterative process converges when $\hat{\xi}_{K+1} = \hat{\xi}$ implying that $\Delta\hat{\xi}_K = 0$. A qualitative trend of J with the number of iterations (k) is shown in Figure 3.3. Usually a limited number of iterations (5-10) are required to obtain convergence. More analytical details on the Maximum Likelihood Method are given in References [1] and [12].

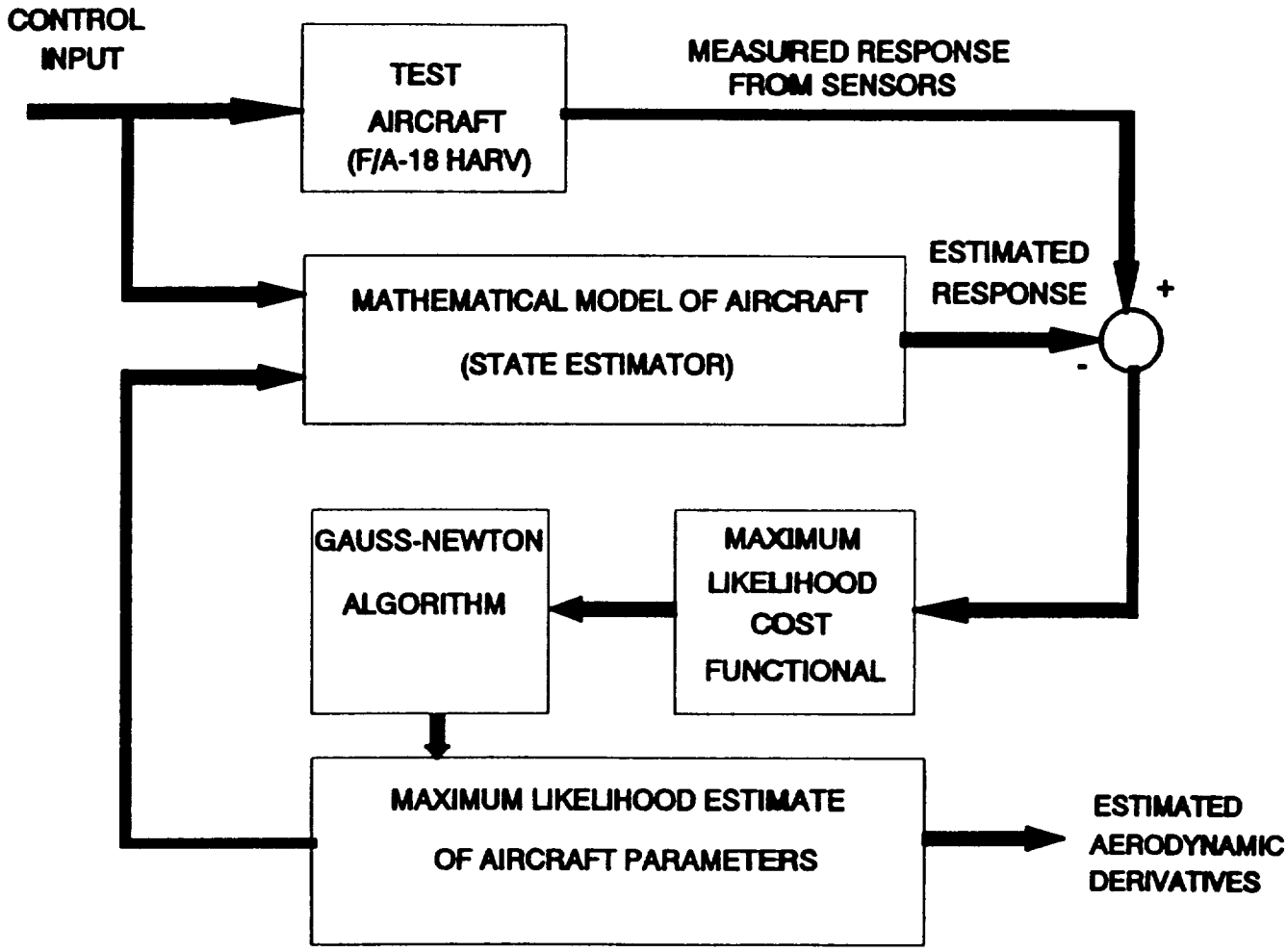

Figure 3.1: The Parameter Estimation Process

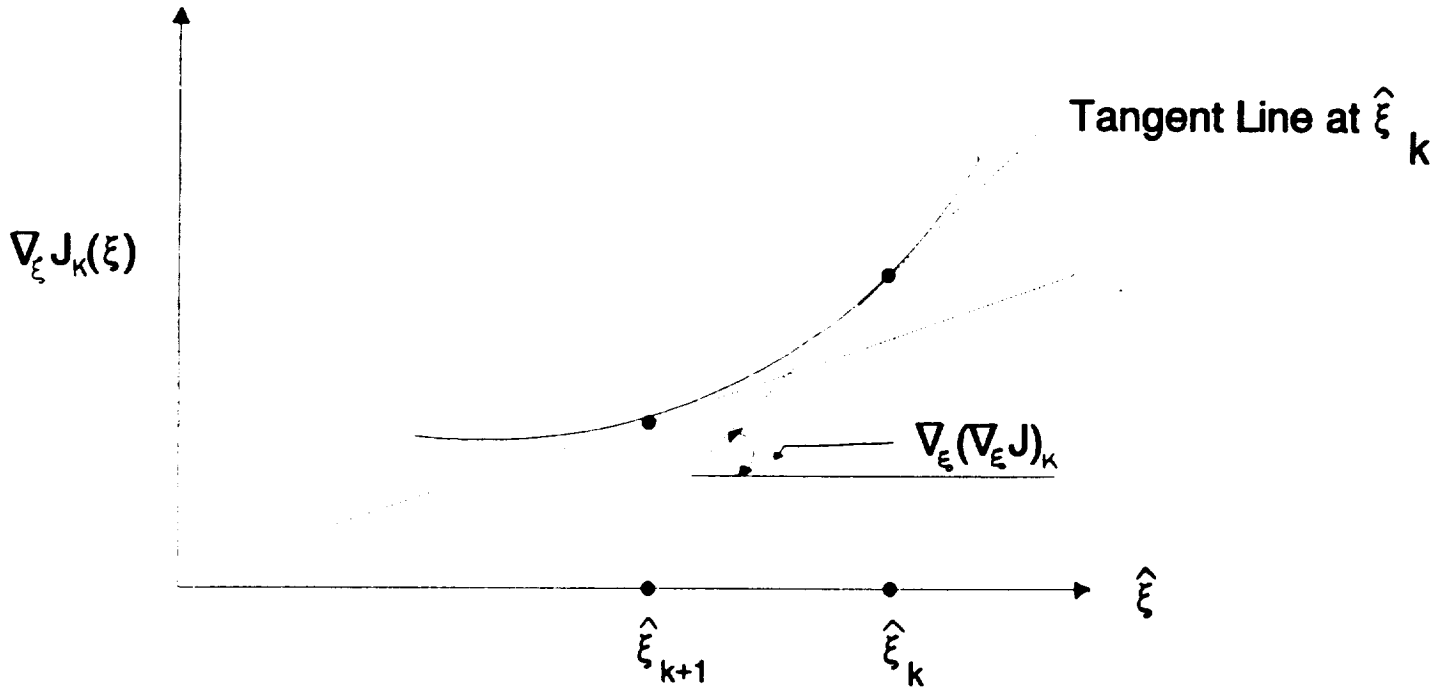

Figure 3.2: Geometric Meaning of the Modified Newton-Raphson Method

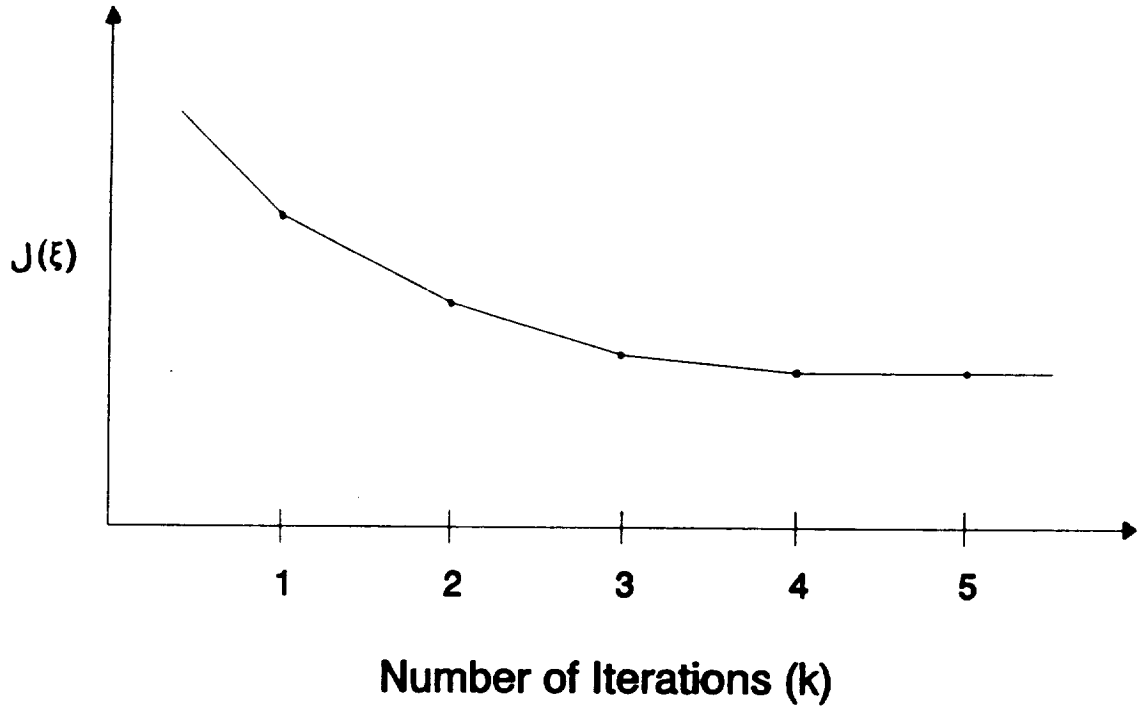

Figure 3.3: A Qualitative Trend of J with the Number of Iterations, K

CHAPTER 4

AIRCRAFT EQUATIONS OF MOTION

This chapter consists of the derivation of the aircraft equations of motion which serve as a basis for any aircraft stability and control analysis.

4.1: NEWTONIAN MECHANICS

The basic equations for linear and angular momentum in a nonrotating inertial axis system fixed relative to the air will be the beginning of the derivation:

$$\bar{F} = \frac{d}{dt}(m\bar{V}) \qquad 4.1$$

$$\bar{M} = \frac{d}{dt}(\bar{h}) \qquad 4.2$$

where $\bar{F}$ is the external applied force, $\bar{V}$ is the velocity vector, $\bar{M}$ is the external applied moment, and $\bar{h}$ is the angular momentum vector. Both the external applied moment and the angular momentum vector are about the center of gravity. Since most of the quantities of interest are referenced to the aircraft geometric body axis, the above equations must be transformed to this coordinate system which is fixed to and rotates with the aircraft. The rotating aircraft body axis system is shown in Figure 4.1. The transformation of the above equations give

$$\bar{F} = \frac{\partial}{\partial t}(m\bar{V}) + \bar{\omega} \times (m\bar{V}) \qquad 4.3$$

$$\bar{M} = \frac{\partial}{\partial t}(\bar{h}) + \bar{\omega} \times (\bar{h}) \qquad 4.4$$

where the angular momentum ($\bar{h}$) is given by:

$$\bar{h} = \begin{bmatrix} I_x & -I_{xy} & -I_{xz} \\ -I_{xy} & I_y & -I_{yz} \\ -I_{xz} & -I_{yz} & I_z \end{bmatrix} \bar{\omega} \qquad 4.5$$

where $\bar{\omega}$ is the angular velocity vector, and the $\partial/\partial t$ operator symbolizes the vector of partial derivatives of the vector components. The components of the angular velocity ($\bar{\omega}$) in the body-axis system are roll rate (p), pitch rate (q), and yaw rate (r), and the components of the velocity vector ($\bar{V}$) are u, v, and w. Substituting the components of $\bar{V}$, $\bar{\omega}$, and $\bar{h}$ into equation 4.3 and 4.4 gives scalar forms of the equations for the external applied forces and moments (F_x, F_y, F_z, M_x, M_y, and M_z)

$$F_x = m(\dot{u} + qw - rv) \qquad 4.6$$

$$F_y = m(\dot{v} + ru - pw) \qquad 4.7$$

$$F_z = m(\dot{w} + pv - qu) \qquad 4.8$$

$$M_x = \dot{p}I_x - \dot{q}I_{xy} - \dot{r}I_{xz} + qr(I_z - I_y) + (r^2 - q^2)I_{yz} - pqI_{xz} + rpI_{xy} \qquad 4.9$$

$$M_y = -\dot{p}I_{xy} + \dot{q}I_y - \dot{r}I_{yz} + rp(I_x - I_z) + (p^2 - r^2)I_{xz} - qrI_{xy} + pqI_{yz} \qquad 4.10$$

$$M_z = -\dot{p}I_{xz} - \dot{q}I_{yz} + \dot{r}I_z + pq(I_y - I_x) + (q^2 - p^2)I_{xy} - rpI_{yz} + qrI_{xz} \quad 4.11$$

4.2: APPLIED FORCES

Now consider the sources of the external forces and moments beginning with the three components of the applied forces: the aerodynamic, gravity, and thrust components.[1] The aerodynamic forces in terms of the nondimensional force coefficients (C_X, C_Y, and C_Z) in the X, Y, and Z axes are

$$F_{X_{aero}} = \bar{q}SC_X \quad 4.12$$

$$F_{Y_{aero}} = \bar{q}SC_Y \quad 4.13$$

$$F_{Z_{aero}} = \bar{q}SC_Z \quad 4.14$$

where $\bar{q}$ is the dynamic pressure and S is the reference area.

Gravity is considered to exert a force mg along the earth Z axis. However, the components given here are referenced to the body axis. Therefore, a transformation of axes is necessary. This transformation is performed with the use of the Euler angles (θ,ϕ,ψ) which will be discussed later in this chapter. The gravitational force components are as follows:

$$F_{X_{grav}} = -mg \sin\theta \quad 4.15$$

$$F_{Y_{grav}} = mg \sin\phi \cos\theta \quad 4.16$$

$$F_{Z_{grav}} = mg\cos\phi\cos\theta \qquad 4.17$$

The third force component is the engine thrust T which is assumed to only act along the body X axis:

$$F_{X_{thrust}} = T \qquad 4.18$$

Thus, combining all components the total applied forces can be written as

$$F = F_{aero} + F_{grav} + F_{thrust} \qquad 4.19$$

and

$$F_X = \bar{q}SC_X - mg\sin\theta + T \qquad 4.20$$

$$F_Y = \bar{q}SC_Y + mg\sin\phi\cos\theta \qquad 4.21$$

$$F_Z = \bar{q}SC_Z + mg\cos\phi\cos\theta \qquad 4.22$$

4.3: APPLIED MOMENTS

Only two components of the applied moment are examined, the aerodynamic and gyroscopic moment. The aerodynamic components are

$$M_{X_{aero}} = \bar{q}SbC_l \qquad 4.23$$

$$M_{Y_{aero}} = \bar{q}ScC_m \qquad 4.24$$

$$M_{Z_{aero}} = \bar{q}SbC_n \qquad 4.25$$

where *b* and *c* are the reference span and chord, and C_l, C_m, C_n are the nondimensional coefficients of rolling moment, pitching moment, and yawing moment.

The other component of the applied moment is the component caused by the gyroscopic effects of the rotating machinery in the engine. Assuming that the engine is oriented along the X axis, the gyroscopic effects contribute to moments along the Y and Z axes:

$$M_{Y_{gyro}} = rNI_{xe} \qquad 4.26$$

$$M_{Z_{gyro}} = -qNI_{xe} \qquad 4.27$$

where *N* is the engine speed in radians per second, and I_{xe} is the moment of inertia of the rotating mass.

The total applied moment can be written as

$$M = M_{aero} + M_{gyro} \qquad 4.28$$

and

$$M_X = \bar{q}SbC_l \qquad 4.29$$

$$M_Y = \bar{q}ScC_m + rNI_{xz} \qquad 4.30$$

$$M_Z = \bar{q}SbC_n - qNI_{xz} \qquad 4.31$$

4.4: EULER ANGLES

In the equations for the external forces, it was noted that the forces are functions of the Euler angles. Therefore, it is necessary to define the angles and present their respective equations.

To describe the orientation of the airplane relative to the earth, it is necessary to describe the orientation of the body-fixed coordinate system XYZ relative to the earth-fixed coordinate system X'Y'Z'. To accomplish this, consider system X'Y'Z' translated parallel to itself until its origin coincides with the center of mass P of the airplane. See Figure 4.2, where this translated system X'Y'Z' has been renamed $X_1Y_1Z_1$.

It is conventional to describe the relative orientation of XYZ to $X_1Y_1Z_1$ by means of three consecutive rotations. Emphasis is placed on "consecutive" because the order of which these rotations are carried out is important because rotations cannot be considered as vectors.

The following rotations are applied:

1. Coordinate system $X_1Y_1Z_1$ is rotated about the Z_1-axis over an angle ψ, positive

as indicated in Figure 4.2. This yields coordinate system $X_2Y_2Z_2$. The angle ψ is referred to as the heading (or yaw) angle.

2. Coordinate system $X_2Y_2Z_2$ is rotated about the Y_2-axis over an angle θ, positive as indicated in Figure 4.2. This yields coordinate system $X_3Y_3Z_3$. The angle θ is referred to as the attitude (or pitch) angle.

3. Coordinate system $X_3Y_3Z_3$ is rotated about the X_3-axis over an angle ϕ, positive as indicated in Figure 4.2. This yields coordinate system XYZ. The angle ϕ is referred to as the bank (or roll) angle.[14]

With these transformation angles it is now possible to describe the way in which the flight path of an airplane with respect to the earth-fixed system can be determined from the knowledge of the body-fixed velocity components u, v, and w. These components are functions of the wind relative velocity, V, the angle of attack, α, and angle of sideslip, β which can be found from

$$V = \sqrt{u^2 + v^2 + w^2} \qquad 4.32$$

$$\alpha = \tan^{-1}\frac{w}{u} \qquad 4.33$$

$$\beta = \sin^{-1}\frac{v}{V} \qquad 4.34$$

Substituting and inverting the above equations gives

$$u = V\cos\alpha\cos\beta \tag{4.35}$$

$$v = V\sin\beta \tag{4.36}$$

$$w = V\sin\alpha\cos\beta \tag{4.37}$$

As a result, the expression for obtaining the flight path of an aircraft is

$$\begin{bmatrix} u_B \\ v_B \\ w_B \end{bmatrix} = \begin{bmatrix} 1 & 0 & 0 \\ 0 & \cos\phi & \sin\phi \\ 0 & -\sin\phi & \cos\phi \end{bmatrix} \begin{bmatrix} \cos\theta & 0 & -\sin\theta \\ 0 & 1 & 0 \\ \sin\theta & 0 & \cos\theta \end{bmatrix} \begin{bmatrix} \cos\psi & \sin\psi & 0 \\ -\sin\psi & \cos\psi & 0 \\ 0 & 0 & 1 \end{bmatrix} \begin{bmatrix} u_E \\ v_E \\ w_E \end{bmatrix} \tag{4.38}$$

This equation is found by means of orthogonal transformations and can be reversed to give the earth-fixed components in terms of the body-fixed components by multiplying the rotation matrices and taking the inverse.

It is now important to find a relationship between the time derivatives of the euler angles and the rotational velocity components. Assuming a flat, nonrotating earth, the total angular velocity can be expressed as the sum of the time derivatives of the Euler angles (ψ,θ,ϕ) components. Transforming all of the components into the body-axis coordinate system with the use of equation 4.38 and equating the sum to the body-axis components of the angular velocity gives

$$\begin{bmatrix} p \\ q \\ r \end{bmatrix} = \begin{bmatrix} 1 & 0 & -\sin\theta \\ 0 & \cos\phi & \sin\phi\cos\theta \\ 0 & -\sin\phi & \cos\phi\cos\theta \end{bmatrix} \begin{bmatrix} \dot{\phi} \\ \dot{\theta} \\ \dot{\psi} \end{bmatrix} \tag{4.39}$$

with the inverse being

$$\dot{\phi} = p + q\tan\theta\sin\phi + r\tan\theta\cos\phi \tag{4.40}$$

$$\dot{\theta} = q\cos\phi - r\sin\phi \qquad 4.41$$

$$\dot{\psi} = r\cos\phi\sec\theta + q\sin\phi\sec\theta \qquad 4.42$$

4.5: VELOCITY COMPONENTS (POLAR FORM)

Since it is possible to measure flow angles that are closely related to angle of attack, α and sideslip angle, β, it is more convenient to have the velocity equations in terms of α, β, and V rather than the spherical components u, v, and w.[1]

In order to derive the α, β, and V equations, equations 4.32-4.34 must first be differentiated as follows:

$$\dot{V} = \frac{1}{V}(u\dot{u} + v\dot{v} + w\dot{w}) \qquad 4.43$$

$$\dot{\alpha} = \frac{u\dot{w} - w\dot{u}}{u^2 + w^2} \qquad 4.44$$

$$\dot{\beta} = \frac{(u^2 + w^2)\dot{v} - vw\dot{w} - vu\dot{u}}{V^2\sqrt{(u^2 + w^2)}} \qquad 4.45$$

Substituting for $\dot{u}$, $\dot{v}$, and $\dot{w}$ from equations 4.6-4.8 and for u, v, and w from equations 4.35-4.37 gives

$$\dot{V} = \frac{F_X}{m}\cos\alpha\cos\beta + \frac{F_Y}{m}\sin\beta + \frac{F_Z}{m}\sin\alpha\cos\beta \qquad 4.46$$

$$\dot{\alpha} = \frac{1}{mV\cos\beta}(F_Z\cos\alpha - F_X\sin\alpha) + q - \tan\beta(p\cos\alpha + r\sin\alpha) \qquad 4.47$$

$$\dot{\beta} = \frac{\cos\beta}{mV}F_Y + p\sin\alpha - r\cos\alpha - \frac{\sin\beta}{mV}(F_Z\sin\alpha + F_X\cos\alpha) \qquad 4.48$$

Then substituting for F_X, F_Y, and F_Z from equations 4.20-4.22 gives

$$\dot{V} = -\frac{\bar{q}S}{m}C_{D_{wind}} + g(\cos\phi\cos\theta\sin\alpha\cos\beta + \sin\phi\cos\theta\sin\beta) + g(-\sin\theta\cos\alpha\cos\beta) + \frac{T}{m}\cos\alpha\cos\beta \qquad 4.49$$

$$\dot{\alpha} = -\frac{\bar{q}S}{mV\cos\beta}C_L + q - \tan\beta(p\cos\alpha + r\sin\alpha) + \frac{g}{V\cos\beta}(\cos\phi\cos\theta\cos\alpha + \sin\theta\sin\alpha) - \frac{T\sin\alpha}{mV\cos\beta} \qquad 4.50$$

$$\dot{\beta} = \frac{\bar{q}S}{mV}C_{Y_{wind}} + p\sin\alpha - r\cos\alpha + \frac{g}{V}\cos\beta\sin\phi\cos\theta + \frac{\sin\beta}{V}(g\cos\alpha\sin\theta - g\sin\alpha\cos\phi\cos\theta + \frac{T}{m}\cos\alpha) \qquad 4.51$$

where

$$C_{D_{wind}} = C_D\cos\beta - C_Y\sin\beta \qquad 4.52$$

$$C_{Y_{wind}} = C_Y\cos\beta + C_D\sin\beta \qquad 4.53$$

and

$$C_L = -C_Z\cos\alpha + C_X\sin\alpha \qquad 4.54$$

$$C_D = -C_X\cos\alpha - C_Z\sin\alpha \qquad 4.55$$

4.6: SIX-DEGREE-OF-FREEDOM EQUATIONS OF MOTION

The following is the full set of the nine coupled nonlinear differential equations of motion which describe the motion of an aircraft.

$$\dot{V} = -\frac{\bar{q}S}{m}C_{D_{wind}} + g(\cos\phi\cos\theta\sin\alpha\cos\beta + \sin\phi\cos\theta\sin\beta) + g(-\sin\theta\cos\alpha\cos\beta) + \frac{T}{m}\cos\alpha\cos\beta \qquad 4.56$$

$$\dot{\alpha} = -\frac{\bar{q}S}{mV\cos\beta}C_L + q - \tan\beta(p\cos\alpha + r\sin\alpha) + \frac{g}{V\cos\beta}(\cos\phi\cos\theta\cos\alpha + \sin\theta\sin\alpha) - \frac{T\sin\alpha}{mV\cos\beta} \qquad 4.57$$

$$\dot{\beta} = \frac{\bar{q}S}{mV}C_{Y_{wind}} + p\sin\alpha - r\cos\alpha + \frac{g}{V}\cos\beta\sin\phi\cos\theta + \frac{\sin\beta}{V}(g\cos\alpha\sin\theta - g\sin\alpha\cos\phi\cos\theta + \frac{T}{m}\cos\alpha) \qquad 4.58$$

Combining equations 4.9-4.11 and equations 4.29-4.31 gives

$$\dot{p}I_x - \dot{q}I_{xy} - \dot{r}I_{xz} = \bar{q}SbC_l + qr(I_y - I_z) + (q^2 - r^2)I_{yz} + pqI_{xz} - rpI_{xy} \quad 4.59$$

$$-\dot{p}I_{xy} + \dot{q}I_y - \dot{r}I_{yz} = \bar{q}ScC_m + rp(I_z - I_x) + (r^2 - p^2)I_{xz} + qrI_{xy} - pqI_{yz} + rNI_{xe} \quad 4.60$$

$$-\dot{p}I_{xz} - \dot{q}I_{yz} + \dot{r}I_z = \bar{q}SbC_n + pq(I_x - I_y) + (p^2 - q^2)I_{xy} + rpI_{yz} - qrI_{xz} - qNI_{xe} \quad 4.61$$

$$\dot{\phi} = p + q\tan\theta\sin\phi + r\tan\theta\cos\phi \quad 4.62$$

$$\dot{\theta} = q\cos\phi - r\sin\phi \quad 4.63$$

$$\dot{\psi} = r\cos\phi\sec\theta + q\sin\phi\sec\theta \quad 4.64$$

4.7: OBSERVATION EQUATIONS

This section is a brief overview of the observation equations corresponding to the measurable aircraft response variables: α, β, V, p, q, r, ψ, θ, ϕ, a_n, a_x, a_y, p, q, r^1. The observation equations are

$$\alpha_z = K_\alpha\left(\alpha - \frac{x_\alpha}{V}q + \frac{y_\alpha}{V}p\right) + \alpha_b \quad 4.65$$

$$\beta_z = K_\beta\left(\beta - \frac{z_\beta}{V}p + \frac{x_\beta}{V}r\right) + \beta_b \quad 4.66$$

$$p_z = p + p_b \tag{4.67}$$

$$q_z = q + q_b \tag{4.68}$$

$$r_z = r + r_b \tag{4.69}$$

$$\Psi_z = \Psi + \Psi_b \tag{4.70}$$

$$\theta_z = \theta + \theta_b \tag{4.71}$$

$$\phi_z = \phi + \phi_b \tag{4.72}$$

$$a_n = \frac{\bar{q}S}{mg} C_N + \frac{x_{a_n}}{g}\dot{q} + \frac{z_{a_n}}{g}(q^2 + p^2) - \frac{y_{a_n}}{g}\dot{p} + a_{n_b} \tag{4.73}$$

$$a_x = -\frac{\bar{q}S}{mg} C_A + \frac{z_{a_x}}{g}\dot{q} - \frac{x_{a_x}}{g}(q^2 + r^2) - \frac{y_{a_x}}{g}\dot{r} + \frac{T}{mg} + a_{x_b} \tag{4.74}$$

$$a_y = \frac{\bar{q}S}{mg} C_Y - \frac{z_{a_y}}{g}\dot{p} + \frac{x_{a_y}}{g}\dot{r} - \frac{y_{a_y}}{g}(p^2 + r^2) + a_{y_b} \tag{4.75}$$

$$\dot{p}_z = \dot{p} + \dot{p}_b \tag{4.76}$$

$$\dot{q}_z = \dot{q} + \dot{q}_b \tag{4.77}$$

$$\dot{r}_z = \dot{r} + \dot{r}_b \tag{4.78}$$

where the parameters x, y, and z with the subscripts α, β, a_n, a_x, and a_y are the positions of the instruments relative to the center of gravity, the variables with the subscript b are biases,

and K_α and K_β are upwash factors for the angle of attack and sideslip.

The above equations are for arbitrary instrument positions. It should be noted that for a rigid aircraft, the sensed flow angles and linear accelerations vary with sensor positions, but the sensed angular accelerations, rates, and attitudes do not vary with sensor positions.

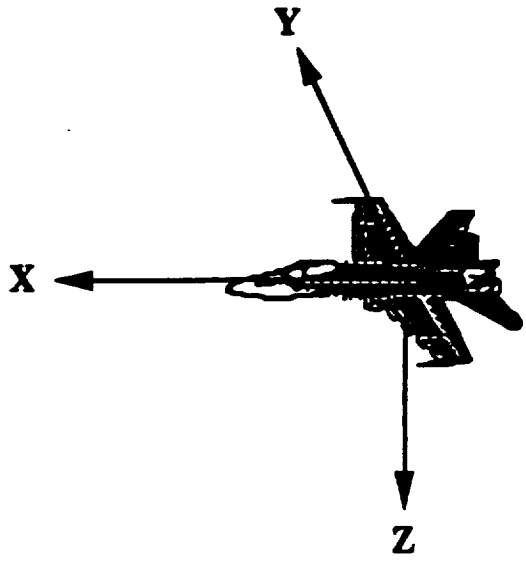

Figure 4.1: Body Axis System

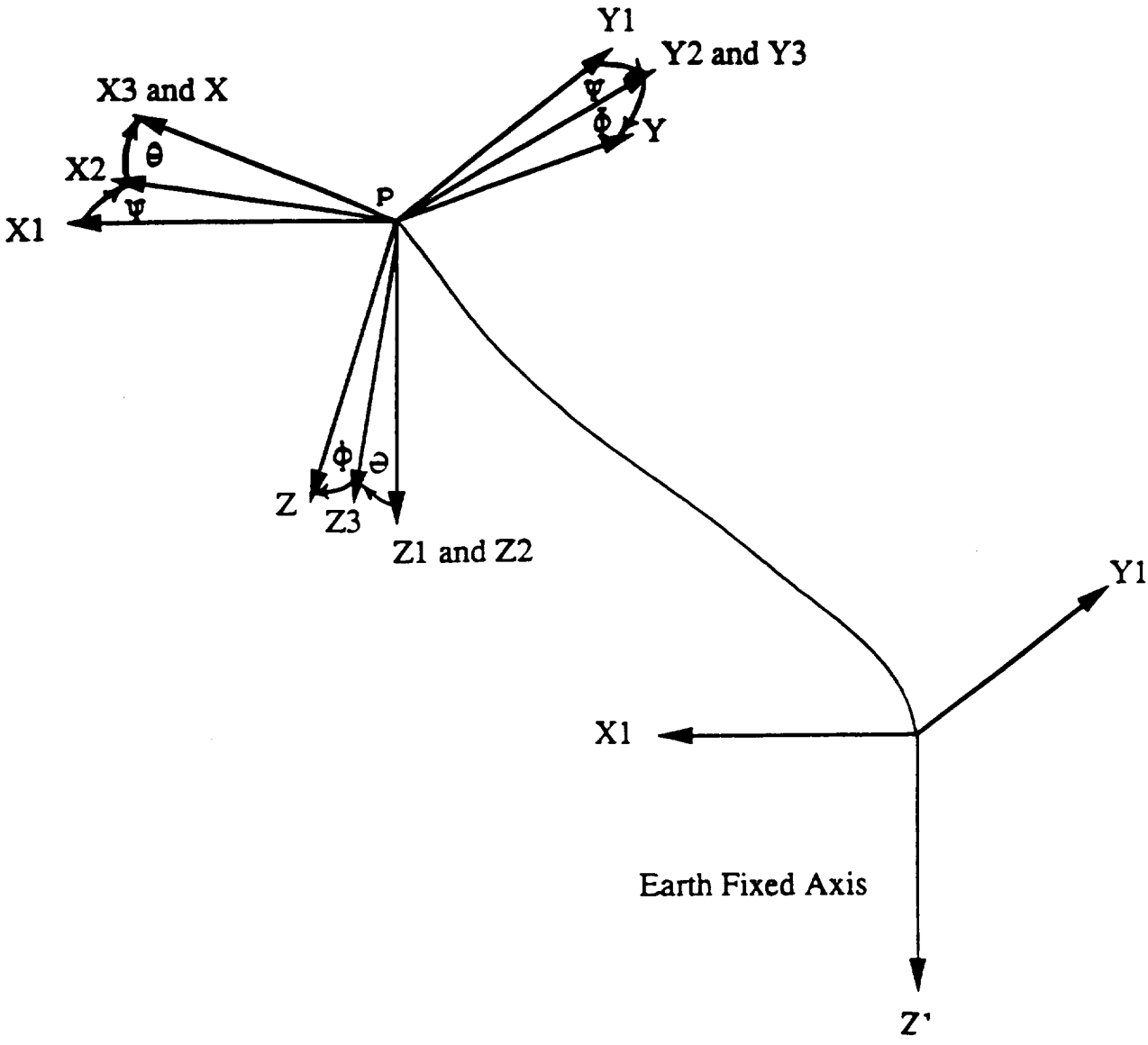

Figure 4.2: Representation of Euler Angles

CHAPTER 5

HIGH ALPHA RESEARCH

5.1: PURPOSE OF THE NASA HIGH ALPHA TECHNOLOGY PROGRAM - (HATP)

The history of air combat has indicated the need of having fighter airplanes with safe, predictable, and usable high-angle-of-attack capabilities. The demand for this increase in agility has been due to the advancements in today's highly lethal point and shoot air-to-air missiles. In a modern combat situation, the ability to rapidly obtain the first shot at the enemy in an engagement may determine the difference between a kill or a failure.

It has been shown through training and combat experience that a fighter's safety and maneuverability are related to its high angle-of-attack characteristics (also known as stall). Pilots who seek to have maximum turning performance and agility will push the aircraft to its maximum controllable angles of attack in order to obtain more lift, make tighter turns, or point at their enemy in the shortest amount of time. Airplanes that have good stability and control characteristics in this separated flow regime will typically outperform those with deficiencies.[15] Thus, the need for an improvement of the performances for a modern military aircraft motivated a research effort in the high alpha technology area.

In the past, high alpha capability was not a design goal: high alpha conditions were regarded as being extremely hazardous and to be avoided. However, as the United States advanced fighter aircraft such as the F-14 and F-15 evolved, their stall characteristics improved. The high alpha design methods were poor, but the experimental prediction

methods such as wind tunnel tests performed during the airplane development provided a sufficient database of the stall/spin characteristics.

On the other hand, more recent fighters such as the F-16 and F-18 were designed to accommodate the goal of achieving high-sustained performance and good stall characteristics. The new designs were based on aerodynamic principles that included vortex lift and automatically scheduled wing flaps. Unfortunately, prediction methods of the aircraft aerodynamics at high alpha for these aircraft were not as valid as those for the previous aircraft. In fact, many discrepancies evolved in the region of maximum lift and beyond (35 - 60 degrees alpha).[16,17] These problems have been thoroughly investigated, but not quite understood. Therefore, it was obvious that further research was needed to produce a better understanding of the experimental methods for high alpha aerodynamics.

NASA's first major effort in high alpha technology started in the mid 1970's. It was a joint effort with the Navy to develop and validate in flight a high alpha control system for the F-14. The outcome of the program was a set of control laws that significantly improved the high alpha maneuverability and spin resistance of the F-14.[18] The success of this program and the shortcomings of the available prediction methods and technology of today's fighter aircraft prompted NASA to formulate the High Alpha Technology Program (HATP).

The HATP began in the mid 1980's with objectives to provide flight-validated prediction/analysis methodology including experimental and computational methods that accurately simulate high-angle-of-attack aerodynamics, flight dynamics, and flying qualities, and to improve agility at high angles of attack and expand the usable high alpha envelope.[15]

Currently, many programs are dedicated to high alpha research. For instance, the

DARPA Enhanced Fighter Maneuverability Program is using two X-31 aircraft to demonstrate the tactical utility of post stall maneuverability with pilots in the loop. Also, the USAF/NASA/DARPA X-29 Program has shown impressive controllability in the stall regime with its forward swept wing and canard configuration. In addition, the USAF F-15 STOL (Short Takeoff and Landing) and Maneuver Technology Demonstrator (S/MTD) is currently using a thrust-vectoring/reversal nozzle highly integrated with the flight control system to show performance gains in takeoff and landing from short runways. Another essential element in the HATP is the High Alpha Research Vehicle (HARV) which is the testbed aircraft for this investigation.

5.2: HIGH ALPHA RESEARCH VEHICLE (HARV) DESCRIPTION

The F-18 HARV (Figure 5.1) is a full-scale development two engine, single seat, fighter/attack airplane built for the U.S. Navy by the McDonnell Douglas Corp. It is powered by two modified General Electric F404-GE-400 afterburning turbofan engines each rated at approximately 16000 lbs. static sea level thrust. The HARV features a midwing configuration with a wing-root leading edge extension. It is highly instrumented for research purposes; the wingtip launching rails and missiles were replaced with specially designed camera pods and airdata sensors. In addition, a pilot-actuated spin chute is onboard in case an uncontrolled spin is entered. It is equipped with five pairs of aerodynamic control surfaces. These include the ailerons, rudders, stabilators, leading-edge flaps, and trailing-edge flaps. The twin vertical stabilizers with trailing edge rudders are canted

outboard at approximately 20° from the vertical. All surfaces except the rudders are capable of moving symmetrically and differentially. A summary of the physical characteristics of the HARV is shown in Table 5.1.

The aircraft was modified by adding a thrust vectoring control system (TVCS) which consists of axisymmetric nozzles and post exit vanes that enable vectoring in both pitch and yaw. Three vanes are positioned about the periphery of each engine nozzle as shown in Figure 5.2. The divergent nozzle and external flaps of the engines were removed to accommodate the vanes which are stowed well out of the exhaust plume. The convergent part of the nozzles remains on the aircraft. During vectoring maneuvers a maximum of two vanes on any engine will be commanded in contact with the flow to help alleviate thermal constraints.[19]

The vanes are commanded by the Research Flight Control System (RFCS). This is another important feature in the modification of the HARV. The RFCS is located in parallel with the primary flight control computer (701E) and communicates with the primary system via dual port ram to receive air data and pilot inputs and to send commands to the airplane control surface actuators. This architecture allows the operation of the RFCS as a non-flight critical system to explore new, innovative flight control laws while using the 701E for primary flight safety.

A subset to the RFCS is the On Board Excitation System (OBES). This system was specially designed to accommodate the needs of parameter estimation. The main purpose for the OBES is to implement single surface excitations. With this system, it is capable of programming maneuvers in which the control surfaces move independently. This capability

is of extreme importance to this investigation and is believed to improve the parameter estimation at higher angles of attack.

5.3: INSTRUMENTATION AND AIRDATA SYSTEMS

Standard aircraft are equipped with instruments that measure control surface positions, linear accelerations, angular rates etc. as well as certain airdata parameters such as angle of attack, angle of sideslip, pressures etc. However, the F-18 aircraft production airdata system was not designed to perform well at high angles of attack. Therefore, new sensors and analysis techniques had to be implemented to the HARV's instrumentation and airdata systems in order to obtain the necessary accuracy in the measurements at high angle of attack flight.

As stated previously, the wingtip missile rails were removed and replaced with special camera pods also used to mount wingtip airdata booms. These booms served as the base for the NACA angle of attack and angle of sideslip flow direction vanes and the specially designed swivel probe that is capable of self-aligning itself with the local flow. The presence of the booms and the aircraft corrupt the static pressure measurements consequently affecting Mach number. This is commonly referred to as static pressure position error and must be determined for all flight conditions. In addition, a correction is also needed for the measurements of angle of attack and angle of sideslip. This is required to take into account the upwash induced by the aircraft. The procedure for these corrections are complex and are thoroughly explained in Reference [20].

Other research measurements obtained on the HARV included: three-axis angular velocities from a body-axis rate gyro package, pitch, roll, and yaw attitudes from a gimballed attitude gyro, and linear accelerations from a set of body-axis accelerometers. The accuracy of these sensors was established from the flight data noise band. Root mean square noise was 0.025 g for the linear accelerometers, 0.2 deg/sec for the three rate gyros, and 0.25 degrees for the three attitudes.

All data were digitally encoded on board the aircraft using pulse code modulation and telemetered to the ground while being displayed in real time and recorded for postflight analysis. The angular rates, attitudes, and accelerations were recorded at 200 samples/sec, and the pressures were recorded at 50 samples/sec.[20]

Table 5.1: Physical Characteristics of the F/A-18 HARV

Parameter	Dimension
Reference Wing Area, ft^2	400
Reference m.a.c., ft	11.52
Reference Span, ft	37.4
Center of Gravity % m.a.c.	23.8
C.G. Fuselage Ref. Station	456.88
Roll Inertia, slug-ft^2	22,789
Pitch Inertia, slug-ft^2	176,809
Yaw Inertia, slug-ft^2	191,744
Product of Inertia, slug-ft^2	-2,305
Overall Length, ft	56
Wing Aspect Ratio	3.5
Stabilator Span, ft	21.6
Stabilator Area, ft^2	86.48
Weight, lb	36,099

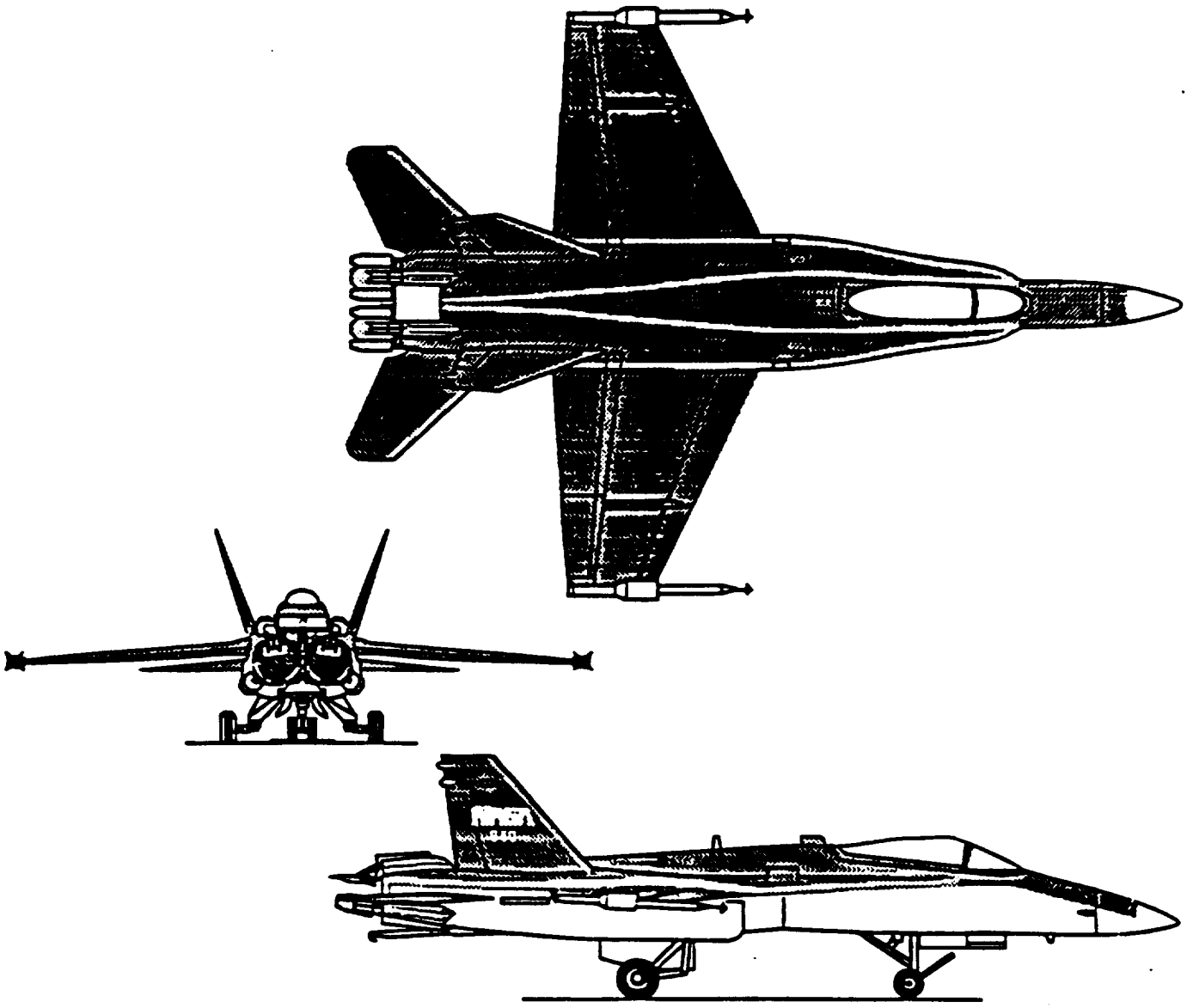

Figure 5.1: Three-view Drawing of the F-18 HARV

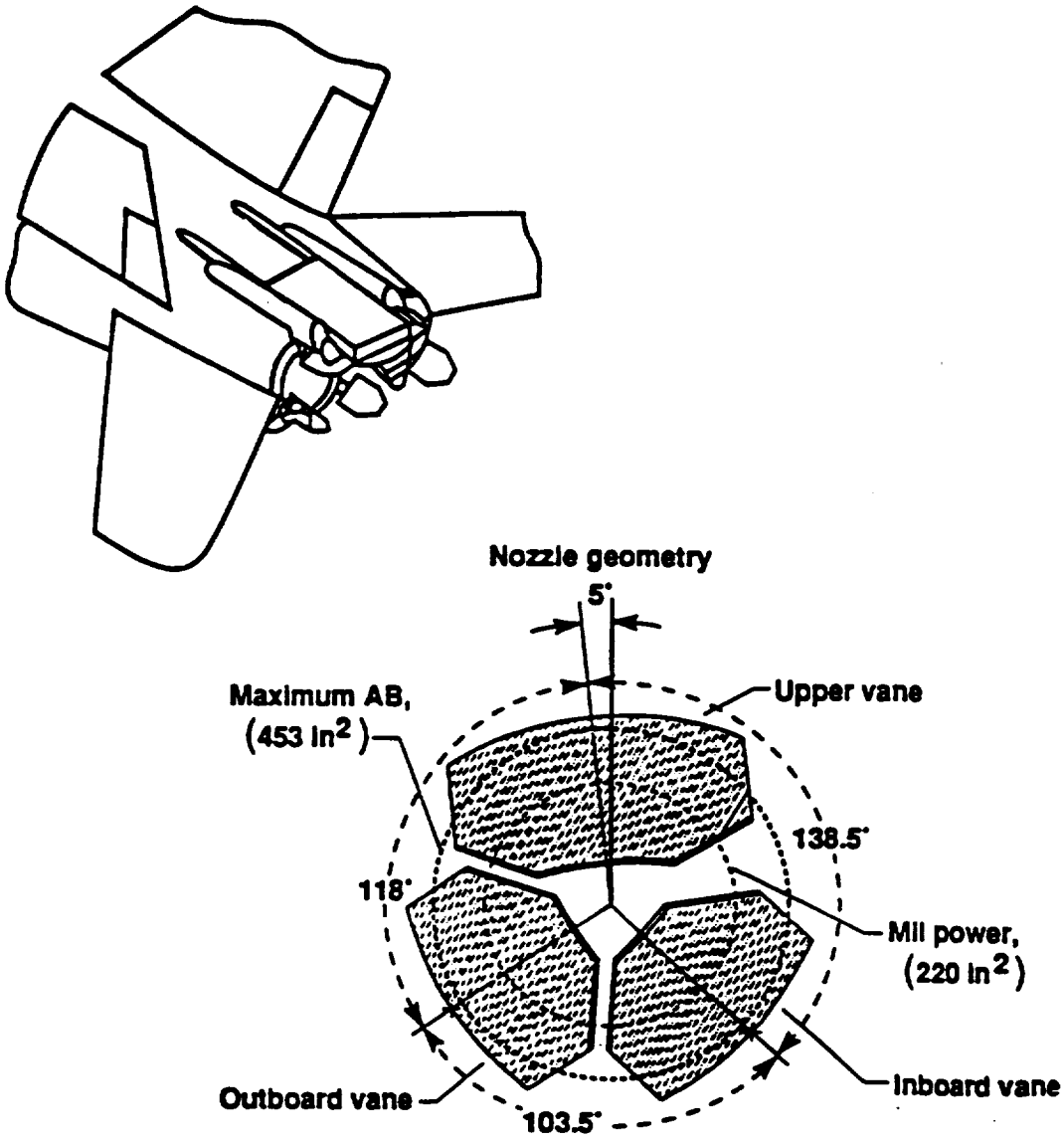

Figure 5.2: F-18 HARV Engine Thrust Vectoring Vane Configuration

CHAPTER 6

FLIGHT TEST MANEUVERS

6.1: DESIGN CONSIDERATIONS

The flight test maneuvers are a key factor in the parameter estimation process. The quality of the estimates is directly related to the quality of the maneuvers; therefore, special consideration must be taken in the design of the inputs that make up the flight test maneuvers. The maneuver design is dependent on the aircraft dynamic characteristics and available control surfaces. In the past, most aircraft were limited to three or four control surfaces, but modern aircraft, especially those that fall into the fighter category, are sometimes equipped with eight or more control surfaces. In these cases, it is first necessary to determine which control surface deflection would induce the most desirable response. It is also important to account for the constraints that may affect the design, such as limits on the control surface position and actuator rates.

To estimate the derivatives, it is necessary to have independent inputs on every control surface used in the maneuver. This is very important because if two surfaces are directly proportional to each other it is practically impossible to determine their individual effectiveness. For example, some airplanes have the aileron and rudder interconnected. If the pilot of an airplane with this setup commands the airplane to roll by moving the stick laterally, the rudder and aileron both move simultaneously. The data from this maneuver would not be useful in the parameter estimation problem because the rudder deflection

actually destroys the aileron effectiveness information. Even though both surfaces move, neither the rudder nor the aileron derivatives could be determined because the motions are dependent. It would be possible however to estimate a combined effectiveness of both surfaces, but the amount that each surface contributes to the effect would be unknown.

The main goal in the design of the inputs for the flight test maneuvers is to properly excite the modes of the aircraft that are of interest. The selection of the control surfaces and the shape of the inputs are two important issues to be considered. A control surface that not only generates a good response but also makes the system mode controllable is desired. The shape of the input is based on the fact that the system modes are best excited by frequencies near the system natural frequencies. This implies that the inputs should be in shapes that cover the range of the system natural frequencies. A good example of this type of input signal shape is a frequency sweep. Other signal shapes such as the 3211 input of Koehler and Wilhelm[21] are also based on the frequency concepts. The 3211 input is a series of four steps that alternate in sign. The first step is three time units long, the second is two, and the last two are each one time unit long. The length of the time unit is varied accordingly in order to center the frequency band of the input around the system natural frequencies.[1] Another type of input shape is that of the pulse-type. This type of input is simple, more easily performed by the pilot, and widely used in recent PID work. As for the size of the pulse and the selection of singlets or doublets, it is necessary to consider the constraints of the control surface positions and actuator rates. Figure 6.1 shows various input shapes.

The design of the maneuvers for the longitudinal cases is based usually on the

short-period mode which is the rigid body dynamic mode with the highest natural frequency. This mode can be excited by a simple doublet by the elevator or any other longitudinal control surface. The length of the pulse should be approximately equal to the natural period of the short-period.

The modes of interest in the lateral direction are the dutch roll, rolling, and spiral. The excitation of these modes can be induced by doublets of the aileron and rudder or any other surface that provides control in roll. It has been determined from past experience that these modes are best excited by rudder and aileron doublets in the same maneuver. The importance of minimizing changes in the flight conditions is a factor in determining the timing and order of the doublets.

6.2: MANEUVERS DEVELOPED FOR THE HARV

As stated previously, one of the objectives of NASA's High-Alpha Technology Program was to obtain a high-alpha database to validate wind tunnel and theoretical predictions. For this reason, the first set of flights included several longitudinal and lateral transient maneuvers intended for estimation of the aircraft aerodynamic parameters. Unfortunately, the results of the initial estimation analysis revealed that insufficient excitation of the transient maneuvers resulted in large scatter of the estimated parameters. This low accuracy was deemed unacceptable. The accuracy of the estimates was further degraded by the near linear dependency of the control surfaces such as the rudder and aileron.[5] The desire to generate independent control surfaces for a better parameter

estimation process was the basis for the design of an additional control system for the HARV. This system has been named OBES (On Board Excitation System) and is essentially a single surface excitation system. It has the capability of exciting the control surfaces one at a time, thus alleviating the problem of dependency. OBES was implemented after the thrust vectoring control system and Research Flight Control System were installed, and it was very successful in reducing the correlation of the control surface deflections. The improvements that OBES introduced are shown in Figures 6.2 - 6.5. Figure 6.2a and 6.2b show time histories of aileron and rudder deflections without the OBES activated, and it is obvious that the two surfaces are correlated. This is also shown in Figure 6.3 where the two deflections are plotted against each other and clearly indicate a somewhat linear relationship. However, with the OBES activated, it can be seen in Figures 6.4a and 6.4b that the simultaneous movements of the surfaces is adequately reduced. The main effect of the OBES activation can be seen in Figure 6.5 which shows the ailerons and the rudder deflections plotted against each other, revealing a much lower correlation.

The size and shape of the inputs programmed into the OBES system software were developed by a trial and error approach in the fixed base simulator at NASA Dryden Flight Research Facility. Different combinations of control surface doublets were tested until the best response was generated. The amplitudes of the doublets were also varied to determine the optimal excitation of the aircraft modes. After several trials, the best maneuvers for each direction were as follows:

Lateral-Directional Inputs

	Small Amplitude Doublets	Large Amplitude Doublets
Differential Tail	+/- 3 deg	+/- 6 deg
Rudder	+/- 10 deg	+/- 15 deg
Aileron	+/- 7 deg	+/- 10 deg
Yaw Vane	+/- 4 deg	+/- 8 deg

Longitudinal-Directional Inputs

	Small Amplitude Doublets	Large Amplitude Doublets
Inboard Trailing Edge Flaps	+/- 15 deg	+/- 25 deg
Symmetric Ailerons	+/- 13 deg	+/- 23 deg
Elevator	+/- 3 deg	+/- 6 deg
Pitch Vane	+/- 2 deg	+/- 4 deg

The doublets were four seconds long - two seconds in the positive sense and two seconds in the negative. Each doublet was separated by one second. The maneuvers were flown at 10°, 25°, 30°, 40°, 50°, and 60° angles of attack. The maneuvers used for this investigation were specified to be low amplitude for all lateral direction test points, and low amplitude for the longitudinal test point of 10° angle of attack. Any point above 10° (for the longitudinal cases) would use large amplitude inputs. The maneuvers are initiated at a stabilized trim condition at approximately 25,000 ft.

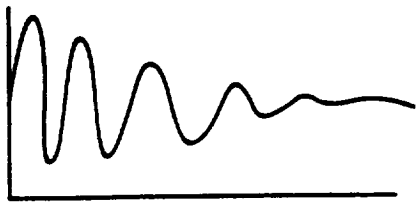

a) Frequency Sweep

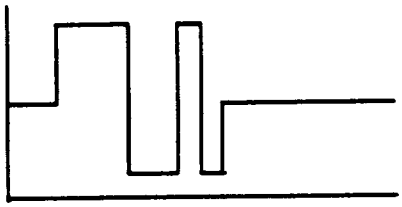

b) 3211

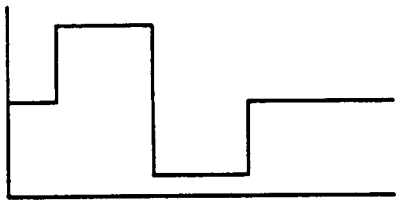

c) Pulse Type

Figure 6.1: Flight Test Maneuver Input Shapes
(a) Frequency Sweep (b) 3211 (c) Pulse-Type (Doublet)

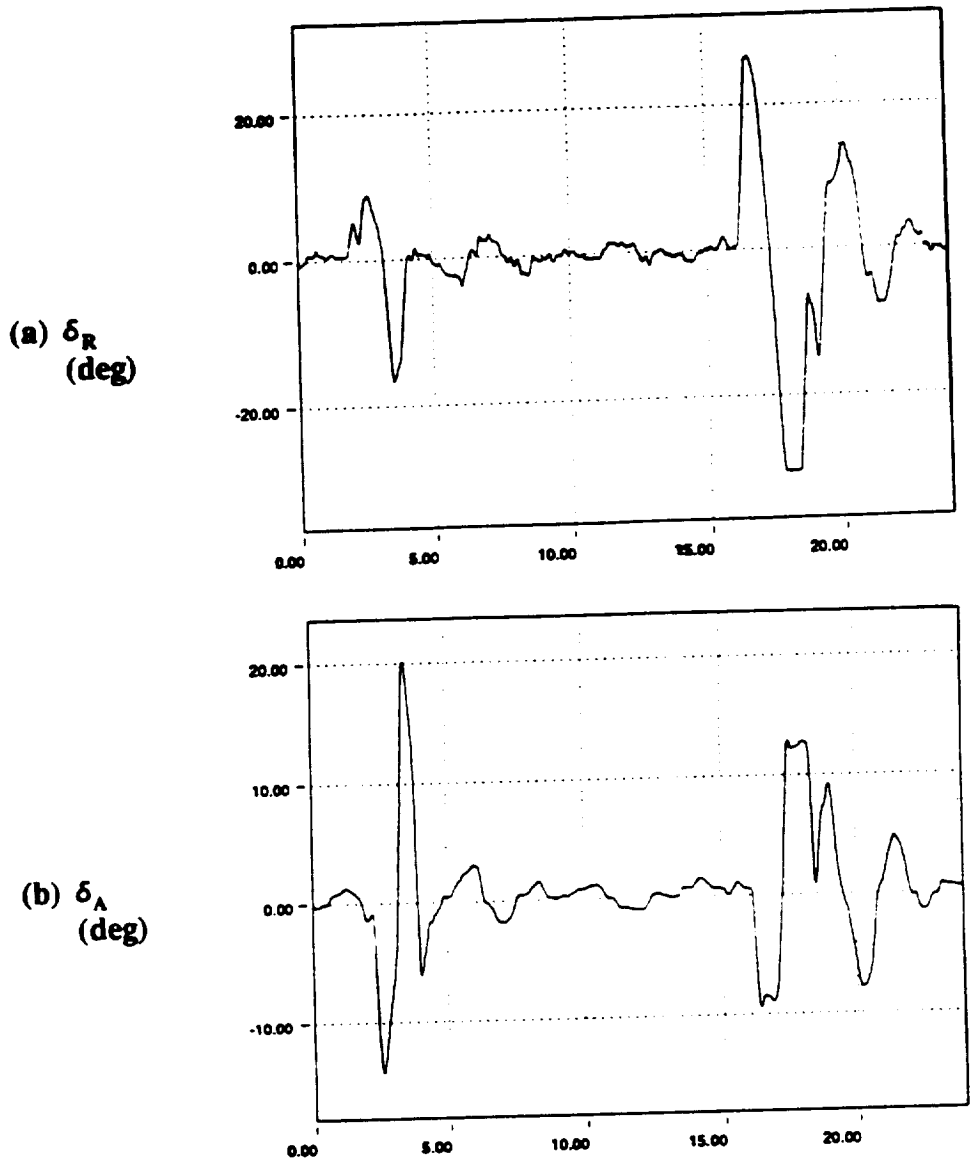

Figure 6.2: Control Surface Deflection Time Histories without OBES
a) Rudder Deflection b) Aileron Deflection

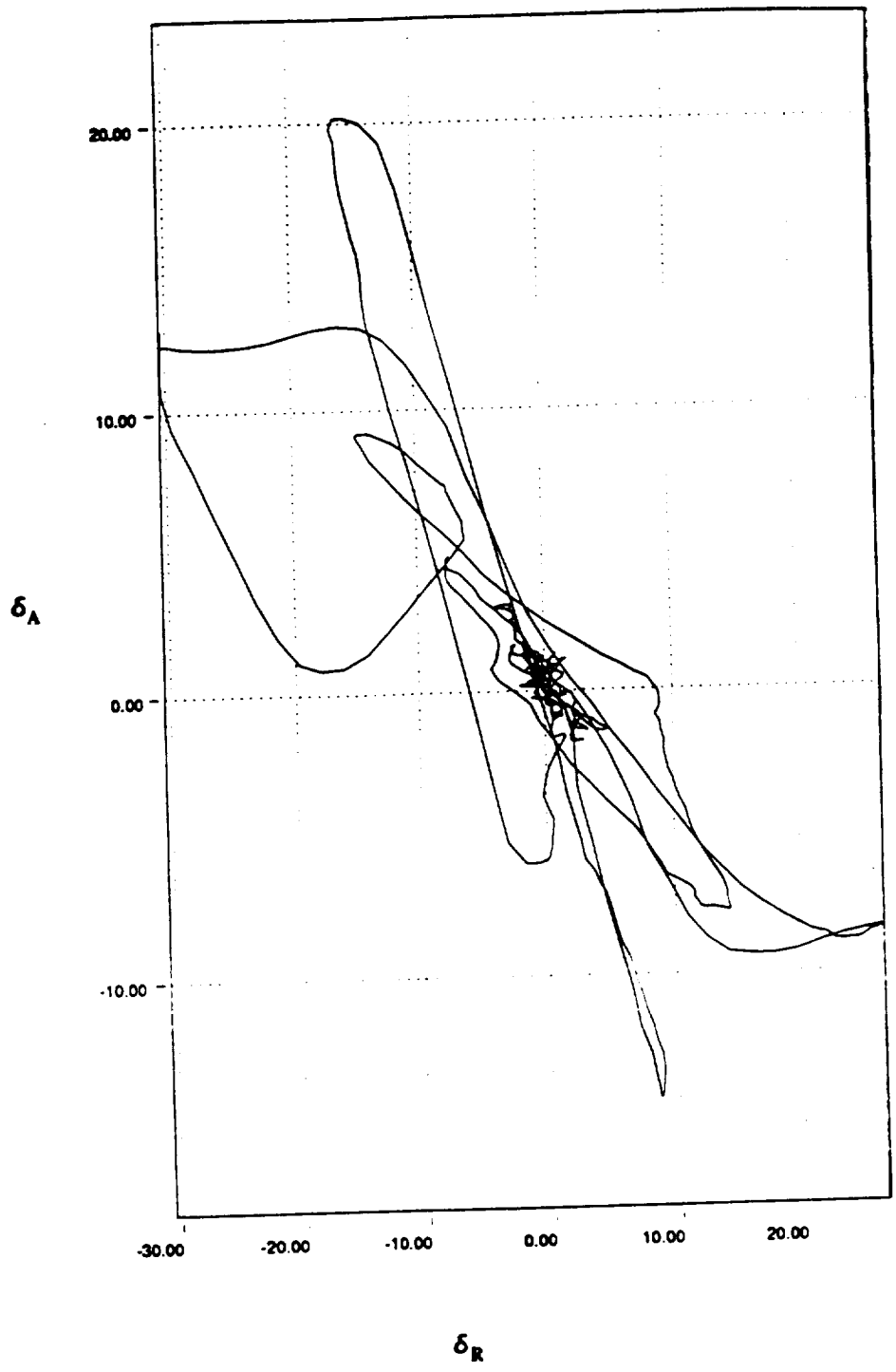

Figure 6.3: Correlation between the Rudder and Aileron Deflections without OBES

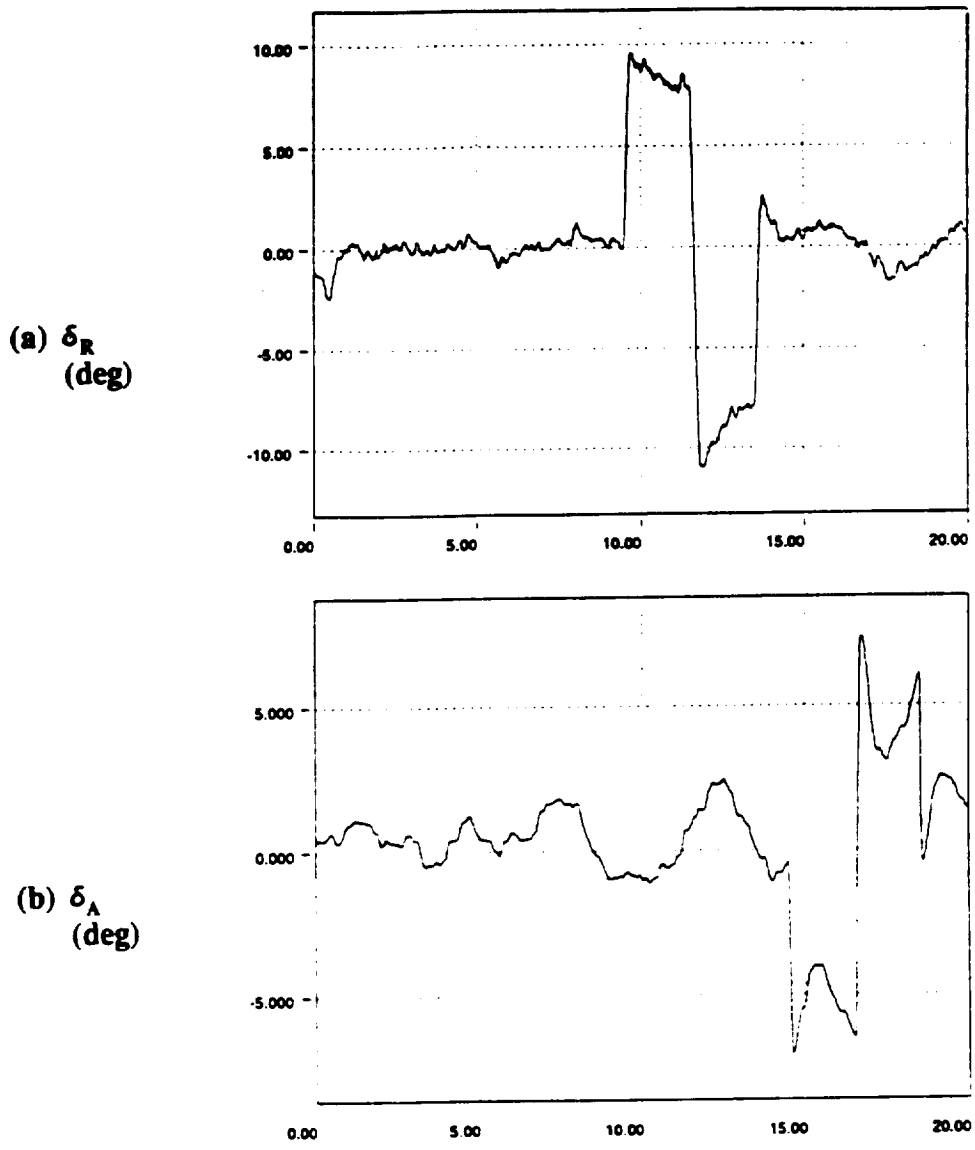

Figure 6.4: Control Surface Deflection Time Histories with OBES
a) Rudder Deflection b) Aileron Deflection

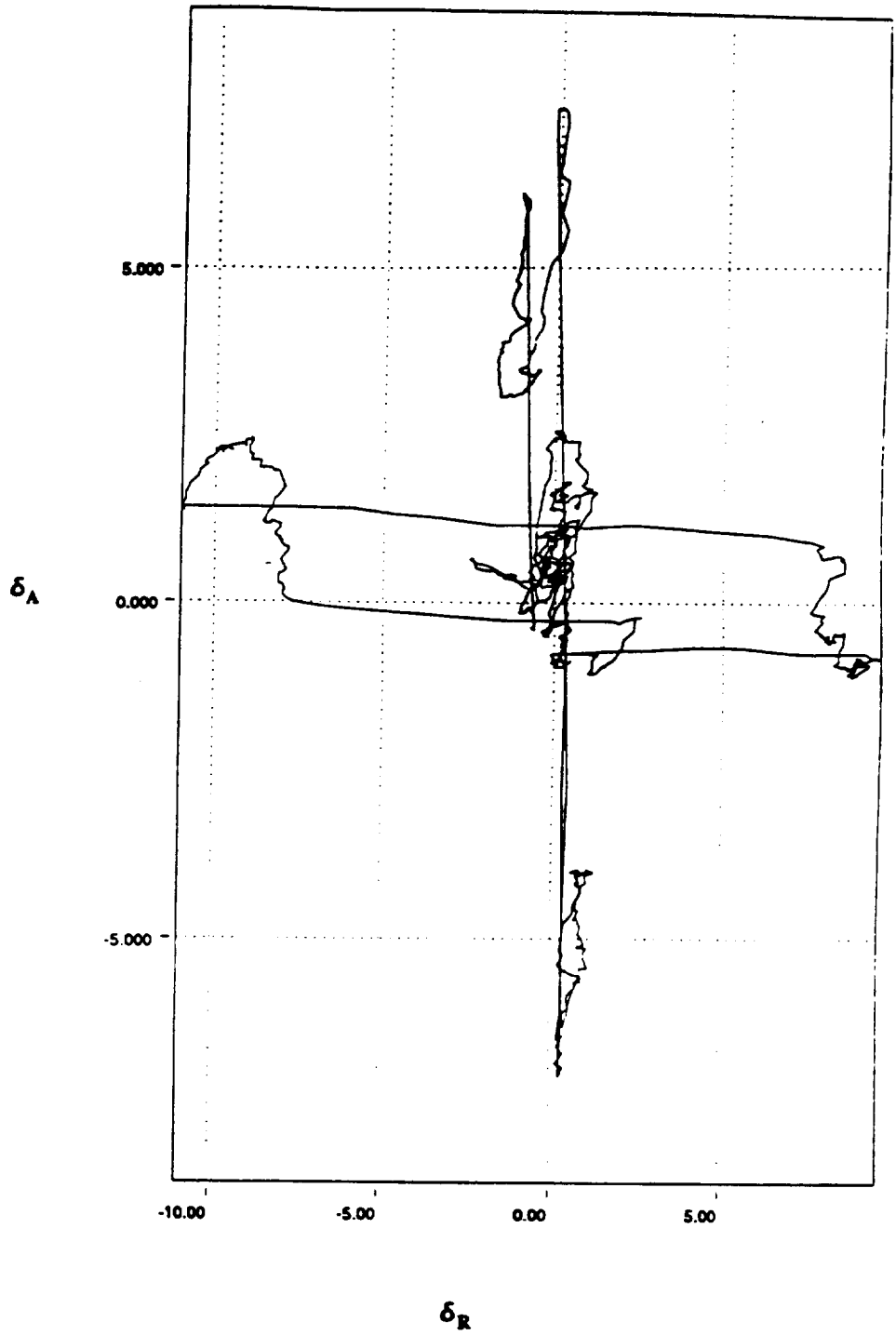

Figure 6.5: Correlation between the Rudder and Aileron Deflections with OBES

CHAPTER 7

HARV AERODYNAMIC MODEL

As stated previously, it is important in the parameter estimation process to use the simplest model possible. In estimating the stability and control derivatives of aircraft, normally an open-loop, bare airframe model is used. The only concern lies with the control surface motions and the aircraft responses. It is irrelevant how or the what causes the surface to deflect. The model includes kinematics and the aerodynamic forces and moments acting on the aircraft. However, only the aerodynamic forces and moments are estimated because the kinematics are well known.

The model is based on the aircraft equations of motion which are a full six degree of freedom set of nonlinear differential equations. These equations were derived in Chapter 4. The equations to be presented assume that the aircraft geometry is fixed, the mass characteristics are constant, and the airplane is flying with relatively no sideslip.

7.1: EQUATION MODIFICATION

The state equations for the longitudinal direction are

$$\dot{\alpha} = q - \tan\beta\,(p\cos\alpha + r\sin\alpha) - \frac{\bar{q}sR}{mV\cos\beta}C_L + \frac{gR}{V\cos\beta}(\cos\theta\cos\phi\cos\alpha + \sin\theta\sin\alpha) \qquad 7.1$$

$$I_y\dot{q} - I_{yz}\dot{r} - I_{xy}\dot{p} = \bar{q}ScC_m R + [pr(I_z - I_x) + (r^2 - p^2)I_{xz} + qrI_{xy} - pqI_{yz}]/R \quad 7.2$$

$$\dot{\theta} = q\cos\phi - r\sin\phi \quad 7.3$$

The lateral directional state equations are

$$\dot{\beta} = p\sin\alpha - r\cos\alpha + \frac{\bar{q}SR}{mV}C_Y + \frac{gR}{V}(\cos\beta\cos\theta\sin\phi) \quad 7.4$$
$$\frac{gR}{V}(-\sin\beta(\cos\theta\cos\phi\sin\alpha - \sin\theta\cos\alpha))$$

$$I_x\dot{p} - I_{xy}\dot{q} - I_{xz}\dot{r} = \bar{q}SbC_l R + [qr(I_y - I_z) + (q^2 - r^2)I_{yz} + pqI_{xz} - prI_{xy}]/R \quad 7.5$$

$$I_z\dot{r} - I_{xz}\dot{p} - I_{yz}\dot{q} = \bar{q}SbC_n R + [pq(I_x - I_y) + (p^2 - q^2)I_{xy} + prI_{yz} - qrI_{xz}]/R \quad 7.6$$

$$\dot{\phi} = p + \tan\theta(r\cos\phi + q\sin\phi) \quad 7.7$$

where b is the reference span, c is the reference chord, S is the reference area, R is a conversion factor (57.2958), V is total velocity, C_L and C_Y are the coefficients of lift and lateral force, and C_l, C_m C_n are the coefficients of rolling, pitching, and yawing moments.

The total force and moment equations for the longitudinal direction are

$$C_N = C_{N_o} + C_{N_\alpha}\alpha + \frac{c}{2VR}C_{N_q}q + C_{N_{\delta E}}\delta E + C_{N_{\delta LEF}}\delta LEF + C_{N_{\delta TEF}}\delta TEF \quad 7.8$$
$$+ C_{N_{\delta SA}}\delta SA + [C_{N_{\delta PV}}\delta PV + C_{N_{\delta YV}}\delta YV]/\bar{q}S$$

$$C_m = C_{m_o} + C_{m_\alpha}\alpha + \frac{c}{2VR}C_{m_q}q + C_{m_{\delta E}}\delta E + C_{m_{\delta LEF}}\delta LEF + C_{m_{\delta TEF}}\delta TEF + C_{m_{\delta SA}}\delta SA \quad 7.9$$

$$C_A = C_{A_o} + C_{A_\alpha}\alpha + \frac{c}{2VR}C_{A_q}q + C_{A_{\delta E}}\delta E + C_{A_{\delta LEF}}\delta LEF + C_{A_{\delta TEF}}\delta TEF \quad 7.10$$
$$+ C_{A_{\delta SA}}\delta SA + [C_{A_{\delta PV}}\delta PV + C_{N_{\delta YV}}\delta YV]/\bar{q}S$$

$$M_Y = \bar{q}ScRC_m + (pr(I_z - I_x) + (r^2 - p^2)I_{xz} + qrI_{xy} - pqI_{yz})/R - (6r[ERPM(I_{xe})])/R + [C_{m_{\delta PV}}\delta PV + C_{m_{\delta YV}}\delta YV]R \quad 7.11$$

and the lateral force and moment equations are

$$C_Y = C_{Y_o} + C_{Y_\beta}\beta + \frac{b}{2VR}(C_{Y_p}p + C_{Y_r}r) + C_{Y_{\delta A}}\delta A + C_{Y_{\delta R}}\delta R + C_{Y_{\delta DHT}}\delta DHT + [C_{Y_{\delta PV}}\delta PV + C_{Y_{\delta YV}}\delta YV]/\bar{q}S \quad 7.12$$

$$C_l = C_{l_o} + C_{l_\beta}\beta + \frac{b}{2VR}(C_{l_p}p + C_{l_r}r) + C_{l_{\delta A}}\delta A + C_{l_{\delta R}}\delta R + C_{l_{\delta DHT}}\delta DHT \quad 7.13$$

$$C_n = C_{n_o} + C_{n_\beta}\beta + \frac{b}{2VR}(C_{n_p}p + C_{n_r}r) + C_{n_{\delta A}}\delta A + C_{n_{\delta R}}\delta R + C_{n_{\delta DHT}}\delta DHT \quad 7.14$$

$$M_X = \bar{q}SbRC_l + (qr(I_y - I_z) + (q^2 - r^2)I_{yz} + pqI_{xz} - prI_{xy})/R + [C_{l_{\delta PV}}\delta PV + C_{l_{\delta YV}}\delta YV]R \quad 7.15$$

$$M_Z = \bar{q}SbRC_n + (pq(I_x - I_y) + (p^2 - q^2)I_{xy} + prI_{yz} - qrI_{xz})/R + (6q[ERPM(I_{xe})])/R + [C_{n_{\delta PV}}\delta PV + C_{n_{\delta YV}}\delta YV]R \quad 7.16$$

The terms δ_E, δ_{SA}, δ_{LEF} and δ_{TEF} are the elevator, symmetric aileron, leading edge flaps and trailing edge flaps deflections, and δ_A, δ_R, δ_{DHT} are the aileron, rudder, and differential horizontal tail deflections. ERPM is the engine revolutions per minute and Ixe is the engine moment of inertia [sl-ft2], and the number 6 in these equations is a conversion factor for revolution per minute to degrees per second.

The symbols δ_{PV} and δ_{YV} represent the vane deflections in the pitch and yaw directions. The signals are a result of a simple averaging technique of the three vane

deflections for each engine. The numbers assigned to each vane, and their corresponding positions are shown in Figure 7.1. The formulation of the pitch and yaw vane deflections are as follows:

$$\delta_{PV} = \frac{1}{2}\left[\delta_{V1} - \left(\frac{\delta_{V2} + \delta_{V3}}{2}\right) + \delta_{V4} - \left(\frac{\delta_{V5} + \delta_{V6}}{2}\right)\right] \qquad 7.17$$

$$\delta_{YV} = \frac{1}{2}\left[\left(\frac{\delta_{V2} - \delta_{V3}}{2}\right) + \left(\frac{\delta_{V6} - \delta_{V5}}{2}\right)\right] \qquad 7.18$$

In this simplistic model it is assumed that the longitudinal aerodynamic coefficients are functions of the angle of attack, pitch rate, and the longitudinal control surface motions. Likewise, the lateral aerodynamic coefficients are dependent on the angle of sideslip, roll rate, yaw rate, and the lateral control surface positions.

As stated above, the force and moment coefficients are linear functions of the aircraft states and controls with the option of adding nonlinear terms.

It should also be noted that during a maneuver it is assumed that the dynamic pressure, velocity, Mach number, Reynolds number, engine parameters and other flight condition parameters are constant. The restriction of having small maneuvers avoids the coupling between longitudinal and lateral-directional dynamics.

7.2: SIGN CONVENTION

The sign convention for the F/A-18 HARV surface deflections is conventional and is as follows. Left rudder deflection is positive and induces a negative yawing moment.

Aileron deflection is found from subtracting the right aileron deflection from the left aileron deflection. This implies that a positive δ_A is left aileron down which induces a positive rolling moment. Finally, the elevator deflection is positive down which gives a negative pitching moment.

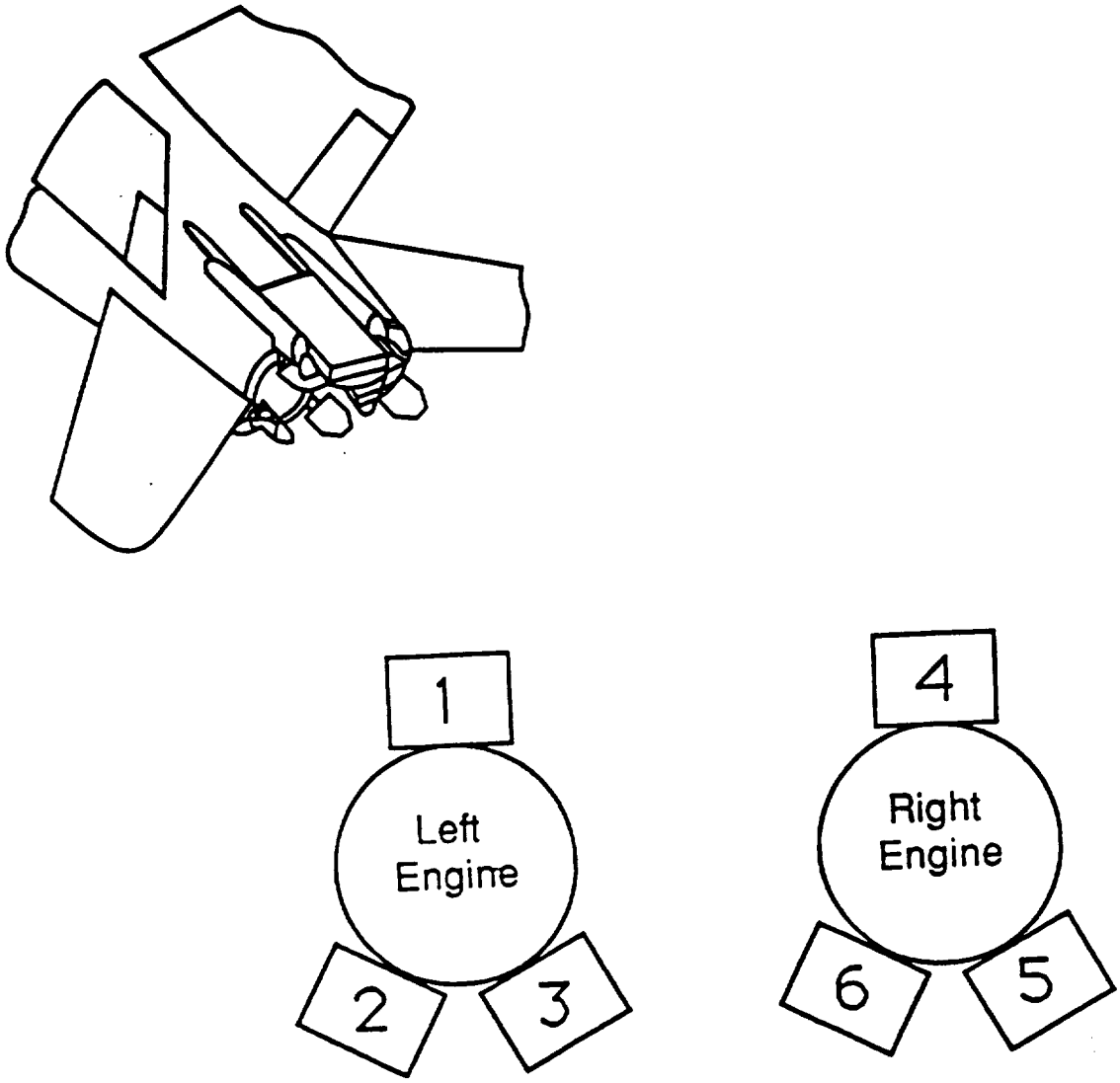

Figure 7.1: Thrust Vectoring Vane Positions

CHAPTER 8

RESULTS AND CONCLUSIONS

The flight tests for this investigation were conducted on September 29, 1992 at NASA Dryden Flight Research Facility in California. The On Board Excitation System (OBES) maneuvers were performed once at 10°, 25°, 30°, 40°, 50°, 60° angles of attack in both the lateral and longitudinal directions. The relevant data was recorded and analyzed at NASA Dryden using the *pEst* code.

It should be noted that the results presented do not represent any information of the thrust vectoring (yaw vane and pitch vane) doublets. The analysis was restricted to incorporate only the three of the four doublets of the OBES flight test maneuvers discussed in Chapter 5. This was done in accordance with International Traffic in Arms Regulations. Recently, the restrictions on the technical diffusion of these data have been lifted.

The results of the derivative values are presented in graphic and numeric forms. The *pEst* code integrates the equations of motion to generate estimates of the derivative values and to produce a time history of the computed variables. All computed variables are first assigned constant default values for the entire time history. These default values for the F/A-18 HARV were chosen from wind tunnel analysis of McDonnell Douglas' clean aerodynamic model of the F/A-18. The program then integrates the equations of motion using current program status, replacing the default values with the computed values as the integration proceeds. The integration continues until the difference between the measured and computed responses is minimized.

The results from *pEst* using the measured flight data are compared with results from a previous parameter estimation analysis of the F/A-18 and values obtained from wind tunnel tests performed by McDonnell Douglas. This previous PID analysis was performed by Dr. K. Iliff at NASA Dryden.[7] It should be noted that the estimates that he obtained and those obtained from McDonnell Douglas' wind tunnel tests were for the F/A-18 before it had the capability of independently moving the control surfaces with the OBES system. An additional comparison was made with values from a *pEst* analysis of data that was obtained from the F/A-18 flight simulator at NASA Dryden. A *pEst* analysis was performed with simulator data because only one maneuver was actually flown at each test point and additional PID maneuvers were not scheduled for several months. It was necessary to obtain extra data at the same flight conditions in order to make a more diverse comparison. However, not much emphasis is placed on the results from the simulator data because several effects are not included in the simulator model.

8.1: LATERAL DIRECTIONAL DERIVATIVES

The time histories of the computed and measured responses of sideslip (β), roll rate (p), yaw rate (r), roll angle (ϕ), and lateral acceleration (ay) for the 10, 25, 30, 40, 50, 60 degree angle of attack (aoa) test points for the lateral direction are shown in Figures 8.1 - 8.6. From these figures it can be seen that for the lower angles of attack (ie. 10° and 25°), the computed responses closely match the measured responses. However; as the aoa increases, the computed response curves seem to deviate slightly from the measured time

histories. This type of deviation implies that the estimated derivative values do not accurately describe the airplane's characteristics. Basically, the more the computed response resembles or fits the measured response, the more the estimated coefficients are accurate. This accuracy of the parameters is also indicated by Cramer-Rao bounds. The Cramer-Rao equality defines the minimum achievable variance for the estimation error of any unbiased estimate.[22]

The effects of the aerodynamic biases, β, p, r, ϕ, δ_A, δ_R, δ_{DHT}, δ_{PV}, and δ_{YV} on the sideforce, rolling moment and yawing moment are shown in Figures 8.7 - 8.15. The square symbols are the coefficient values computed by *pEst* using the flight data, the circles are values obtained from Dr. K. Iliff's analysis for the F/A-18. The triangles represent the results obtained from *pEst* of the data recorded from the F/A-18 flight simulator, and the x's are the coefficient values from McDonnell Douglas' wind tunnel tests. Notice that the results from Iliff are only for aoa's of 10° - 40°, and that some of the values from the wind tunnel tests are not available. The vertical bars on the estimated derivative values symbolize the Cramer Rao bounds. To accentuate the bounds on the plotted results, they were multiplied by a scale factor of 5.

Figure 8.8 includes plots of the effect of sideslip (C_{Y_β}, C_{l_β}, and C_{n_β}). C_{Y_β} is the change in side-force coefficient due to a sideslip angle, and it is generally negative. All four values at each aoa compare reasonably with exception to the flight determined data at 30° and 40°. The scatter of these data points could be due to the unsteady behavior of the vortical flow fields associated with the forebody and wings, coupled with the rolling degree of freedom of the aircraft. This dynamic phenomenon that plagues many slender-wing

aircraft is called wing rock and is basically a single-degree-of-freedom, limit cycle, roll oscillation. Previous wing rock investigations for the HARV have indicated a rising trend of motion between 30° and 40° angles of attack.[23]

The C_{l_β} term indicates the change in rolling moment coefficient due to a sideslip angle and is also known as the airplane dihedral effect. All values in Figure 8.8b are negative, as expected, and similar in magnitude. The estimates from flight data compare well with the other values except for the 40° aoa. This scatter may be attributed to the noise level of the lateral acceleration signal at the 40° aoa as shown in Figure 8.4e. The sideslip and sideforce terms are directly related to the lateral acceleration. Hence, if the signal is not clear the estimates may not be valid.

C_{n_β} is the change in yawing moment coefficient due to a sideslip angle. This term is primarily responsible for the aircraft directional dynamic stability, and it is expected to be positive. Figure 8.8c shows a close comparison among the values at 10° - 40° aoas. The Cramer Rao bounds are small thus implying a good accuracy.

The contributions of the rolling moment, p, to sideforce, rolling moment, and yawing moment are shown in Figure 8.9. The C_{Y_p} and C_{n_p} shown in figures 8.9a and 8.9c are two less important derivatives. As it can be seen the data points are somewhat scattered with large Cramer Rao bounds, thus indicating that the accuracy is poor. The arrows on the graphs symbolize data points that were off the vertical scale. The appropriate values and Cramer Rao bounds for these points are located in the legend to the right of the graph.

The C_{l_p} graph in Figure 8.9b shows favorable agreement among each of the values for the lower aoas; however, after 30° aoa the scatter tends to increase. The sign of the

values is positive as expected.

Figure 8.10 contains the yawing moment effects. The more important of these three derivatives is the derivative C_{nr}. The C_{lr} terms are very similar in magnitude with exception to the 30° and 40° aoa, and the C_{Yr} graph shows considerable distribution of the flight data values. The Cramer Rao bounds are quite large, therefore the estimates are considered to be a poor representation of the yawing moment's effect on the sideforce. In a similar manner to the values of C_{lp}, the C_{nr} values decrease in accuracy in the higher aoa range.

The effects of the aileron control surface deflections are represented in Figure 8.11. The plot of $C_{Y\delta A}$ shows a change in sign of the values as the aoa changes. There is no visible trend of the flight data values. More data points at each aoa are needed to determine the tendency of the results. However, the $C_{l\delta A}$ estimates depict a good representation of the aileron effect on the rolling moment. The small Cramer Rao bounds on both the simulator and flight data results suggest that the values are valid. The values decrease in almost a linear fashion from approximately 0.0026 to 0.000015 as the aoa increases. The positive sign of the values is expected because a positive aileron deflection (which is one half of a positive left aileron minus a negative right aileron) generates a positive rolling moment. The large uncertainty of the results from Iliff's analysis could be due to the insufficient excitation of the rolling mode. Recall that in his investigation, the F/A-18 was not yet equipped with the OBES system. He concluded that the differences in the derivatives the he obtained was due to the lack of independent control surface deflections.[7] The results for this particular derivative show that the single surface excitations from OBES definitely improve the estimation.

The values for $C_{n\delta A}$ from the flight data, simulator data and Iliff's analysis notably agree throughout the aoa range. The generally negative sense of this derivative implies that a positive aileron deflection induces an adverse yawing situation.

The rudder effects are shown in Figure 8.12. The more important of the three δR coefficients are $C_{Y\delta R}$ and $C_{n\delta R}$. Figure 8.12a indicates that the largest uncertainty of the estimates for $C_{Y\delta R}$ lies within the aoa range of 30° - 40°. The estimates for $C_{Y\delta R}$ are expected to be positive. The tendency of the $C_{n\delta R}$ estimates obtained from the flight data first decreases slightly in magnitude to 40° aoa then increases at the higher angles.

The differential horizontal tail contributions are shown in Figure 8.13. The derivatives were only estimated up to a 50° angle of attack because past 50° the differential horizontal tail is ineffective due to flow detachment. This control surface acts in a similar manner to the ailerons because it produces a positive rolling moment when deflected positively. However, the same positive deflection is expected to yield a proverse yawing situation unlike the ailerons which induce adverse yaw when deflected positively. This proverse yaw is due to the increase in the amount of drag on the right side of the tail section.

The thrust vector derivatives are shown in Figures 8.14 and 8.15. It should be noted again that the thrust vector control surfaces were not used to independently excite the aircraft's motion. Therefore, the results presented here are not the best representation of the thrust vectoring effects. Even though the pitch vane is almost negligible in the lateral sense, the corresponding derivatives were also estimated. This was done in order to get a better perspective of the way in which the thrust vector controls were modeled. As it is

evident, each of the coefficients are large in magnitude and vary throughout the aoa range.

The validity of the estimates for $C_{n\delta YV}$ and $C_{Y\delta YV}$ was examined by comparing the calculated moment arm of the deflected thrust force to the real moment arm defined from the aircraft dimensions. The calculated thrust moment arm was found by dividing the yawing moment derivative $C_{n\delta YV}$ by the sideforce derivative $C_{Y\delta YV}$. These values were calculated from the estimates at each angle of attack and are shown in Figure 8.16. The real thrust moment arm was found as the distance between the aircraft center of gravity and the point were the exhaust plume was deflected. This value was determined to be -20.1 feet. The negative sign indicates that the distance is aft of the center of gravity. As seen in Figure 8.16, the calculated moment arm is never -20.1 feet. This suggests that the estimates are not accurately describing these characteristics.

It is not possible however, to imply that the modeling of the thrust vector terms is completely wrong. The insufficient amount of data does not allow a complete comparison of results. Additional data is needed at the same conditions in order to verify the modelling techniques.

8.2: LONGITUDINAL DIRECTIONAL DERIVATIVES

Even though the lateral derivative estimates were more of a concern, a preliminary set of longitudinal derivatives was estimated to generate a complete set of values for each direction.

The computed response time histories are compared to the measured responses for

the longitudinal direction at 10°, 25°, 30°, 40°, 50°, 60° angles of attack in Figures 8.17 - 8.22. Essentially, the fits of the computed and measured times histories are good. However, the *pEst* program had difficulty matching the measured responses of the axial acceleration, a_x because of the noise level in the ax measurements. Therefore, the accuracy of the axial force coefficient estimates is degraded.

The amount of noise of the normal acceleration and the angle of attack signals also decreases as the airplane is subjected to the more dynamic conditions at the higher angles of attack. At the higher angles of attack, the airplane undergoes an ample amount of changes. For instance, the amount of structural vibration increases, the aerodynamics turn nonlinear, wing rock occurs, and many others. All of these events may affect the shape or amount of noise on the signals.

The offsets in the fits of the computed and measured responses could also be the results of time shifts in the data. For instance, in Figure 8.19c it can be seen that the computed response begins to estimate a change in the pitch angle before the actual measured response changes. This type of situation suggests that a lead in the data transfer is present because *pEst* begins to compute the response as soon as it detects movement of the control surfaces. The computed response starts to indicate a change in the aircraft motion before the measured response shows a change, it is possible that the data for the control surface deflection was not transferred at the exact time that the surface moved. However, in order to determine if in this case the offsets are due to time shifts in the data transfer, additional maneuvers are needed. The additional maneuvers would allow a better comparison of responses.

The longitudinal derivative estimates are shown in Figures 8.23 - 8.31. Essentially, the small Cramer Rao bounds on the more important of the derivatives such as C_{N_α}, C_{m_α}, C_{m_q}, $C_{m_{\delta TEF}}$, $C_{m_{\delta SA}}$, $C_{m_{\delta E}}$ imply that the estimates are a valid representation of the longitudinal stability and control characteristics. Notice that the uncertainty of the estimates at the 10° aoa is larger than other data points. This could be due to the fact that the low amplitude doublets used at the 10° aoa did not sufficiently excite the aircraft modes. It is expected that the large amplitude maneuvers would improve that results.

Again, the large amount of scatter of the thrust vector terms is possibly due to the fact that the vanes were not used to independently induce the motion of the aircraft. Inclusion of the thrust vectoring (pitch vane and yaw vane) doublets would possibly raise the accuracy of these estimates.

Note that the axial force coefficients estimated from the simulator data are expected to be invalid. This is because the effect of changing angle of attack on the thrust is not modelled in the simulator.

8.3: CONCLUSIONS

In the previous chapters, the procedure for estimating the aircraft stability and control derivatives was presented. It was shown how the aircraft equations of motion were developed and incorporated in the maximum likelihood method to generate estimates for the derivatives.

For this investigation, a particular application of parameter estimation was applied to the NASA F/A-18 High Alpha Research Vehicle. Discussions of the vehicle and why it is being used to study the characteristics in the high angle of attack regime are included. The design of the flight test maneuvers and mathematical modelling of the airplane are also addressed.

The results of the analysis provide a reasonable base for further research in this area. From the results it can be concluded that the single surface excitation system (OBES) greatly improved the derivative estimates. This is due to the fact that the system effectively reduced the correlation among the deflection of different control surfaces.

In addition, this investigation includes results of the first attempt to model the thrust vectoring effects. Unfortunately, the flight data which included the thrust vectoring doublets could not be used for this analysis due to the International Traffic in Arms Regulations. Therefore, the results presented for the thrust vector derivatives can be deemed as only initial predictions of the thrust vectoring characteristics. Additional research is required to determine an accurate method of modelling these effects.

The estimates at the higher angles of attack suggest that problems do exist in this

region. For example, the uncertainty of the estimates in the 30° - 60° angle of attack is possibly due to occurrences of wing rock, turbulence and separated flow conditions. However, it is difficult to determine the exact problem with only one estimate at each flight condition. Essentially, additional data is needed to verify the modelling techniques and gather a complete understanding of the airplane characteristics at these high angle of attack conditions.

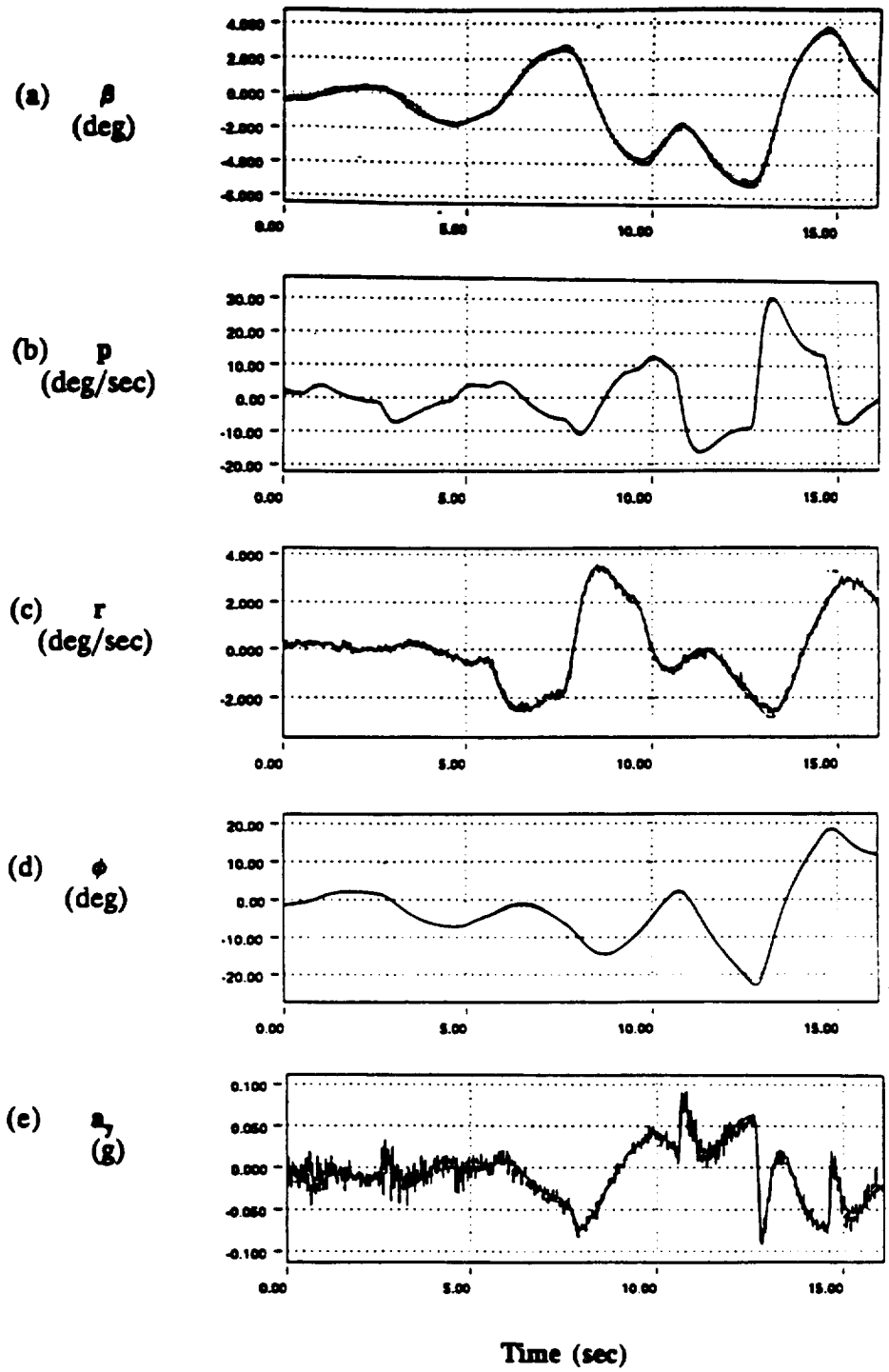

Figure 8.1: Computed (--) and Measured (——) Response Time Histories for $\alpha = 10°$ in the Lateral Direction for (a) Sideslip Angle (b) Rolling Moment (c) Yawing Moment (d) Roll Angle (e) Lateral Acceleration

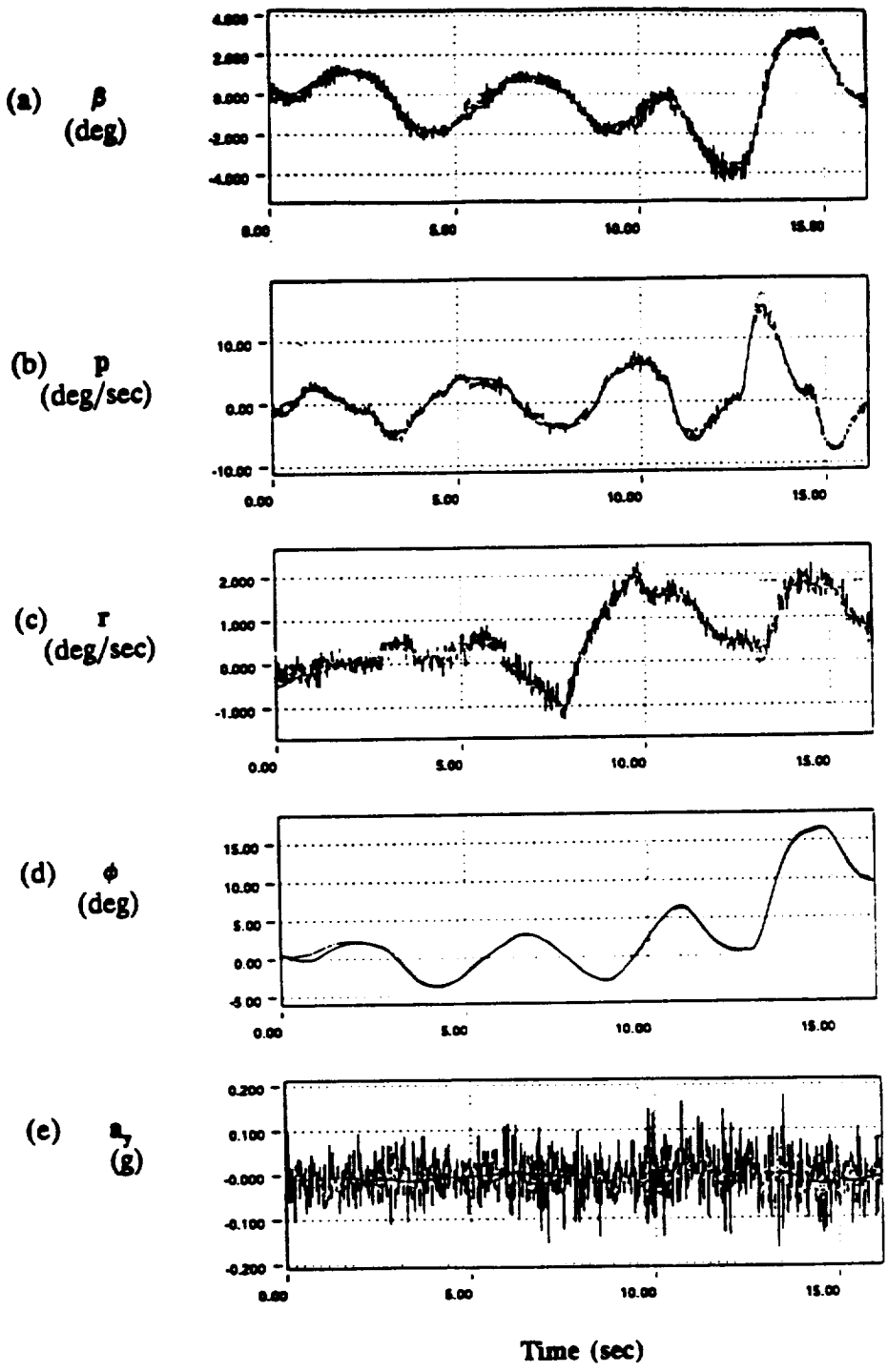

Figure 8.2: Computed (--) and Measured (——) Response Time Histories for $\alpha=25^{\circ}$ in the Lateral Direction for (a) Sideslip Angle (b) Rolling Moment (c) Yawing Moment (d) Roll Angle (e) Lateral Acceleration

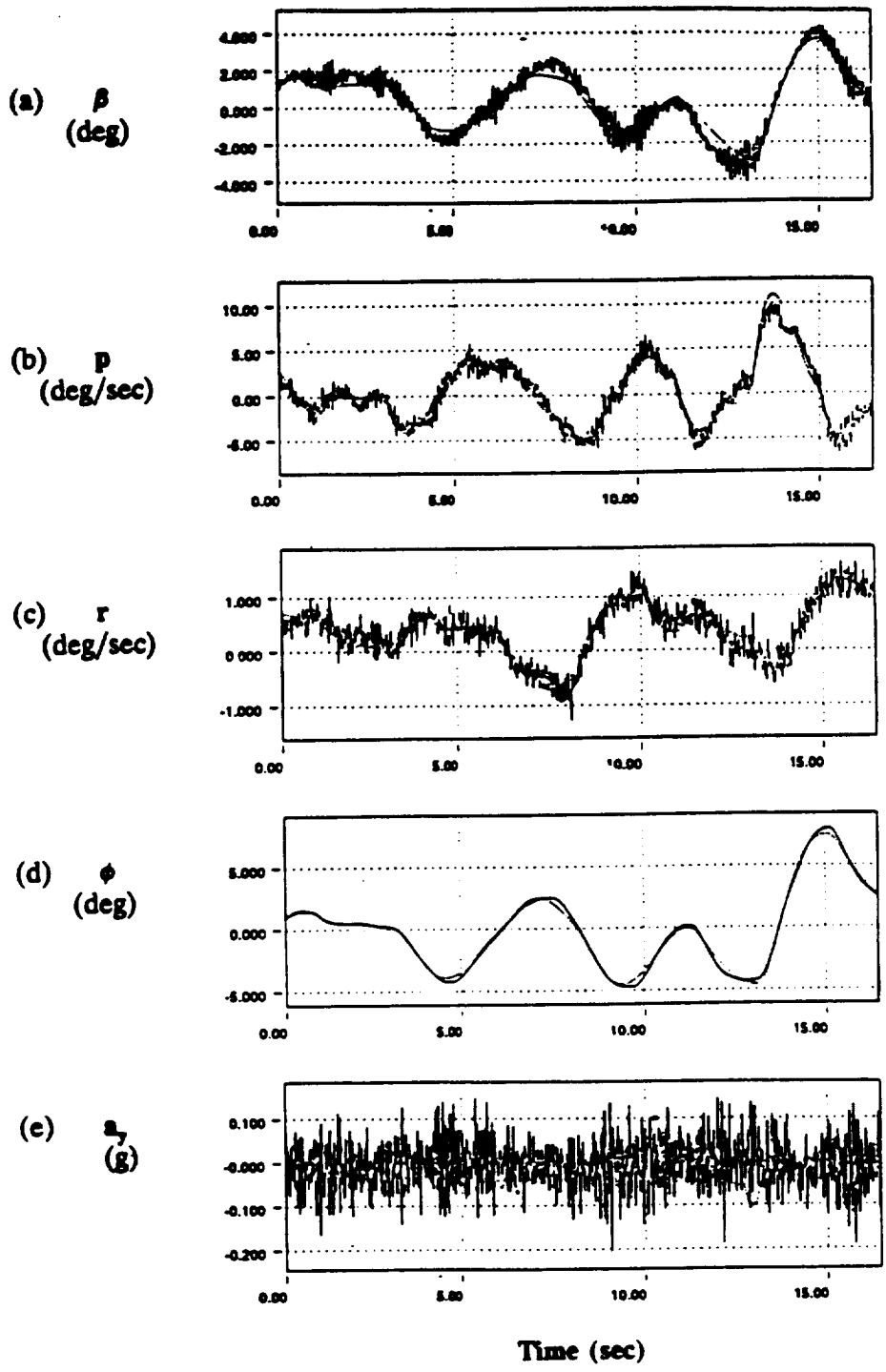

Figure 8.3: Computed (--) and Measured (——) Response Time Histories for $\alpha = 30°$ in the Lateral Direction for (a) Sideslip Angle (b) Rolling Moment (c) Yawing Moment (d) Roll Angle (e) Lateral Acceleration

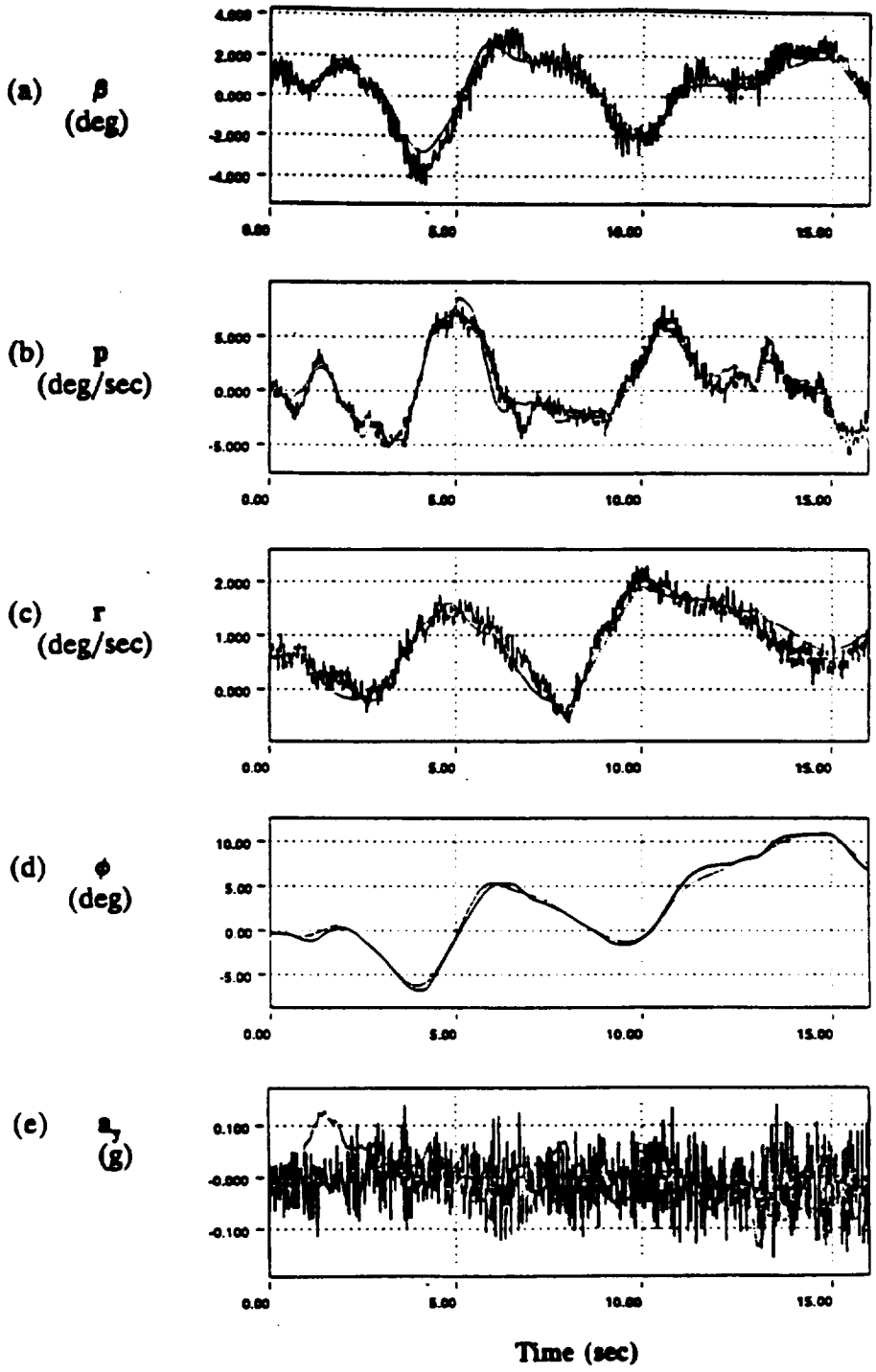

Figure 8.4: Computed (--) and Measured (——) Response Time Histories for $\alpha = 40°$ in the Lateral Direction for (a) Sideslip Angle (b) Rolling Moment (c) Yawing Moment (d) Roll Angle (e) Lateral Acceleration

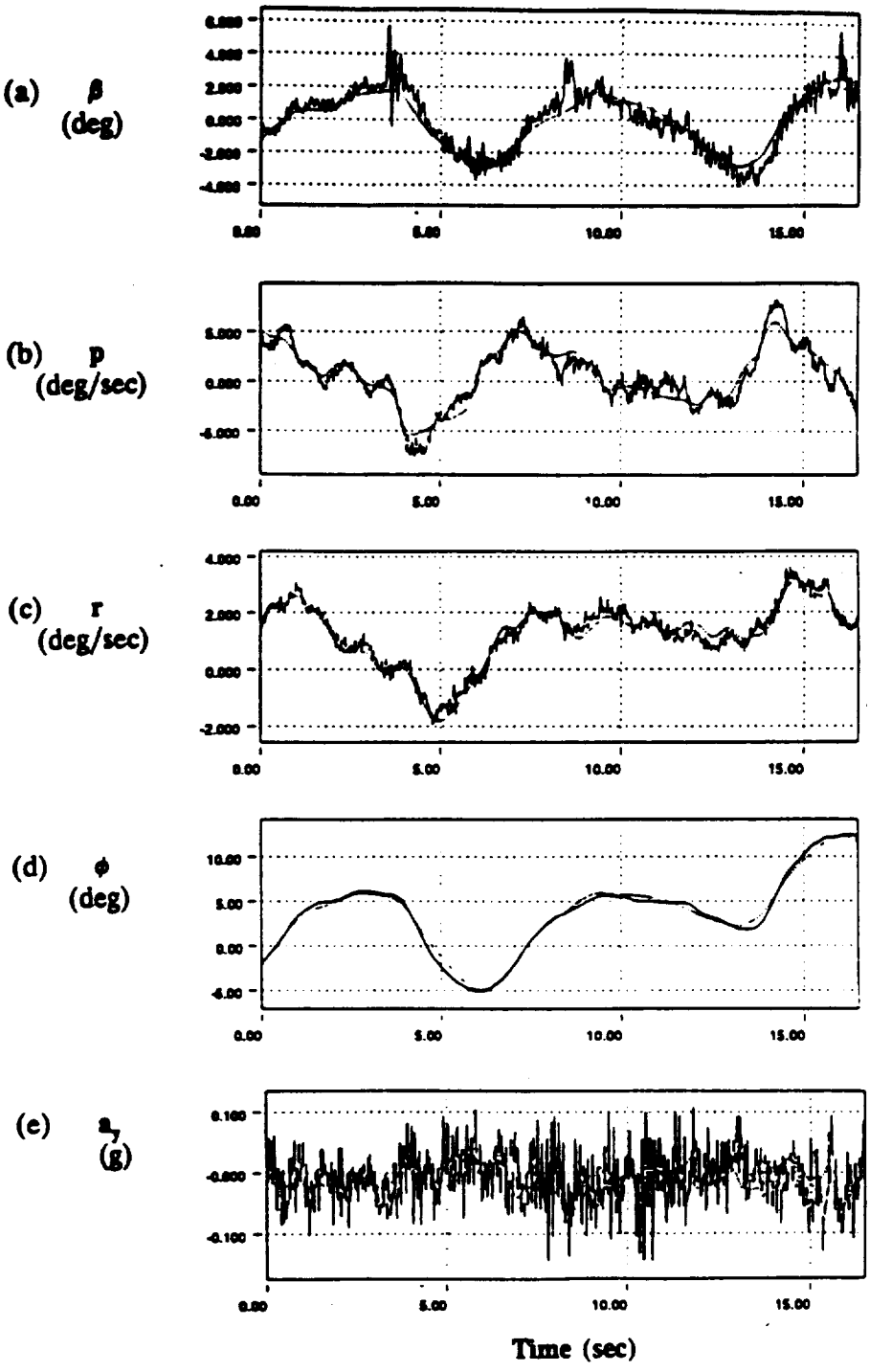

Figure 8.5: Computed (--) and Measured (——) Response Time Histories for $\alpha = 50°$ in the Lateral Direction for (a) Sideslip Angle (b) Rolling Moment (c) Yawing Moment (d) Roll Angle (e) Lateral Acceleration

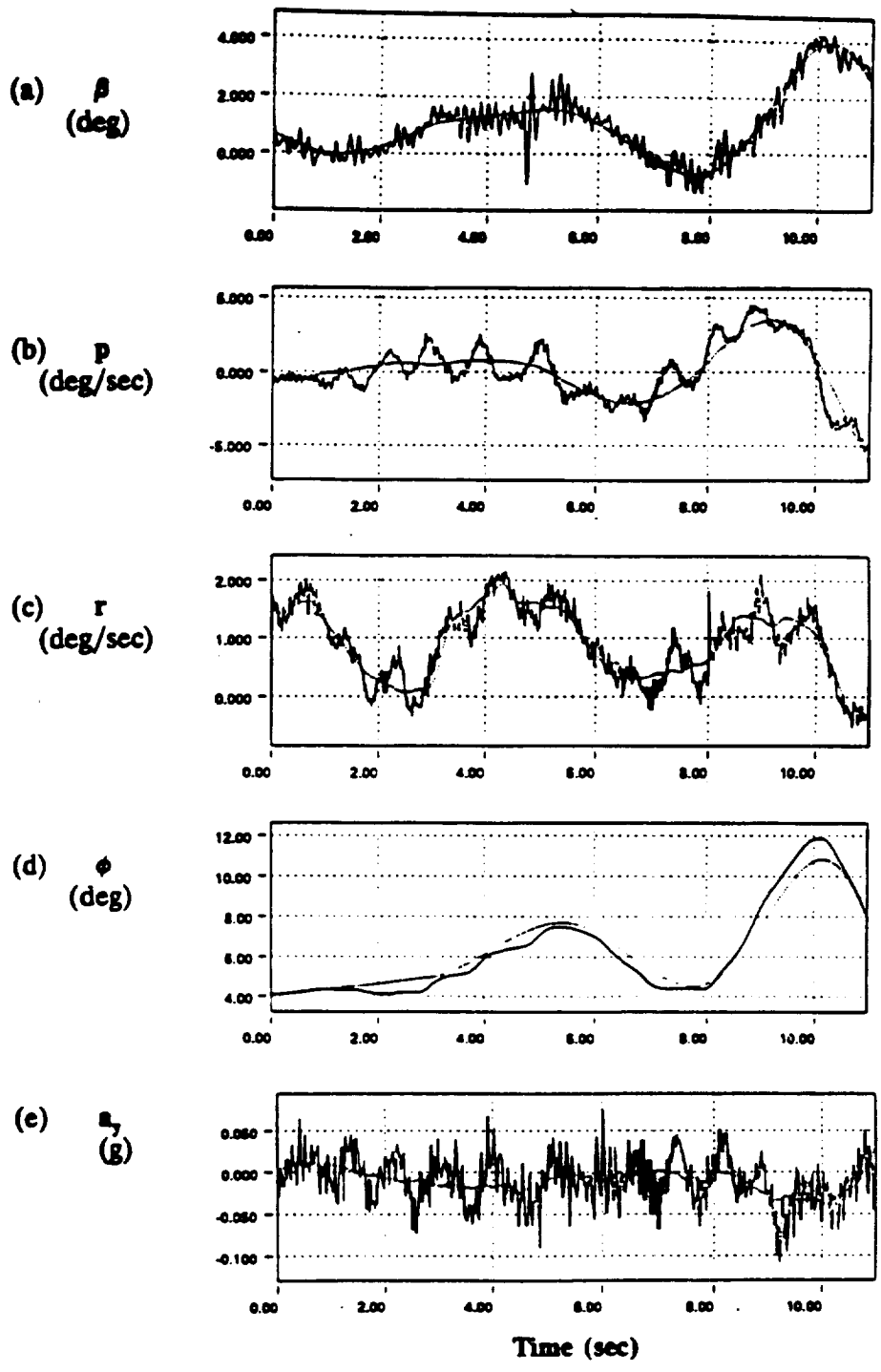

Figure 8.6: Computed (--) and Measured (——) Response Time Histories for $\alpha = 60°$ in the Lateral Direction for (a) Sideslip Angle (b) Rolling Moment (c) Yawing Moment (d) Roll Angle (e) Lateral Acceleration

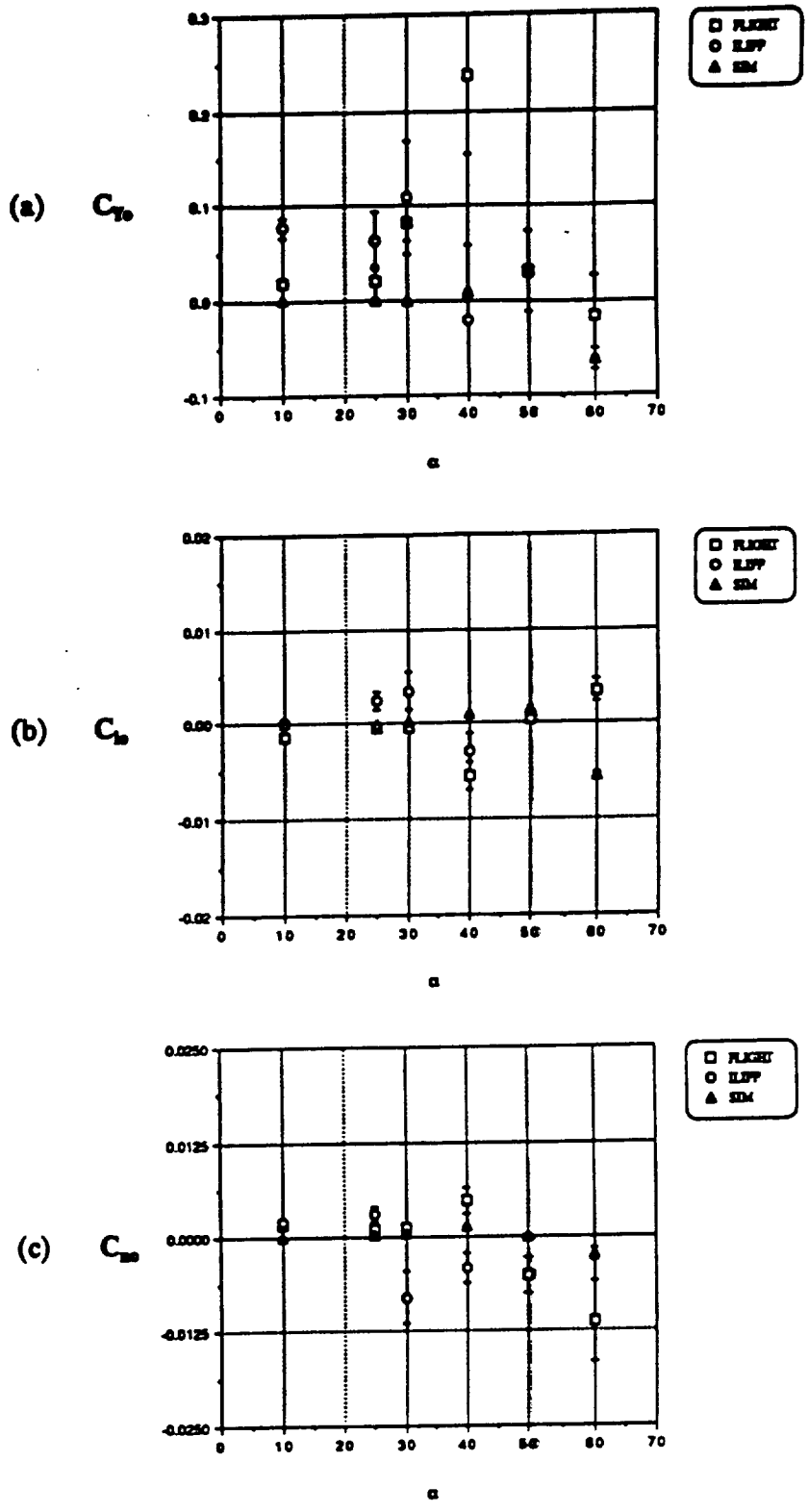

Figure 8.7: Aerodynamic Bias Derivatives (Lateral-Directional)
(a) Lateral Force (b) Rolling Moment (c) Yawing Moment

C-2

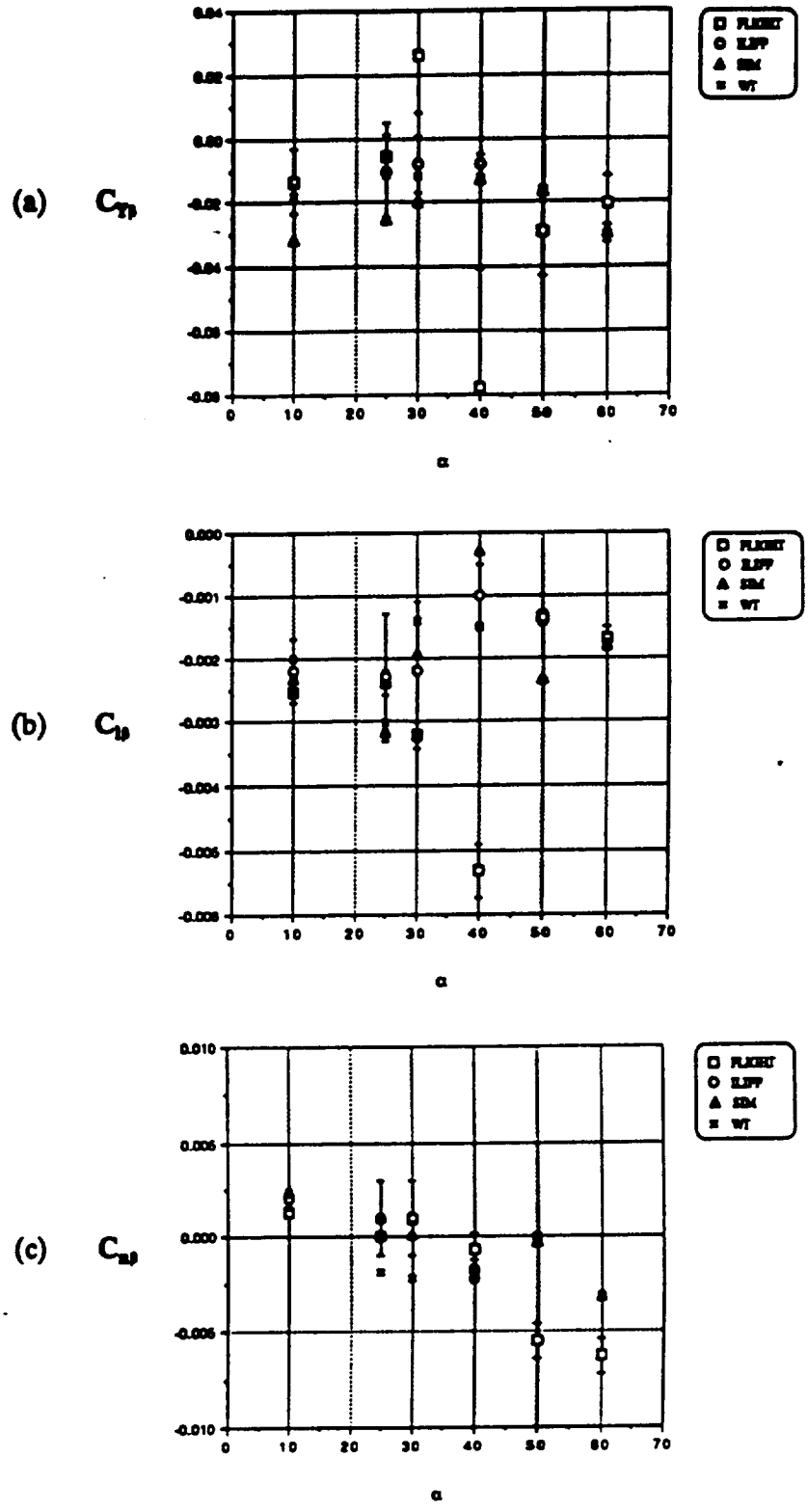

Figure 8.8: Sideslip Derivatives (Lateral-Directional)
(a) Lateral Force (b) Rolling Moment (c) Yawing Moment

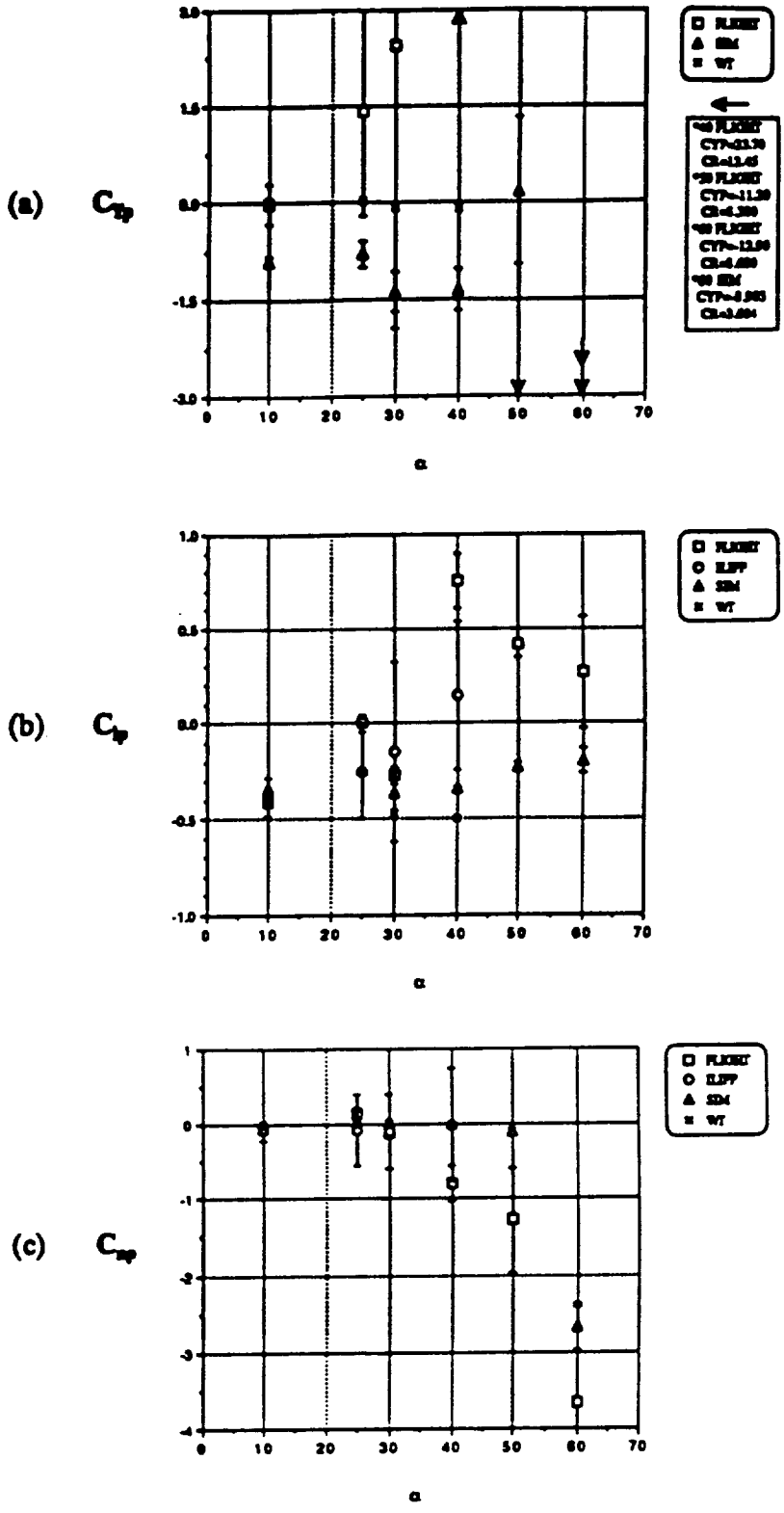

Figure 8.9: Roll Rate Derivatives (Lateral-Directional)
(a) Lateral Force (b) Rolling Moment (c) Yawing Moment

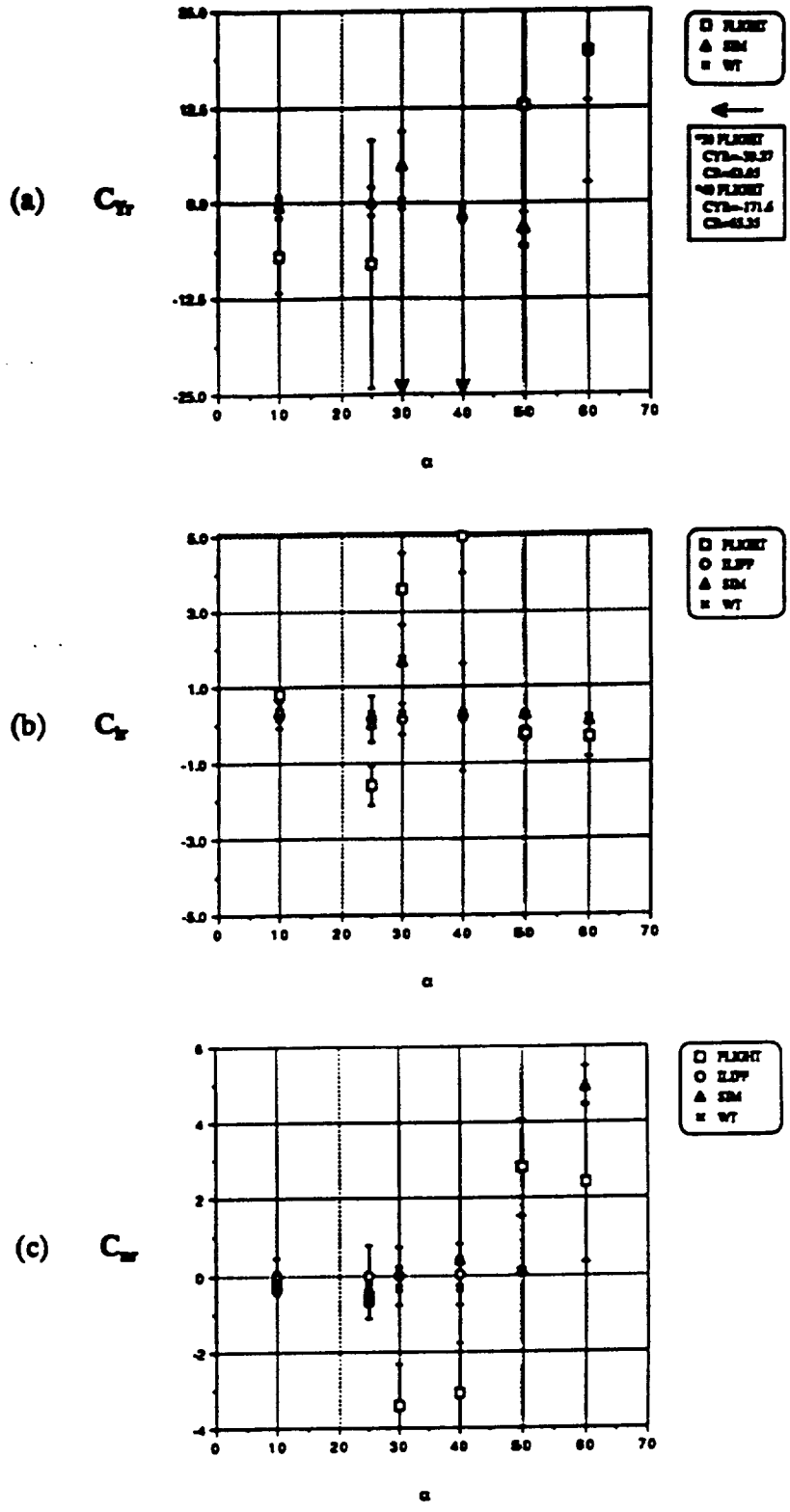

Figure 8.10: Yaw Rate Derivatives (Lateral-Directional)
(a) Lateral Force (b) Rolling Moment (c) Yawing Moment

(a) $C_{Y_{\delta A}}$

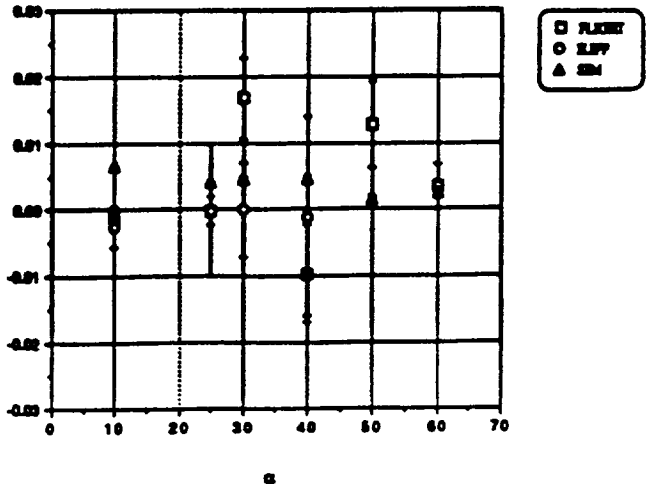

(b) $C_{l_{\delta A}}$

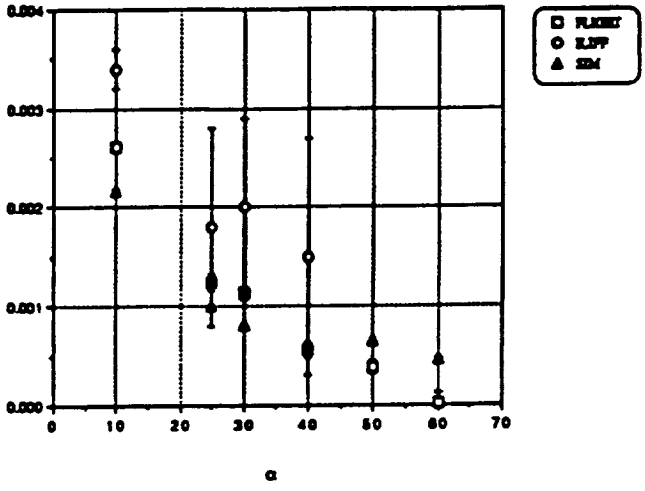

(c) $C_{n_{\delta A}}$

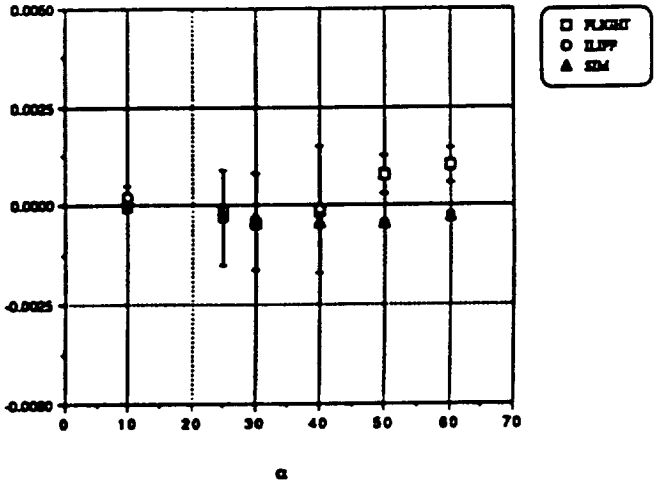

Figure 8.11: Aileron Derivatives (Lateral-Directional)
(a) Lateral Force (b) Rolling Moment (c) Yawing Moment

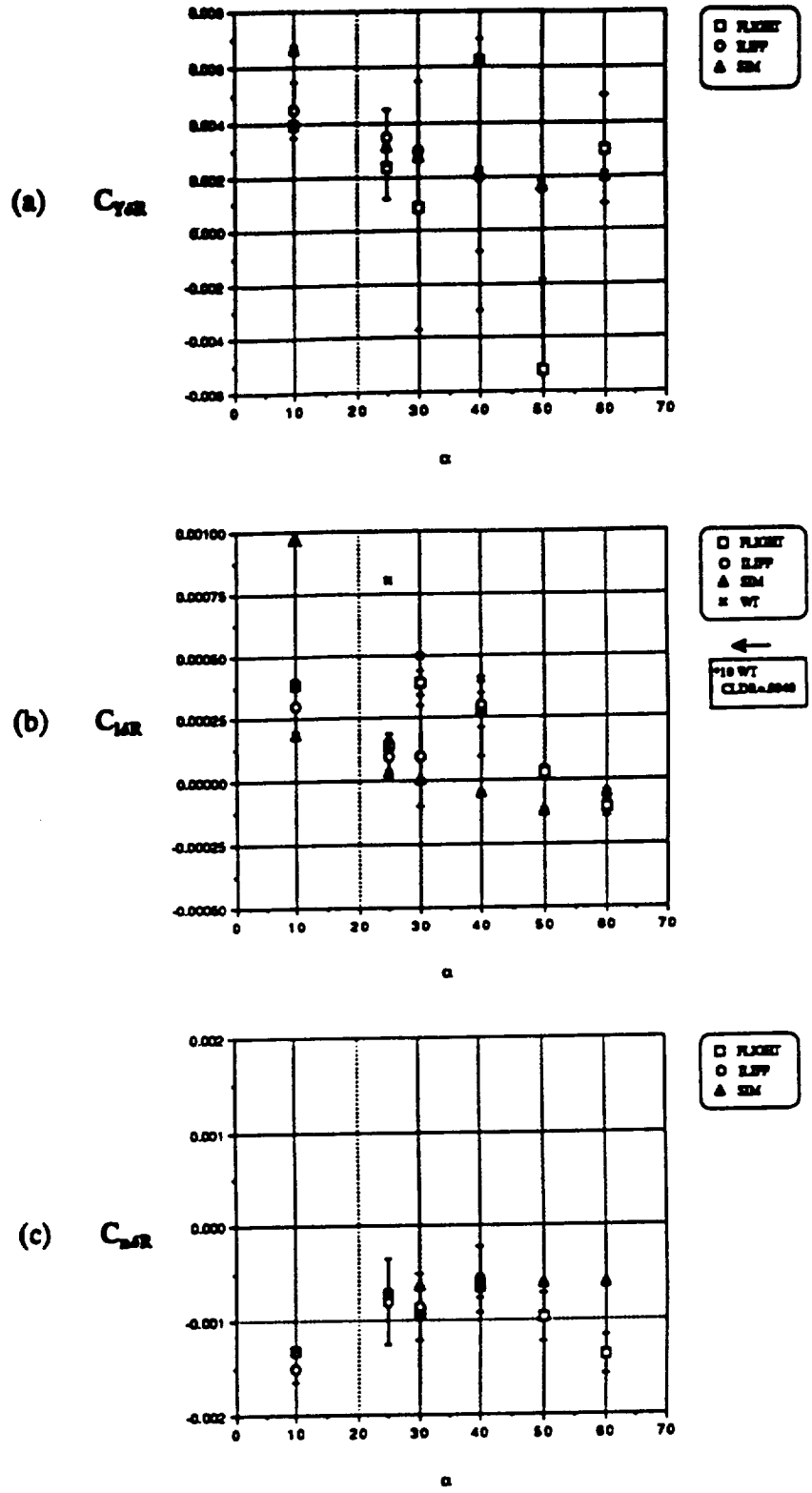

Figure 8.12: Rudder Derivatives (Lateral-Directional)
(a) Lateral Force (b) Rolling Moment (c) Yawing Moment

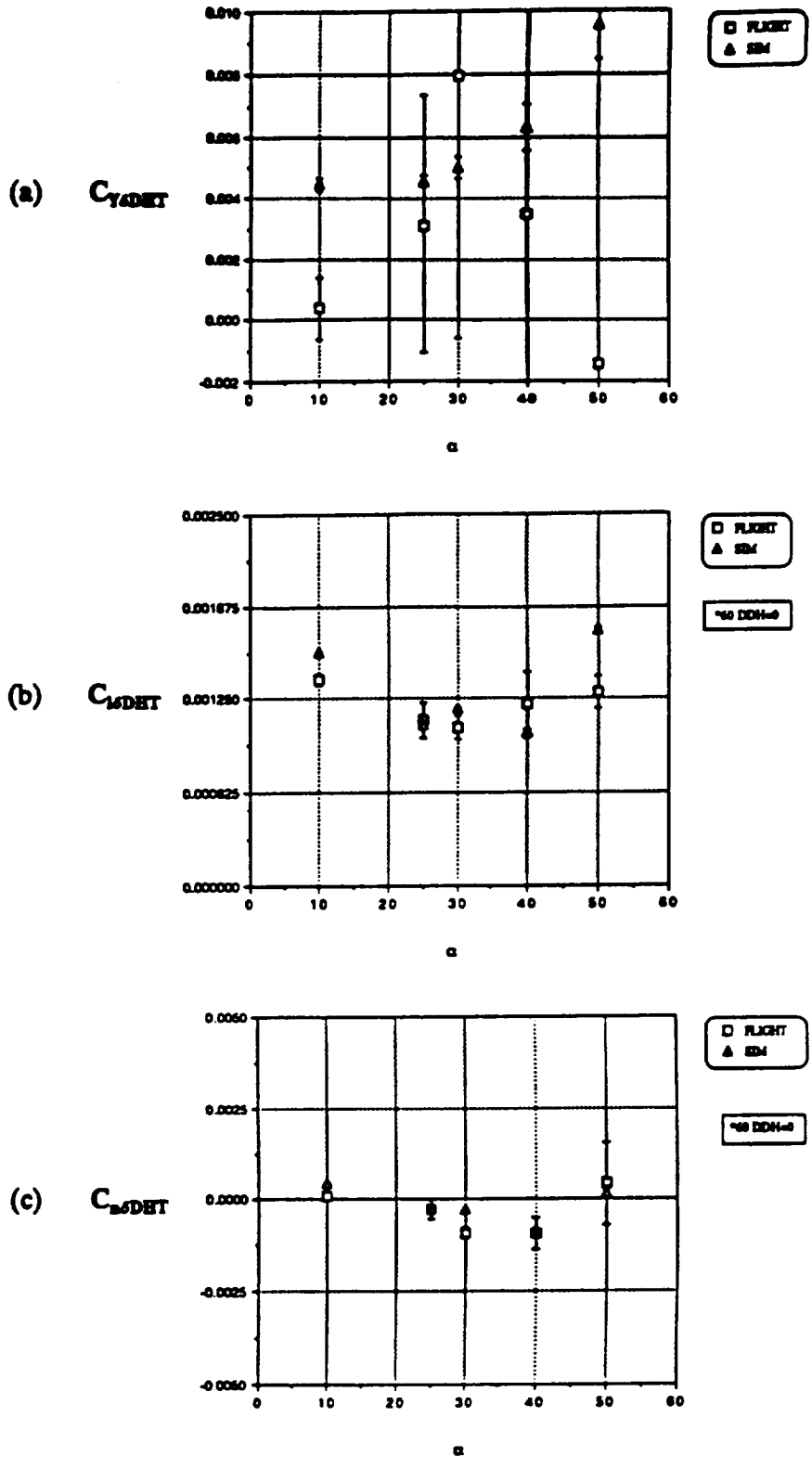

Figure 8.13: Differential Horizontal Tail Derivatives (Lateral-Directional) (a) Lateral Force (b) Rolling Moment (c) Yawing Moment

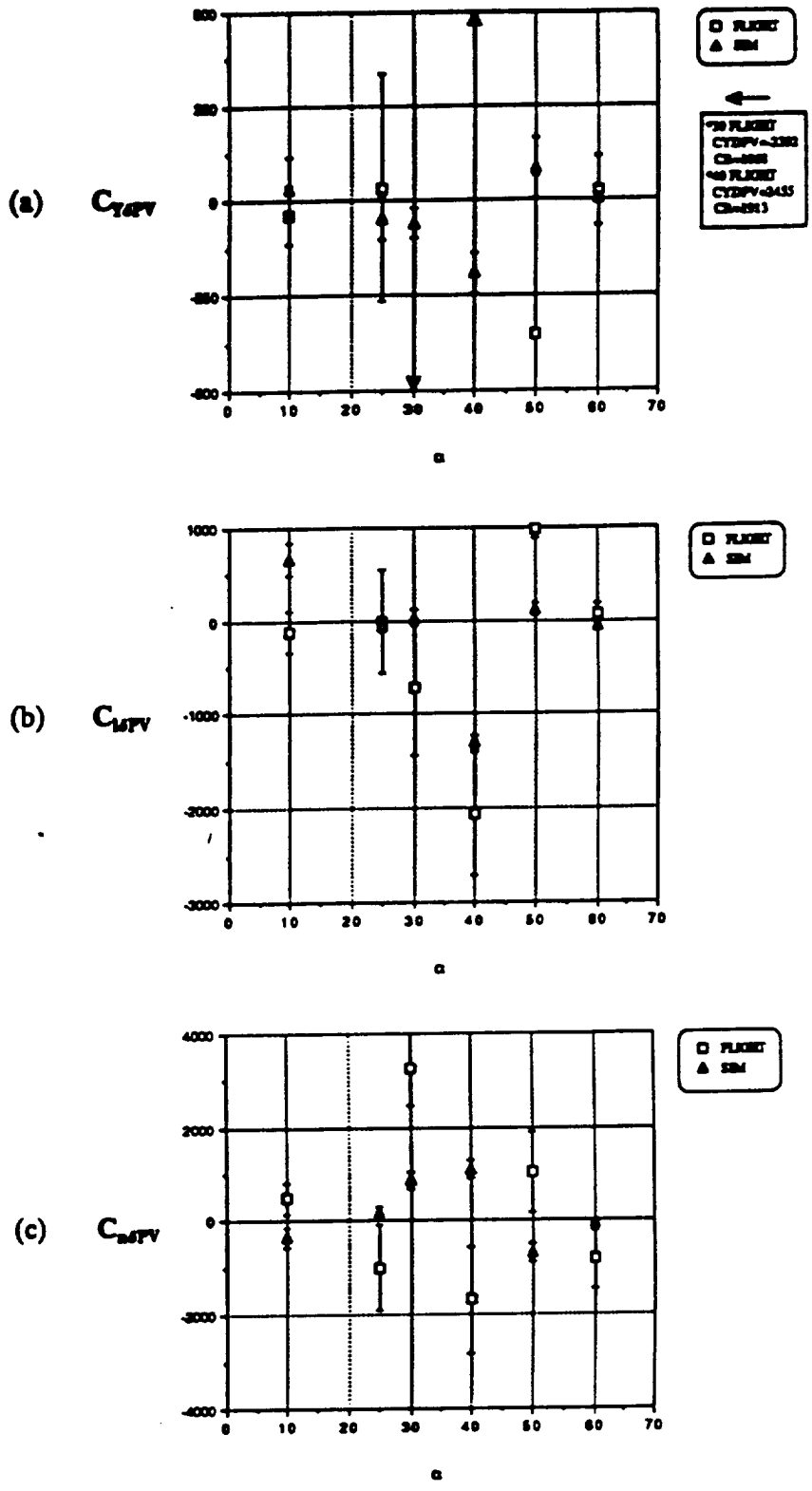

Figure 8.14: Pitch Vane Derivatives (Lateral-Directional)
(a) Lateral Force (b) Rolling Moment (c) Yawing Moment

(a) $C_{Y_{\delta YV}}$

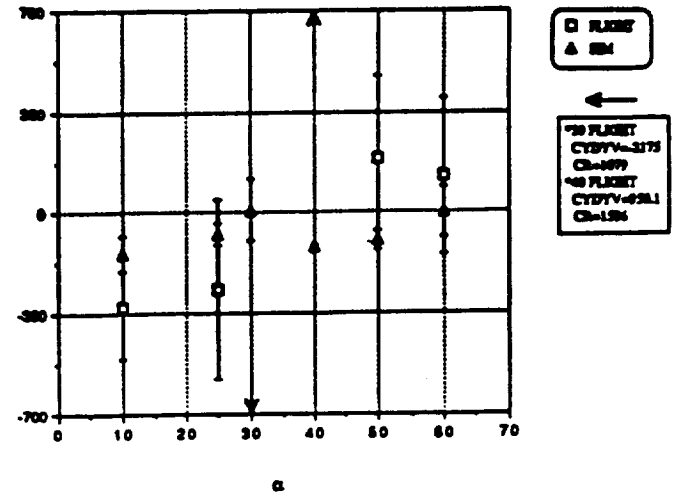

(b) $C_{l_{\delta YV}}$

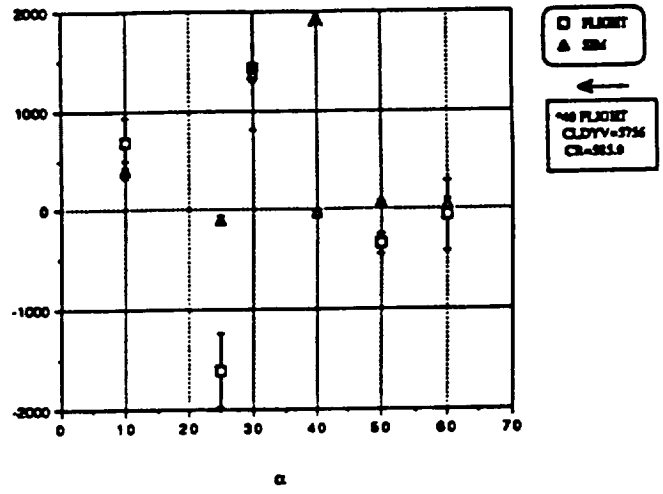

(c) $C_{n_{\delta YV}}$

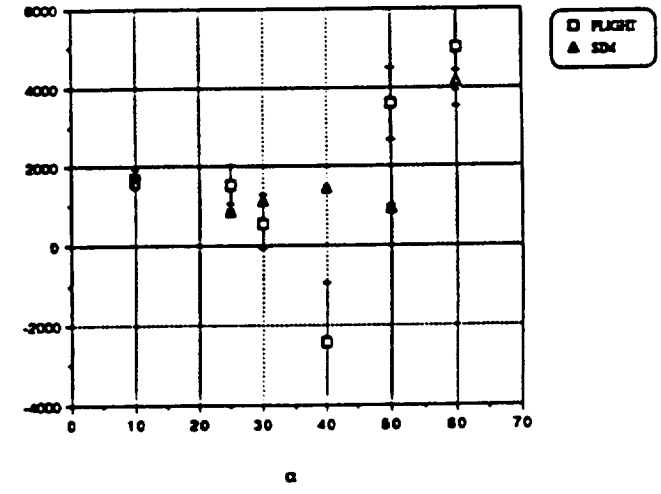

Figure 8.15: Yaw Vane Derivatives (Lateral-Directional)
(a) Lateral Force (b) Rolling Moment (c) Yawing Moment

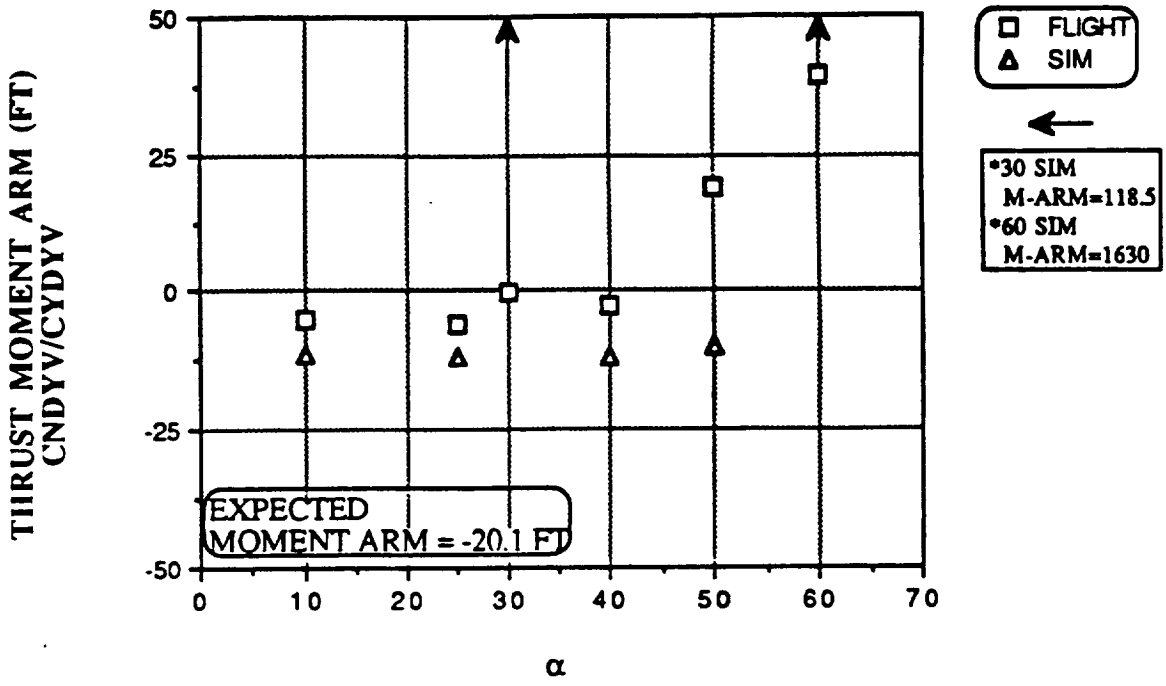

Figure 8.16: Calculated Thrust Moment Arm at Varying Angles of Attack

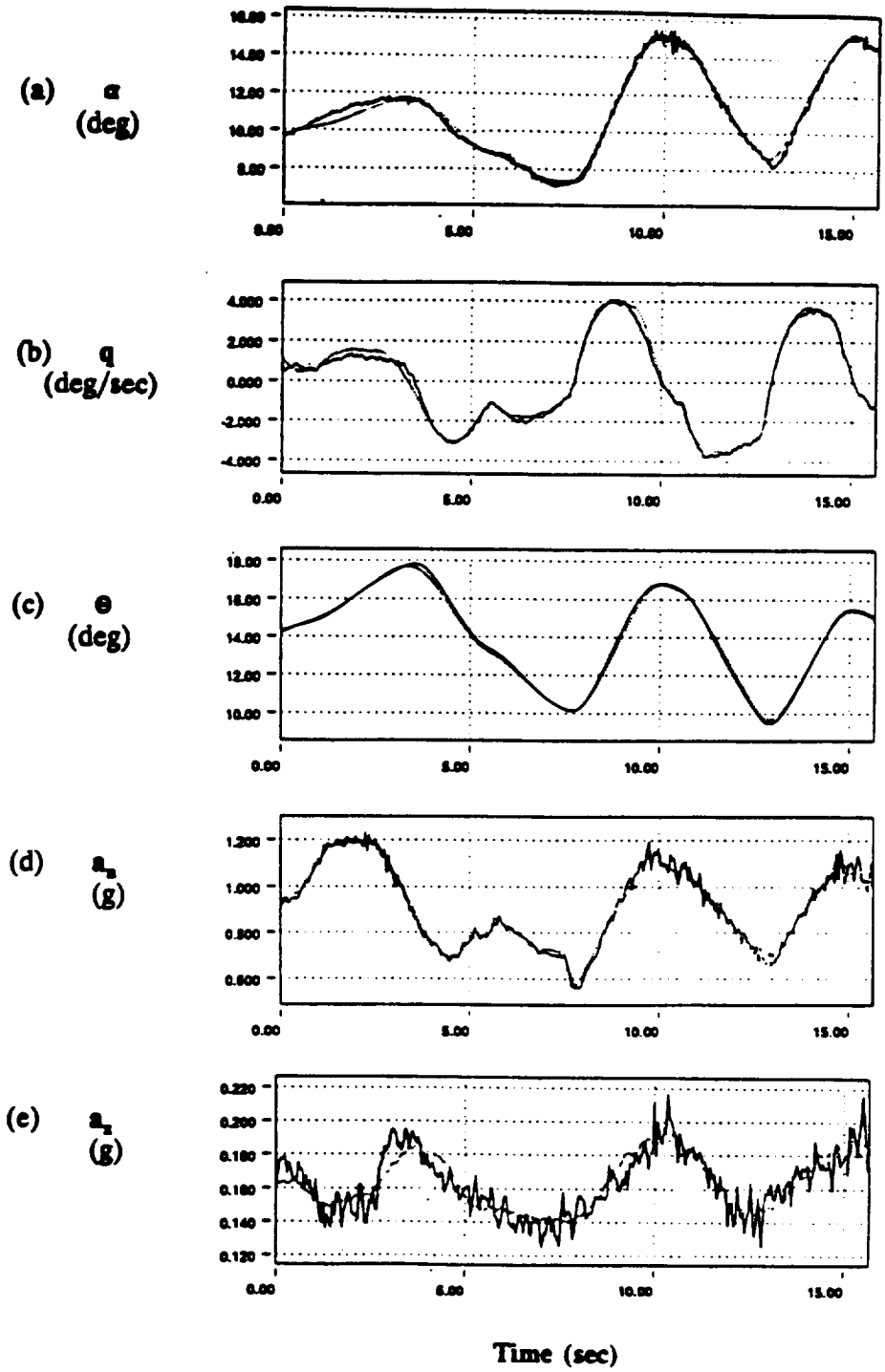

Figure 8.17: Computed (--) and Measured (——) Response Time Histories for $\alpha = 10°$ in the Longitudinal Direction for (a) Angle of Attack (b) Pitching Moment (c) Pitch Angle (d) Normal Acceleration (e) Axial Acceleration

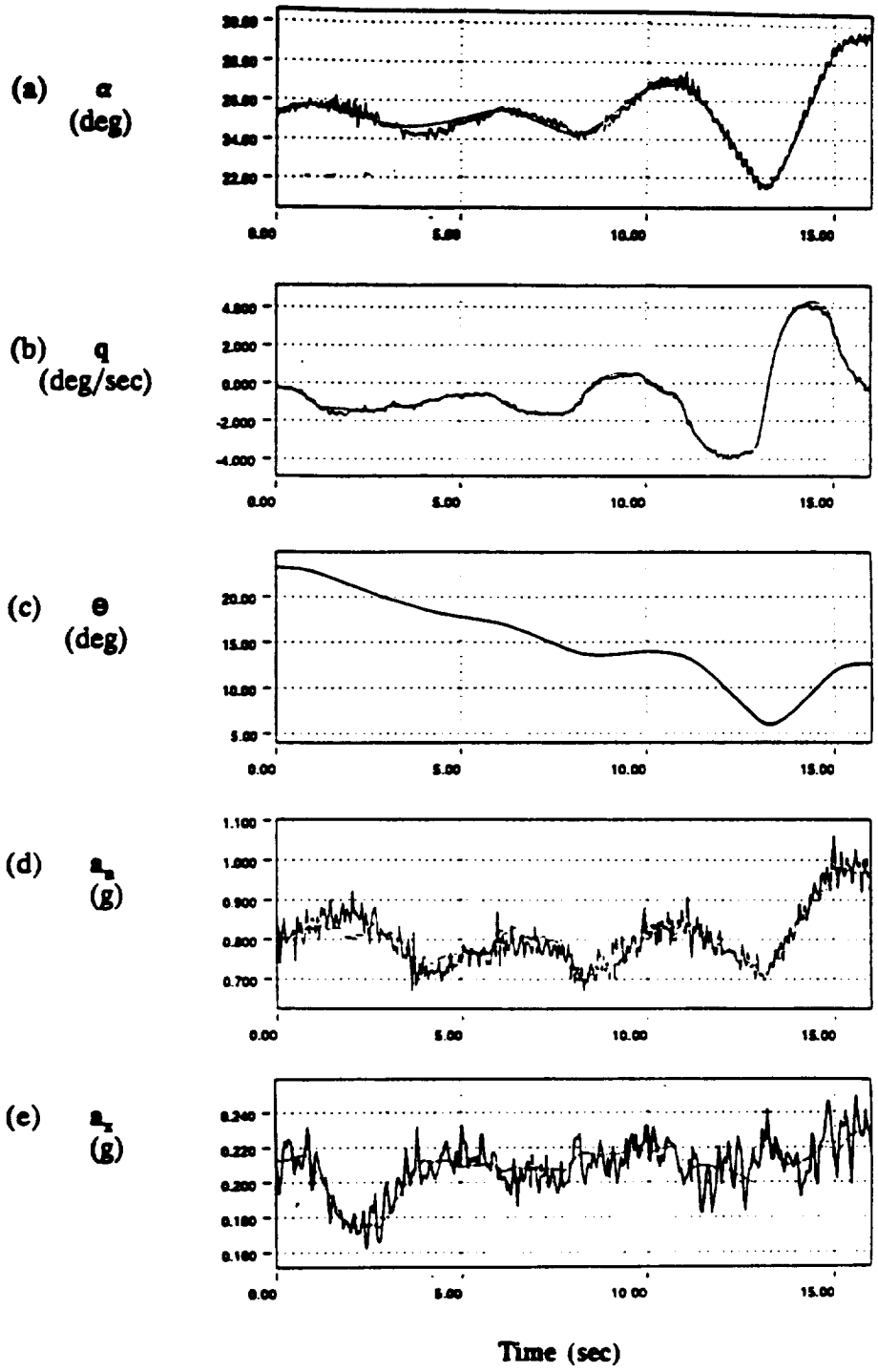

Figure 8.18: Computed (--) and Measured (——) Response Time Histories for $\alpha = 25^{\circ}$ in the Longitudinal Direction for (a) Angle of Attack (b) Pitching Moment (c) Pitch Angle (d) Normal Acceleration (e) Axial Acceleration

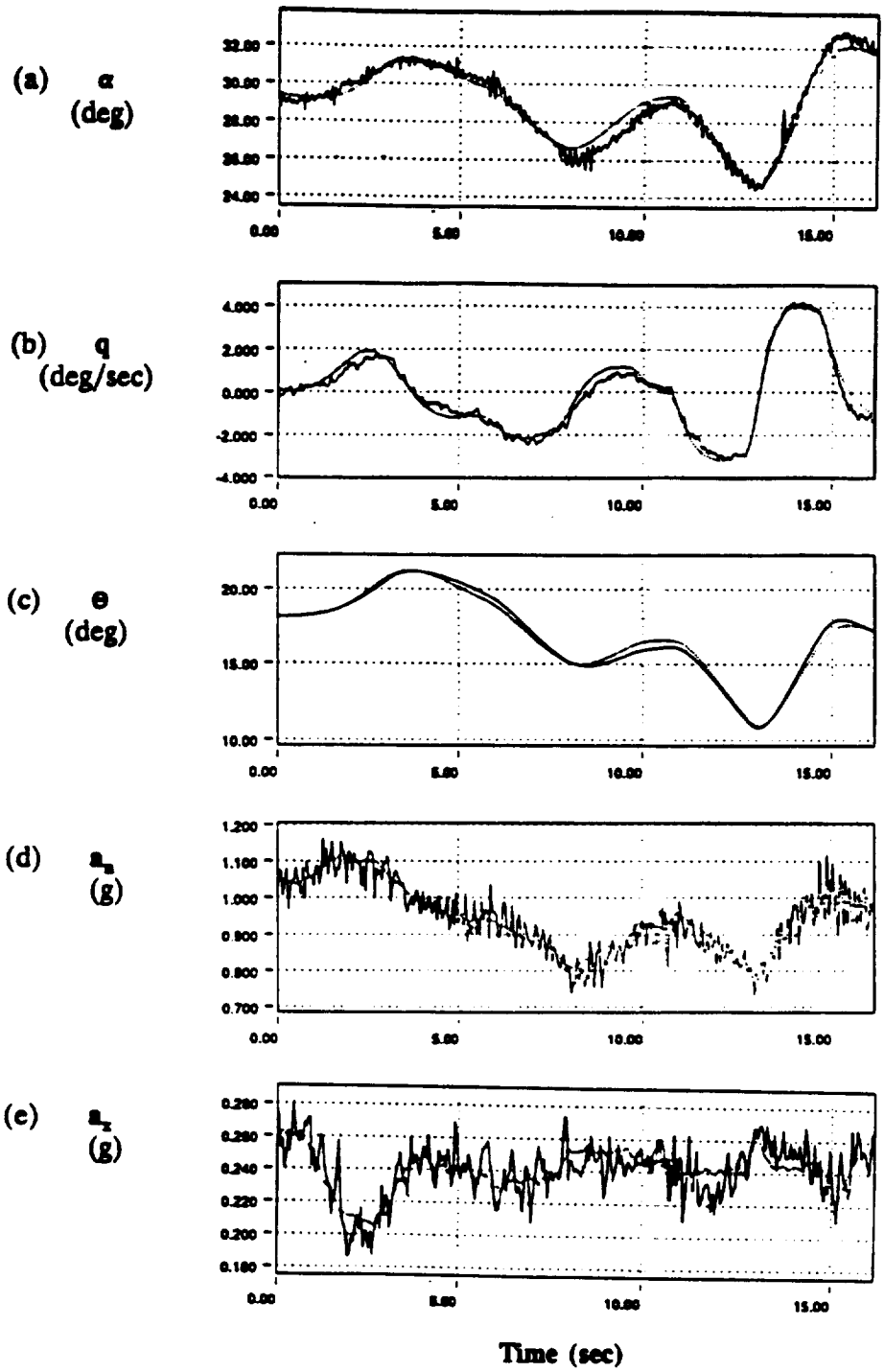

Figure 8.19: Computed (--) and Measured (——) Response Time Histories for $\alpha = 30°$ in the Longitudinal Direction for (a) Angle of Attack (b) Pitching Moment (c) Pitch Angle (d) Normal Acceleration (e) Axial Acceleration

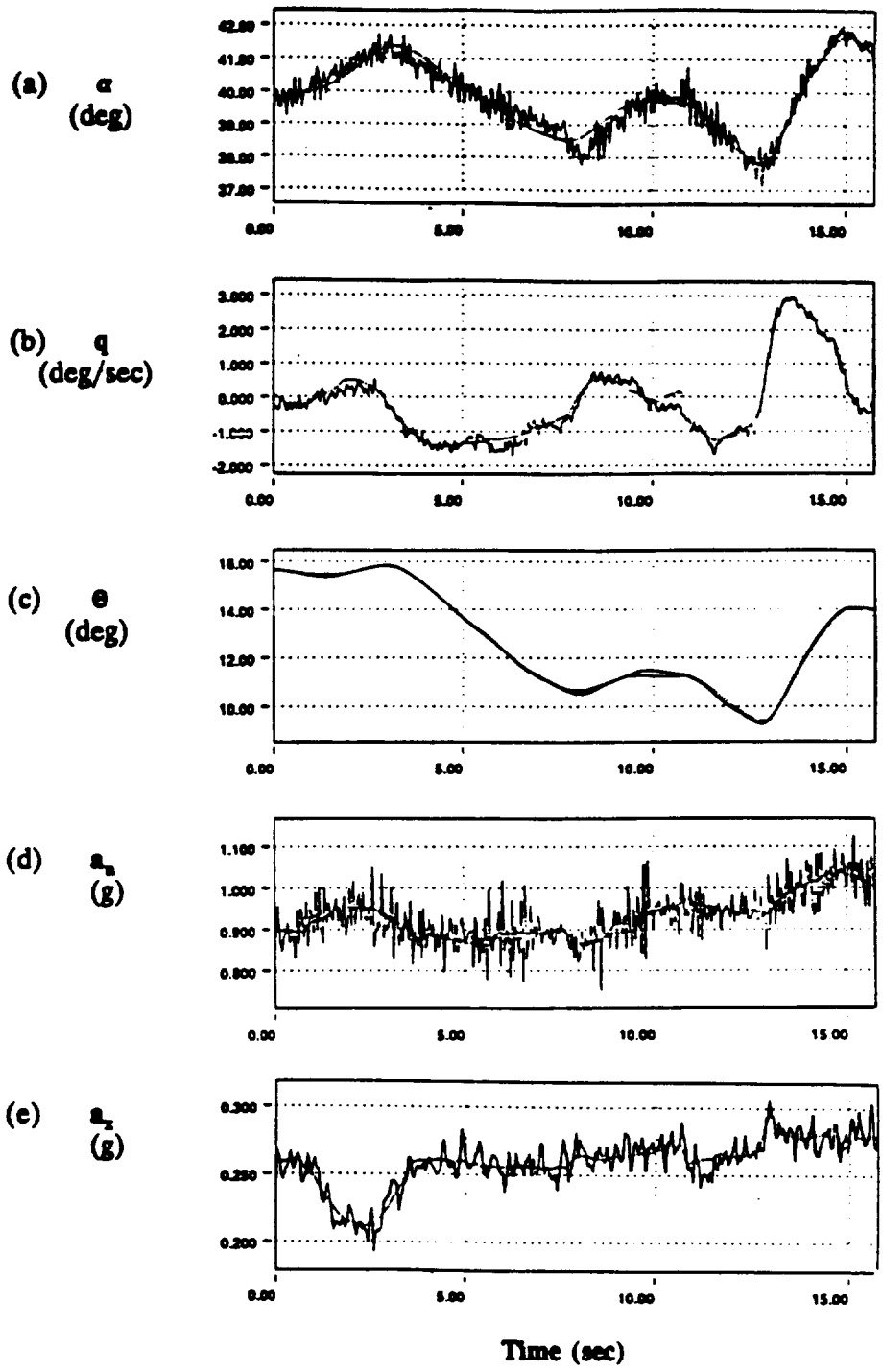

Figure 8.20: Computed (--) and Measured (——) Response Time Histories for $\alpha=40°$ in the Longitudinal Direction for (a) Angle of Attack (b) Pitching Moment (c) Pitch Angle (d) Normal Acceleration (e) Axial Acceleration

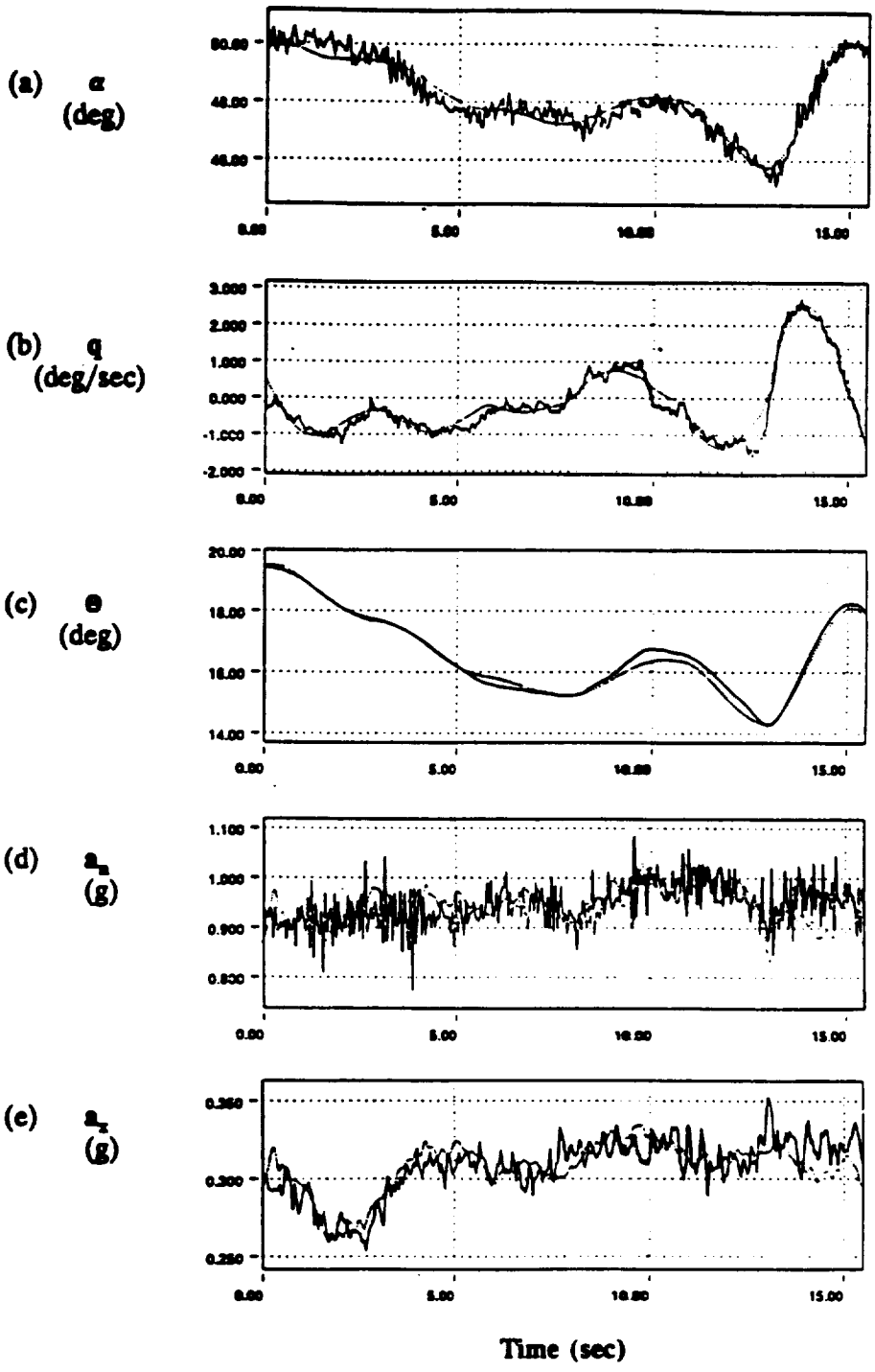

Figure 8.21: Computed (--) and Measured (——) Response Time Histories for $\alpha = 50°$ in the Longitudinal Direction for (a) Angle of Attack (b) Pitching Moment (c) Pitch Angle (d) Normal Acceleration (e) Axial Acceleration

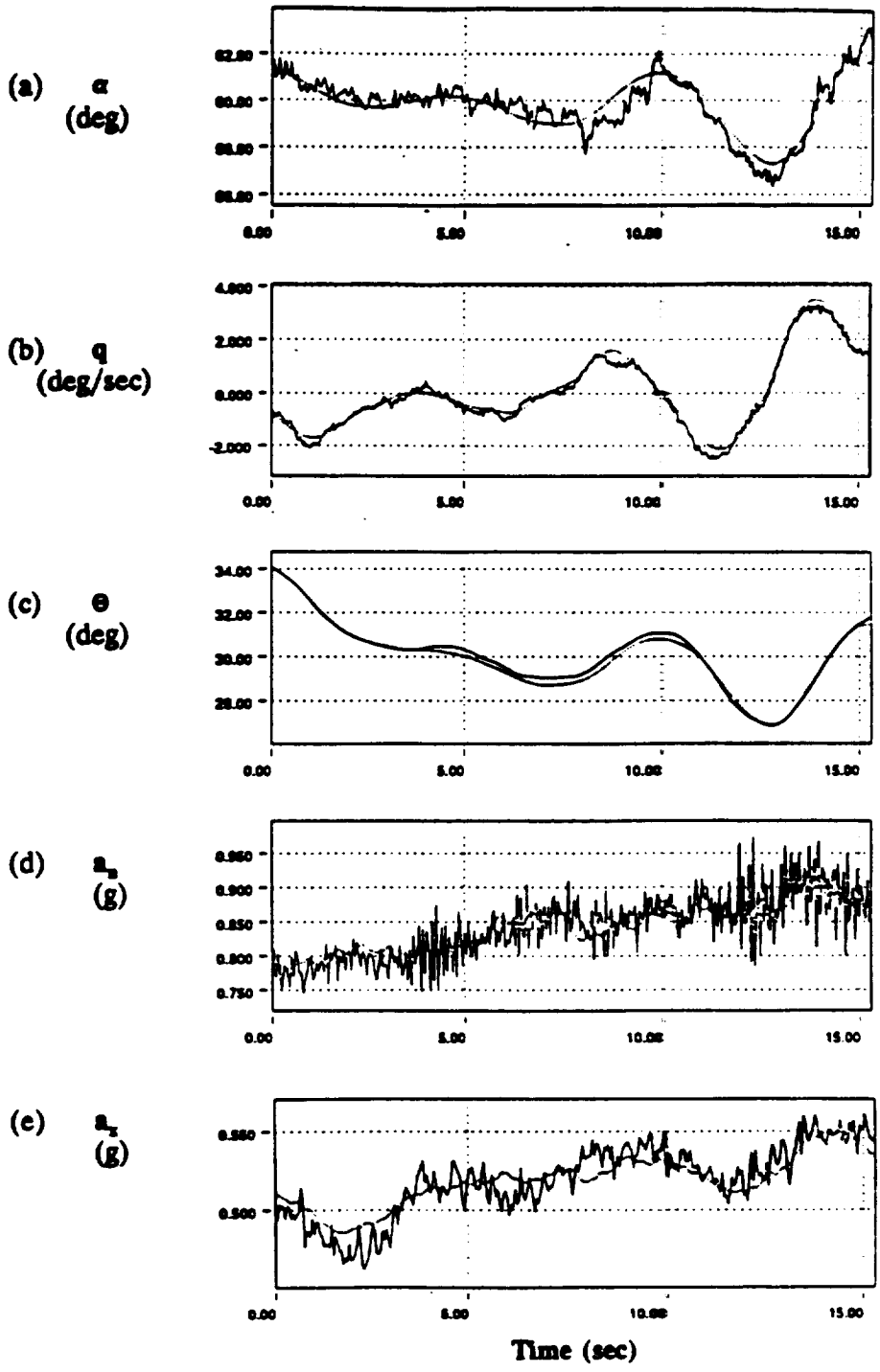

Figure 8.22: Computed (--) and Measured (——) Response Time Histories for $\alpha = 60°$ in the Longitudinal Direction for (a) Angle of Attack (b) Pitching Moment (c) Pitch Angle (d) Normal Acceleration (e) Axial Acceleration

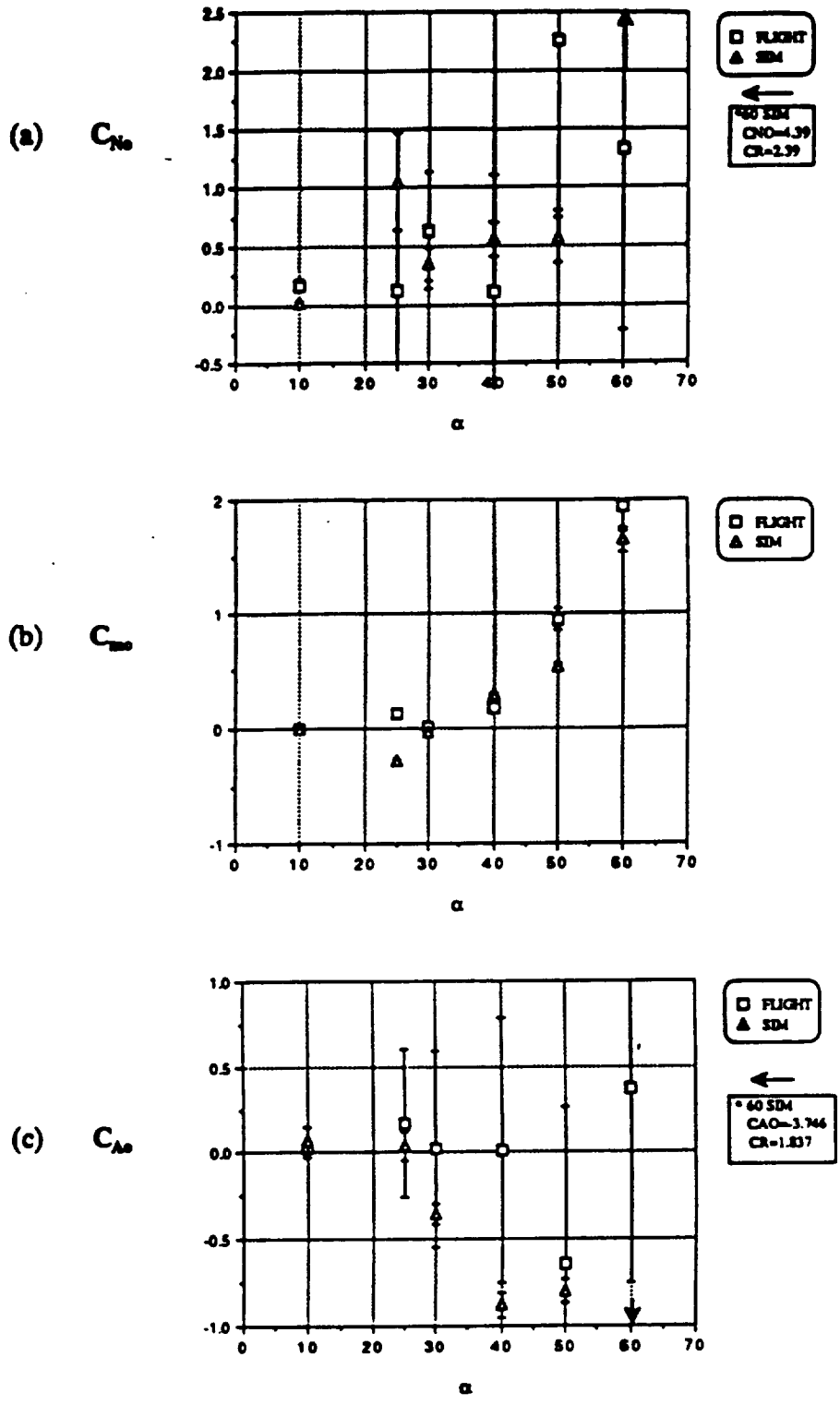

Figure 8.23: Aerodynamic Bias Derivatives (Longitudinal-Directional)
(a) Normal Force (b) Pitching Moment (c) Axial Force

(a) $C_{N\alpha}$

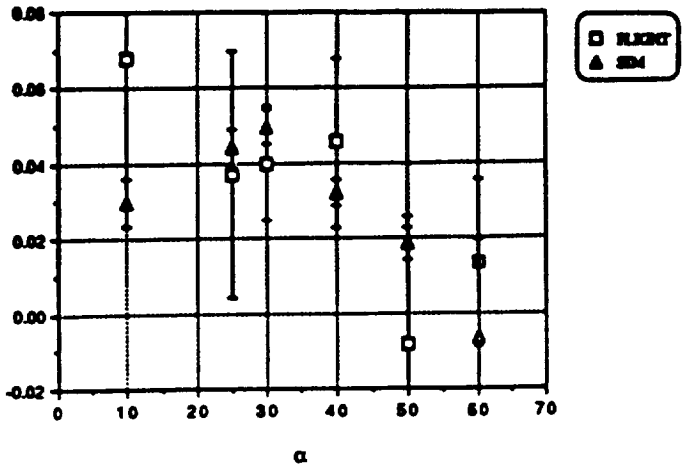

(b) $C_{m\alpha}$

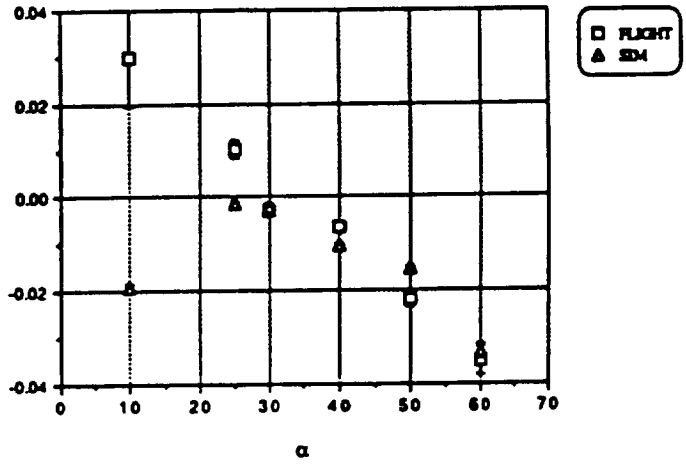

(c) $C_{A\alpha}$

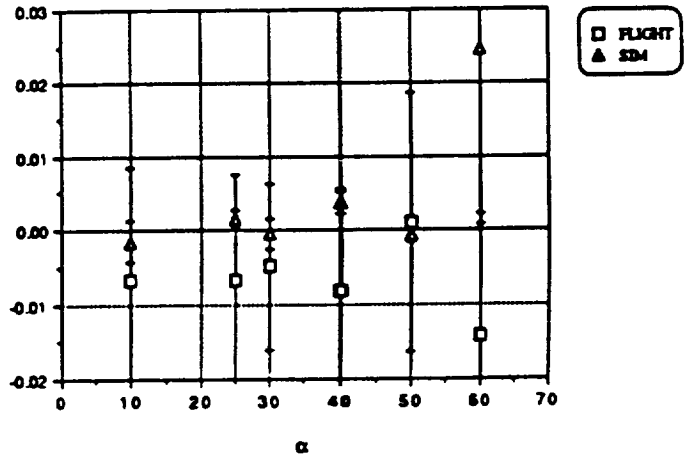

Figure 8.24: Angle of attack Derivatives (Longitudinal-Directional)
(a) Normal Force (b) Pitching Moment (c) Axial Force

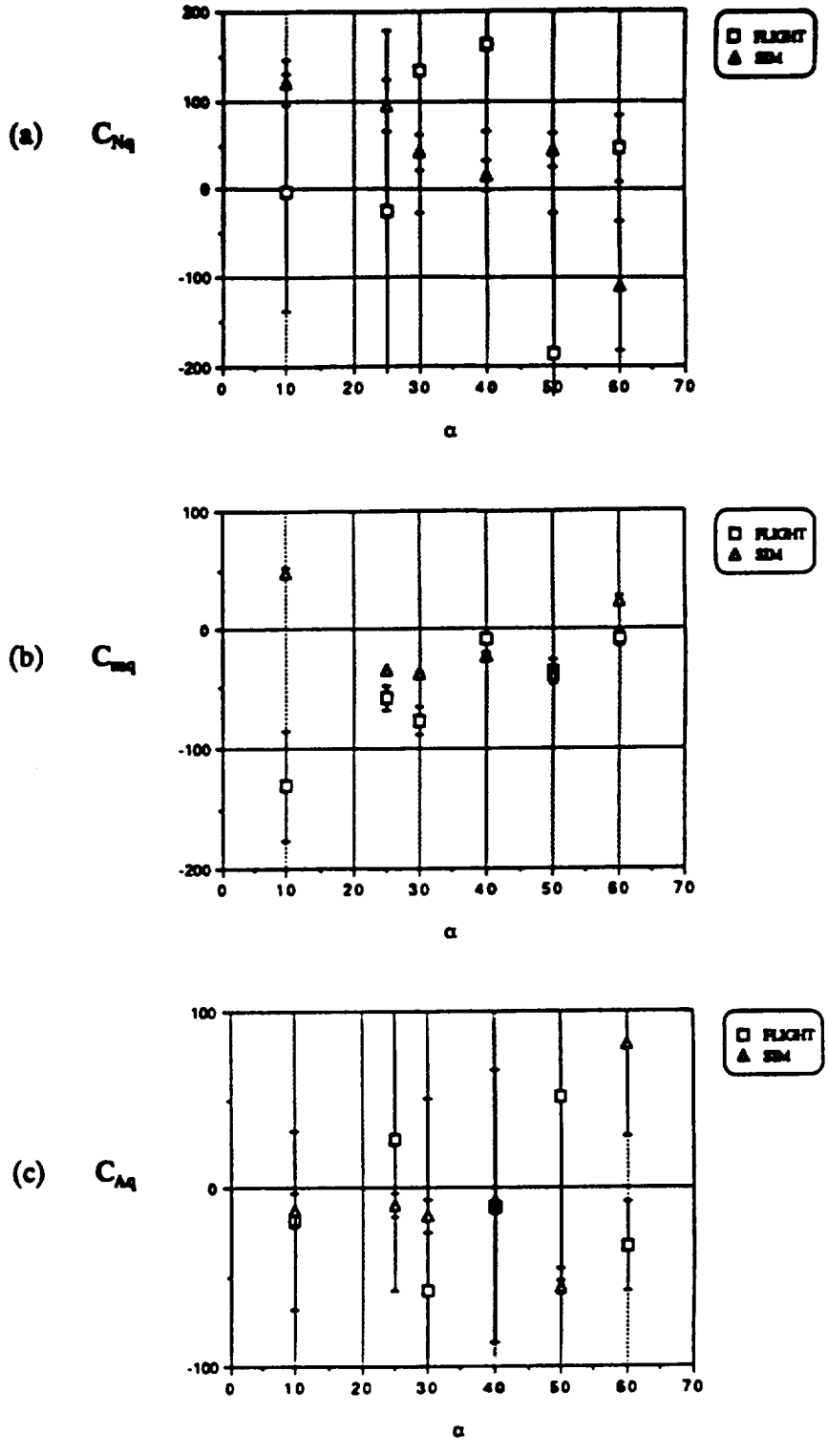

Figure 8.25: Pitch Rate Derivatives (Longitudinal-Directional)
(a) Normal Force (b) Pitching Moment (c) Axial Force

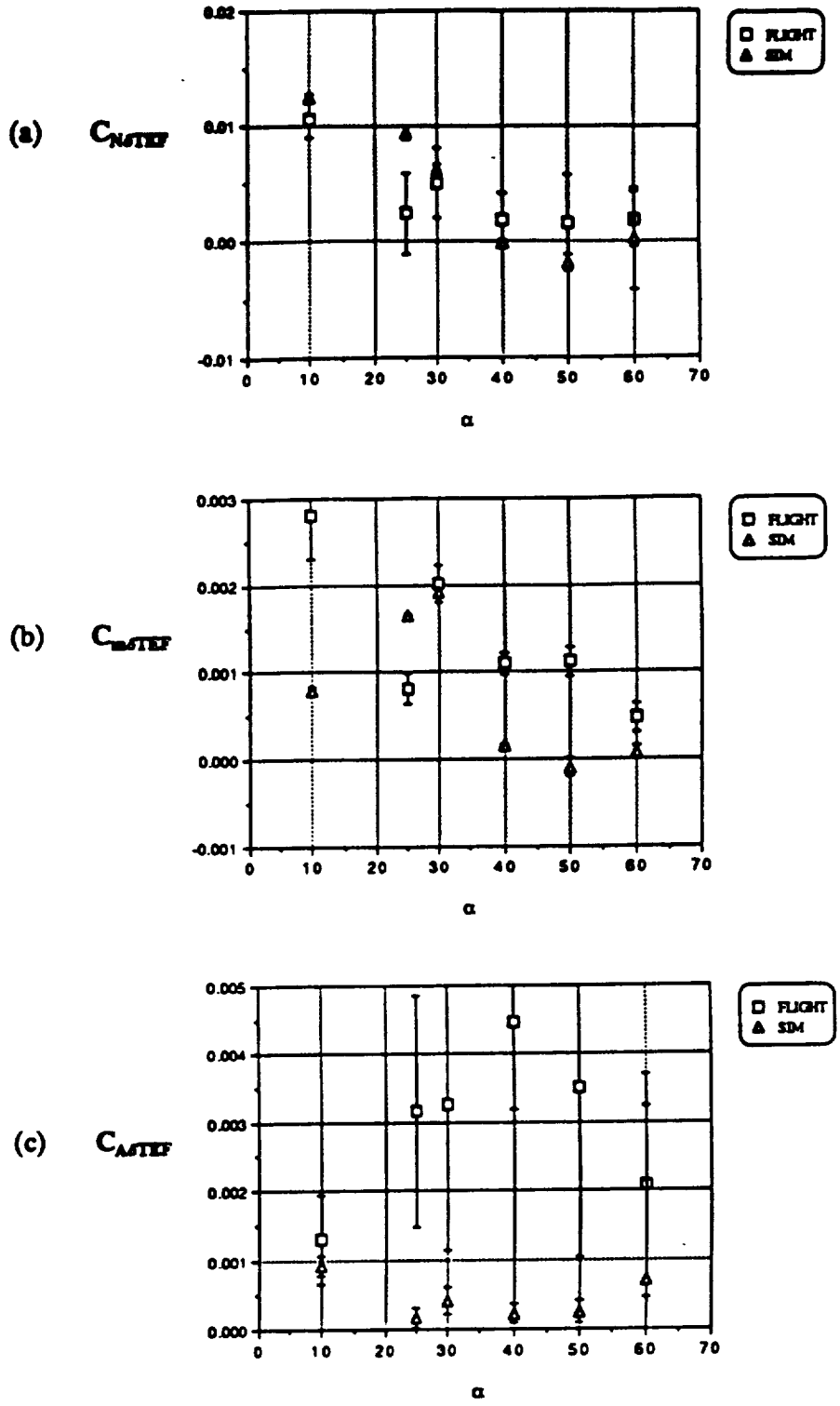

Figure 8.26: Trailing Edge Flap Derivatives (Longitudinal-Directional) (a) Normal Force (b) Pitching Moment (c) Axial Force

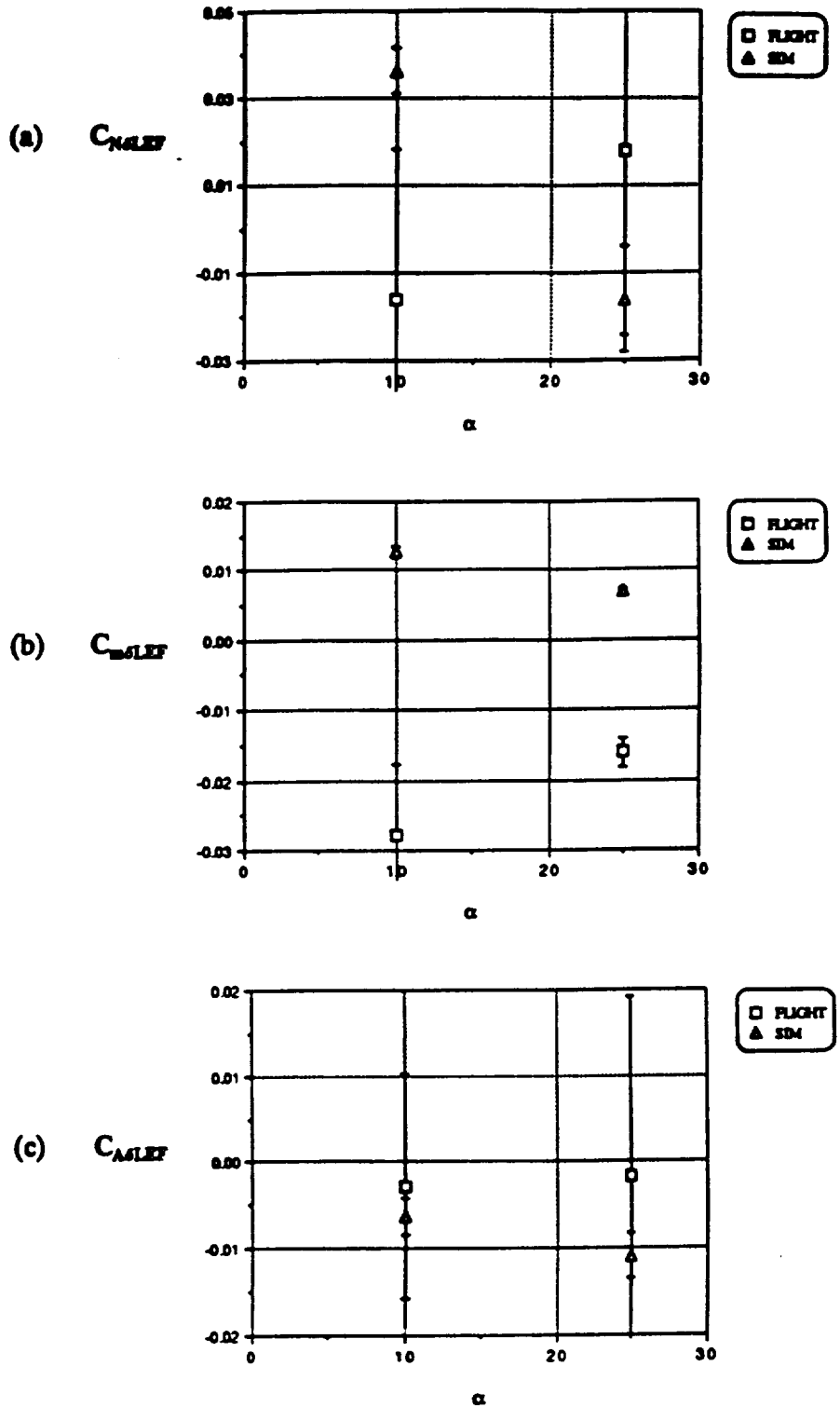

Figure 8.27: Leading Edge Flap Derivatives (Longitudinal-Directional)
(a) Normal Force (b) Pitching Moment (c) Axial Force

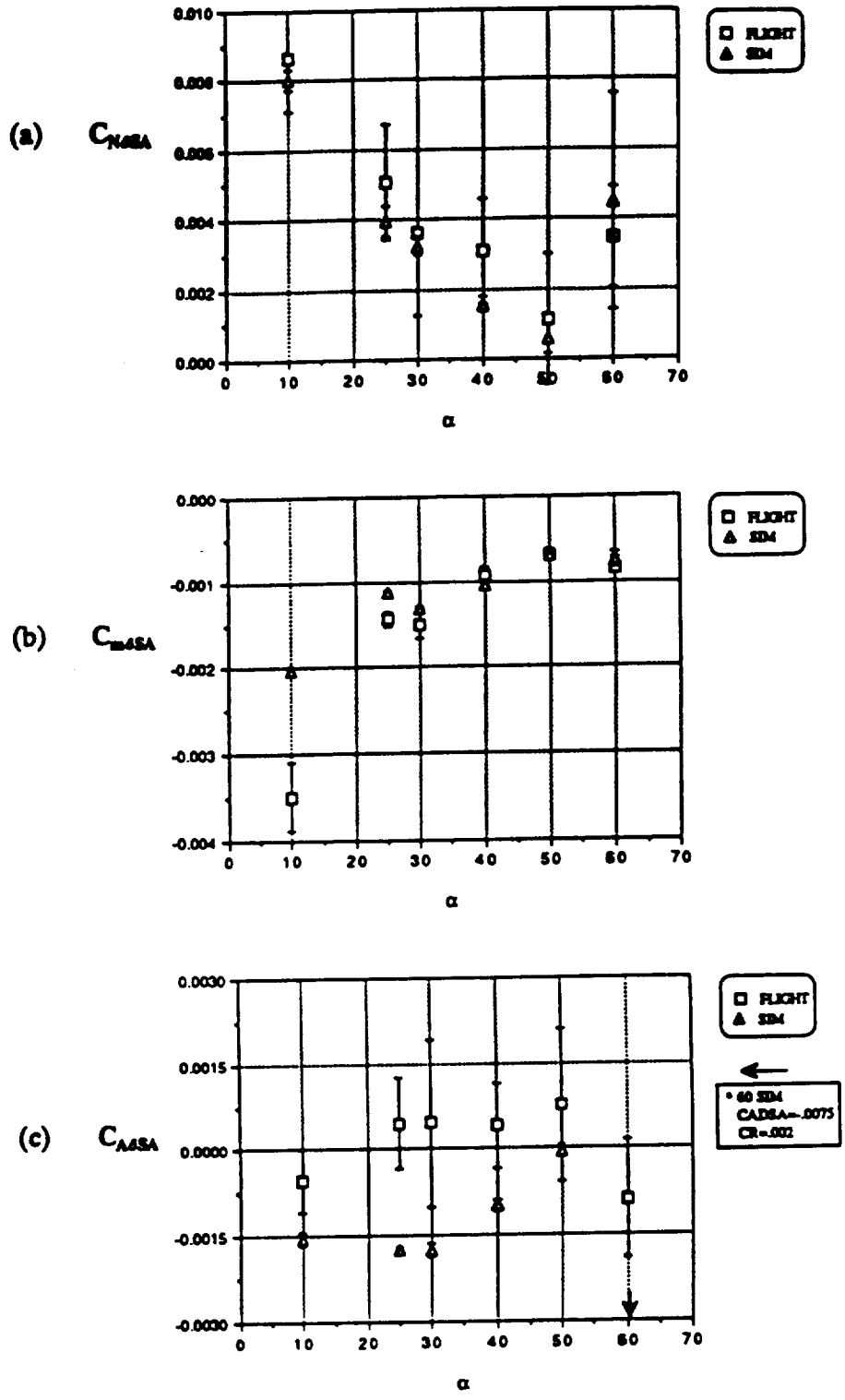

Figure 8.28: Symmetric Aileron Derivatives (Longitudinal-Directional) (a) Normal Force (b) Pitching Moment (c) Axial Force

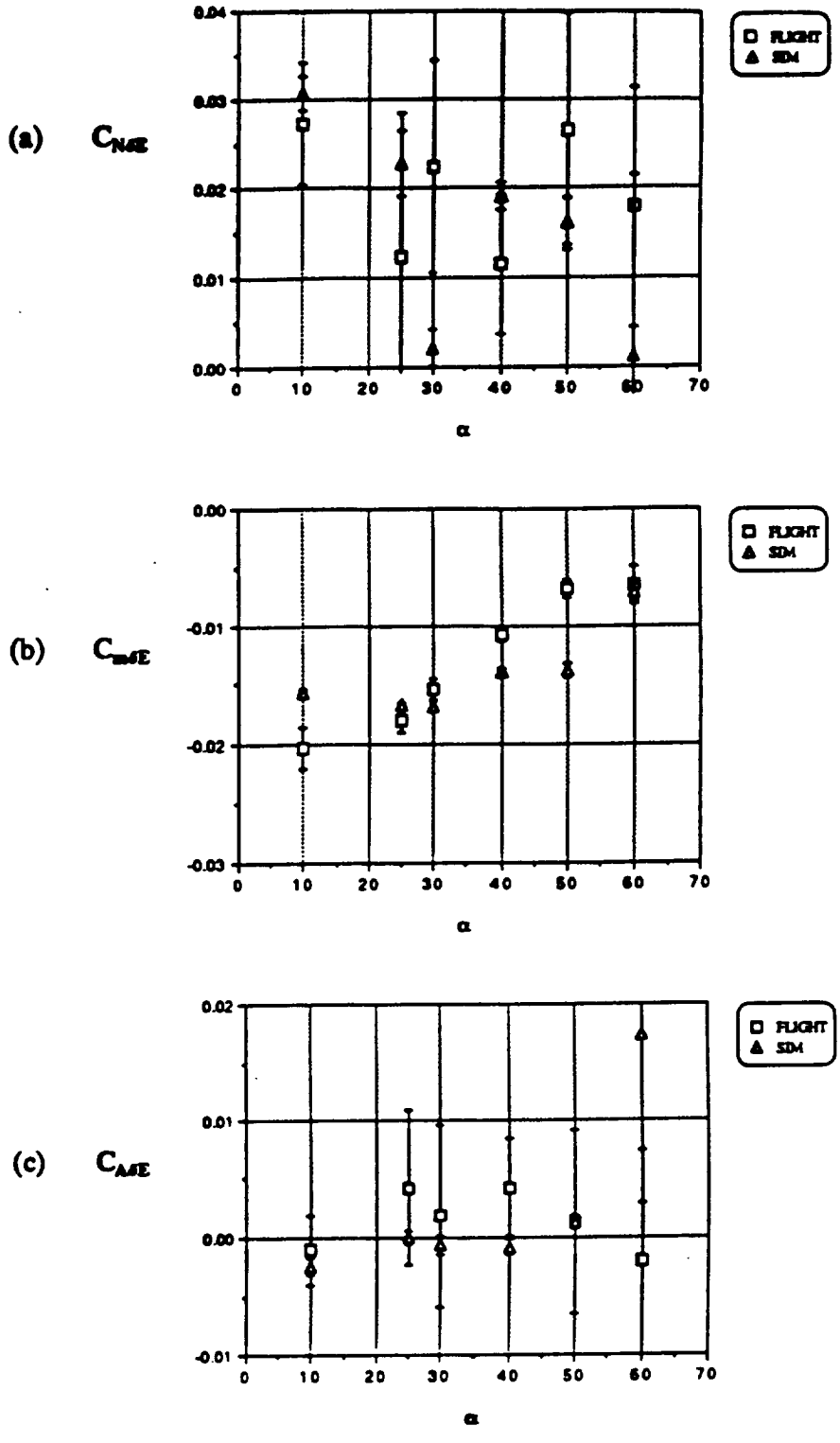

Figure 8.29: Elevator Derivatives (Longitudinal-Directional)
(a) Normal Force (b) Pitching Moment (c) Axial Force

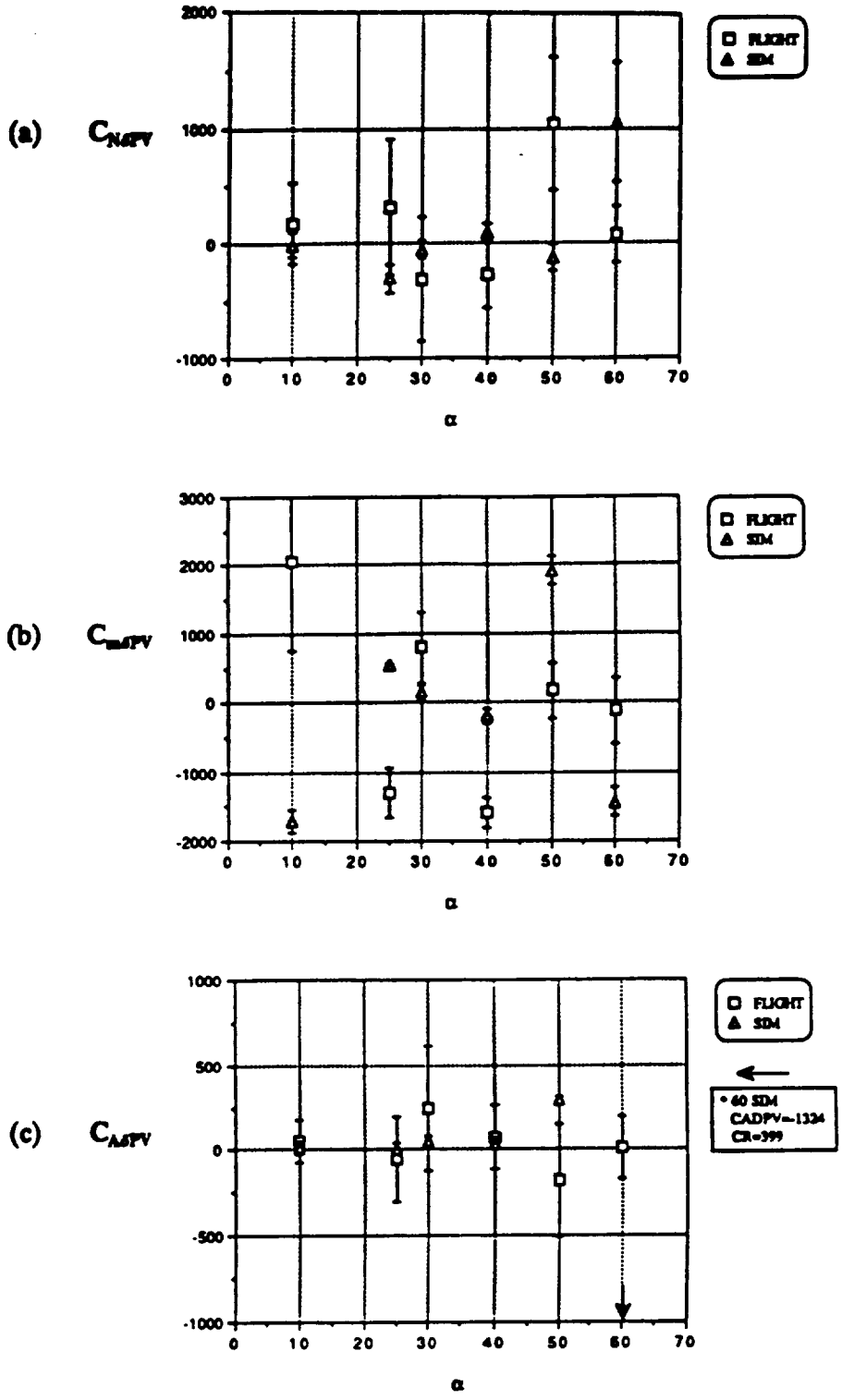

Figure 8.30: Pitch Vane Derivatives (Longitudinal-Directional)
(a) Normal Force (b) Pitching Moment (c) Axial Force

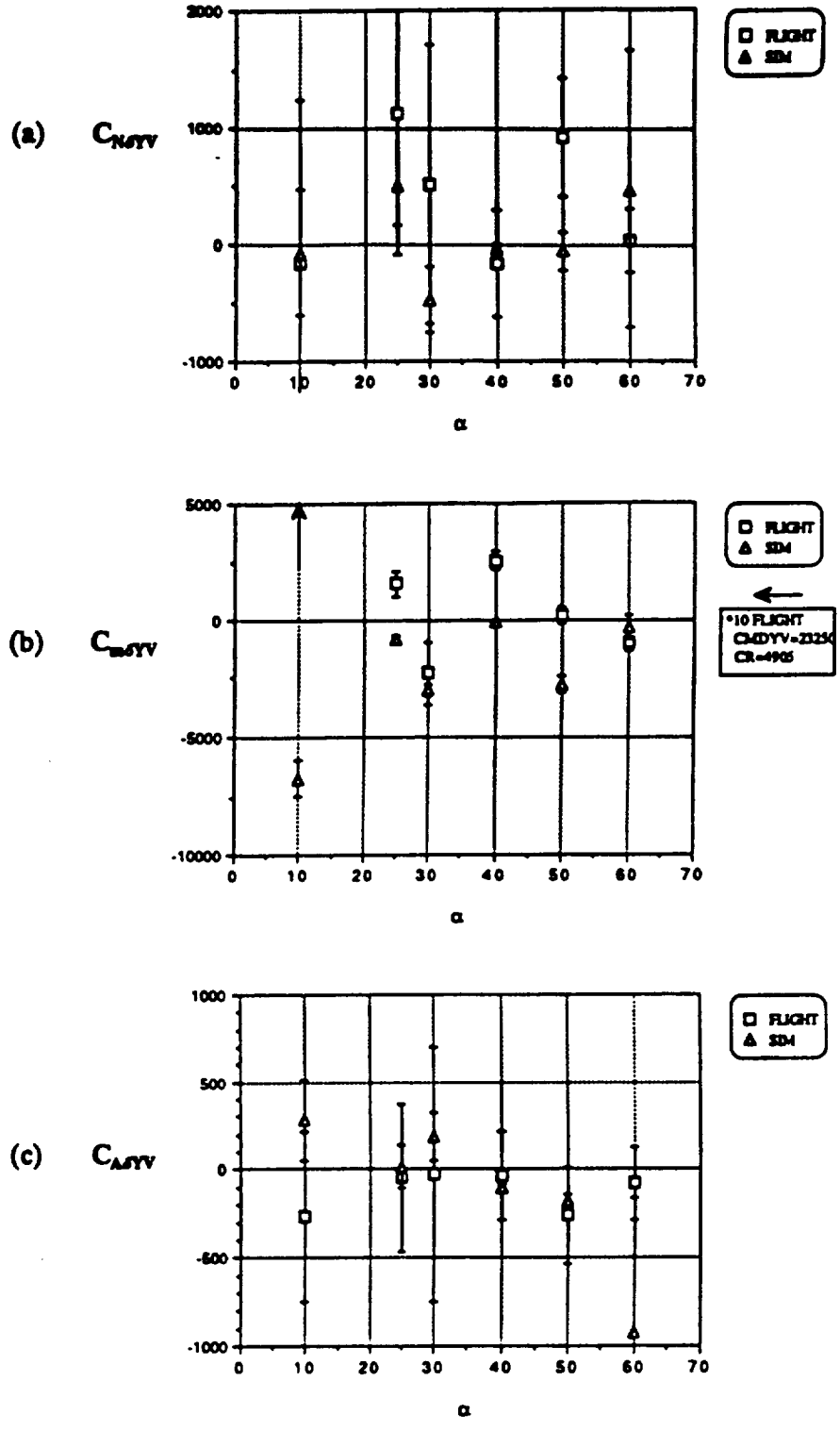

Figure 8.31: Yaw Vane Derivatives (Longitudinal-Directional)
(a) Normal Force (b) Pitching Moment (c) Axial Force

REFERENCES

1. Maine, Richard E.; and Iliff, Kenneth W.: *Application of Parameter Estimation to Aircraft Stability and Control - The Output-Error Approach*. NASA RP-1168, 1986.

2. Maine, Richard E.; and Murray, James E.: *Application of Parameter Estimation to Highly Unstable Aircraft*. NASA TM-88266, 1986.

3. Sim, Alex G.; and Curry, Robert E.: *Flight-Determined Aerodynamic Derivatives of the AD-1 Oblique-Wing Research Airplane*. NASA TP-2222, 1984.

4. Pellicano, Paul; Krumenacker, Joseph; and Vanhoy, David: *X-29 High Angle-of-Attack Flight Test Procedures, Results, and Lessons Learned*.

5. Klein, Vladislav; Breneman, Kevin P.; and Ratvasky, Thomas P.: *Aerodynamic Parameters of an Advanced Fighter Aircraft Estimated from Flight Data, Preliminary Results*. NASA TM-101631, 1989.

6. Rohlf, D.; Plaetschke, E; and Weiss, S.: *X-31A Model Evaluation and Validation via System Identification*. AIAA Atmospheric Flight Mechanics Conference, New Orleans, LA, August 12-14, 1991, Paper No. 91-2875.

7. Iliff, Kenneth W.: Updated Stability and Control Derivatives for F-18. Memo 1990.

8. Klein, Vladislav: *Determination of Stability and Control Parameters of a Light Airplane from Flight Data Using Two Estimation Methods*. NASA TP-1306, 1979.

9. Bryan, G.H.: *Stability in Aviation*, Macmillan, London, England, 1911.

10. Nelson, Robert C.: *Flight Stability and Automatic Control*, McGraw-Hill Book Co., New York, 1989.

11. *USAF Stability and Control DATCOM*, Flight Control Division, Air Force Flight Dynamics Laboratory, Wright-Patterson Air Force Base, OH.

12. Maine, Richard E.; and Iliff, Kenneth W.: *User's Manual for MMLE3, A General FORTRAN Program for Maximum Likelihood Parameter Estimation*. NASA TP-1563, 1980.

13. Murray, James E.; and Maine, Richard E.: *pEst Version 2.1 User's Manual*. NASA TM-88280, 1987.

14. Roskam, Jan: *Airplane Flight Dynamics and Automatic Flight Controls, Part I*, Roskam Aviation and Engineering Corp., Ottawa, Kansas, 1979.

15. Gilbert, William P.; and Gatlin, Donald H.: *Review of the NASA High-Alpha Technology Program.*

16. Hammett. L. N., Jr.: *An Investigation of the F-16 High Angle-of-Attack Pitching Moment Discrepancy*. Technical Report AFWAL-TR-81-3107.

17. Erickson, Gary E.: Water Tunnel Flow Visualization and Wind-Tunnel Data Analysis of the F/A-18. NASA CR 165859, May 1982.

18. Dornheim, Michael A.: *NASA Control Laws Boost F-14 High Angle-of Attack Performance*. Aviation Week and Space Technology, Page 71, October 14, 1985.

19. Bowers, Albion H.; Noffz, Gregory; Grafton, Sue B.; Mason, Mary L.; and Peron, Lee R.: *Multiaxis Thrust Vectoring Using Axisymmetric Nozzles and Postexit Vanes on an F/A-18 Configuration Vehicle*. NASA TM 101741, 1991.

20. Moes, Timothy R.; and Whitmore, Stephen A.: *A Preliminary Look at Techniques Used to Obtain Airdata from Flight at High Angles of Attack*. NASA TM 101729, 1990.

21. Koehler, R.; and Wilhelm, K.: Auslegung von Eingangssignalen fur die Kennwertermittlung. IB 154-77/40, DFVLR Institut fur Flugmechanik, Braunschweig, Federal Republic of Germany, 1977.

22. Maine R.E.; and Iliff, K.W.: *Identification of Dynamic Systems - Theory and Formulation*. NASA RP-1138, 1985.

23. Williams, David; Quast, Thomas; and Nelson, Robert C.: *Comparison of Flight and Sub-scale Model Wing Rock Characteristics of an F-18 Aircraft*. Final Report for NASA Grant NCA2-513, 1993.